Synthesis and Evaluation of Sterically Demanding Ruthenium Dithiolate Catalysts for Stereoretentive Olefin Metathesis

T. Patrick Montgomery,[†] Jessica M. Grandner,[‡] K. N. Houk,[‡] and Robert H. Grubbs[†]*

[†]*The Arnold and Mabel Beckman Laboratory of Chemical Synthesis, Division of Chemistry and Chemical Engineering, California Institute of Technology, Pasadena, California 91125, USA*
[‡]*Department of Chemistry and Biochemistry, University of California, Los Angeles, CA 90095, USA*

Table of Contents:

I. Catalyst Initiation Studies

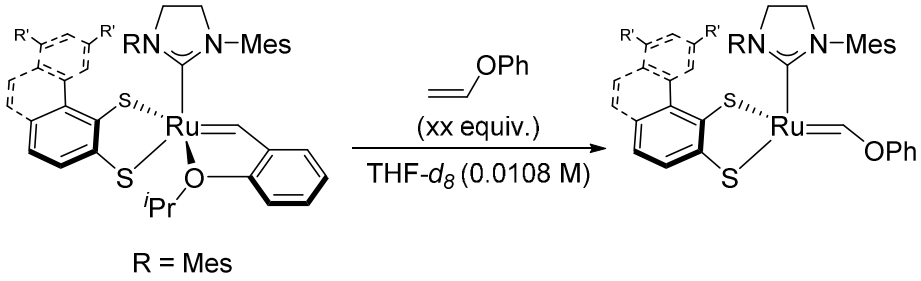

R = Mes

Scheme S1. Catalyst initiation using phenyl vinyl ether.

Data for **II**:

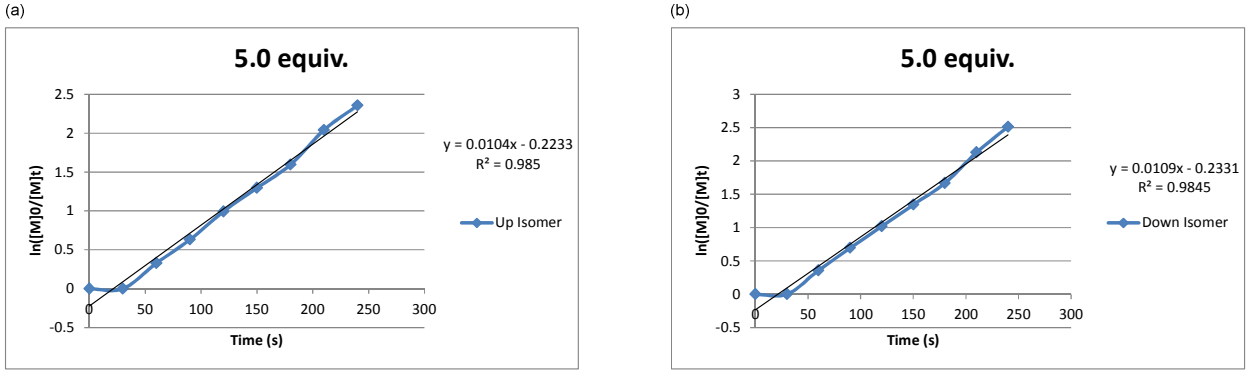

Figure S1. Initiation data for **II** using 5.0 equiv. of phenyl vinyl ether. (a) *up*-**II**. (b) *down*-**II**.

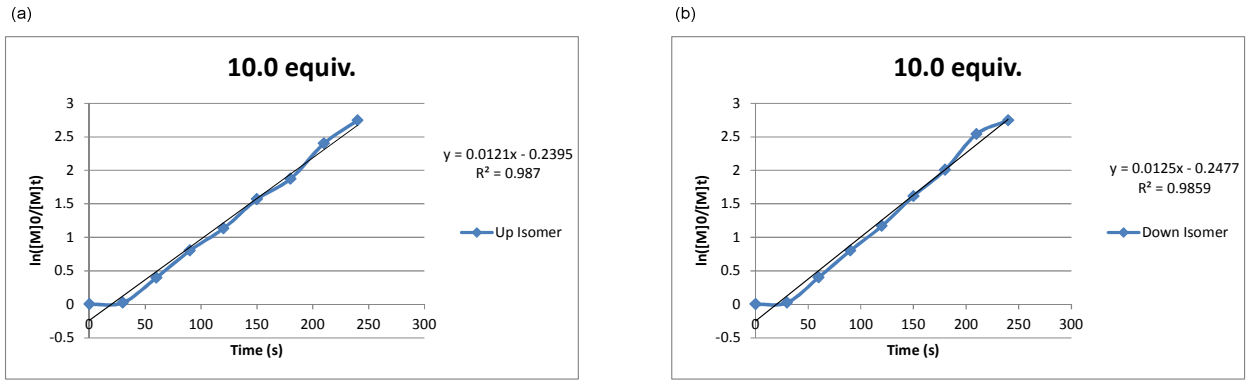

Figure S2. Initiation data for **II** using 10.0 equiv. of phenyl vinyl ether. (a) *up*-**II**. (b) *down*-**II**.

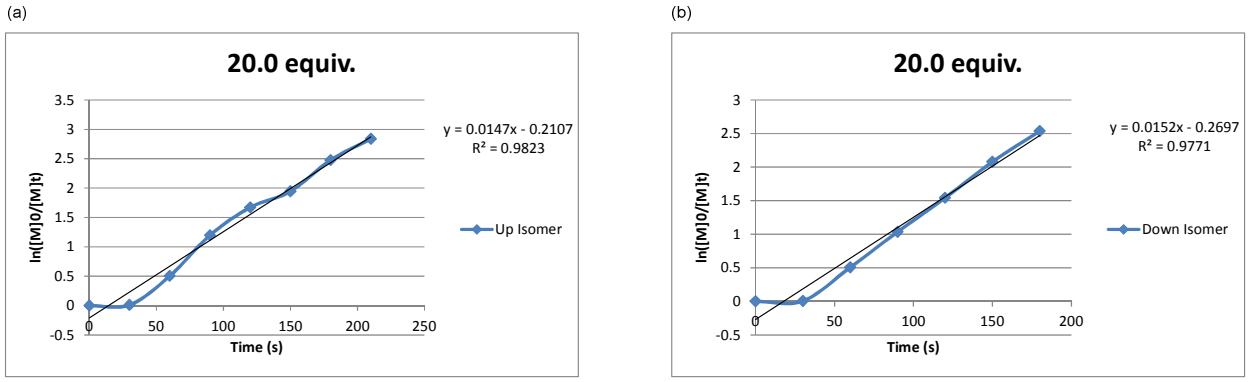

Figure S3. Initiation data for **II** using 10.0 equiv. of phenyl vinyl ether. (a) *up*-**II**. (b) *down*-**II**.

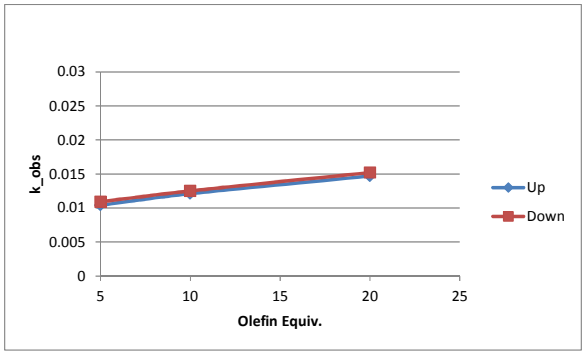

Figure S4. Initiation data for **II** comparing *up*-**II** and *down*-**II**.

Data for **III**:

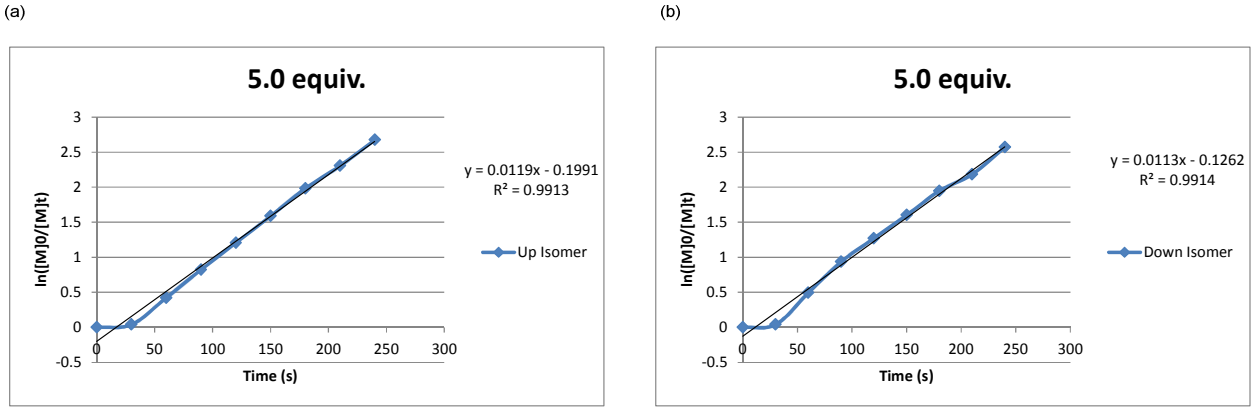

Figure S5. Initiation data for **III** using 5.0 equiv. of phenyl vinyl ether. (a) *up*-**III**. (b) *down*-**III**.

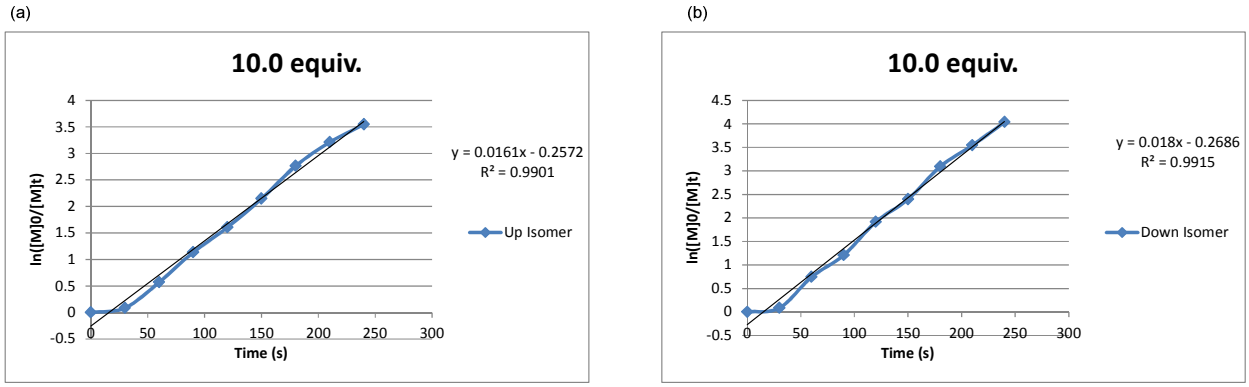

Figure S6. Initiation data for **III** using10.0 equiv. of phenyl vinyl ether. (a) *up*-**III**. (b) *down*-**III**.

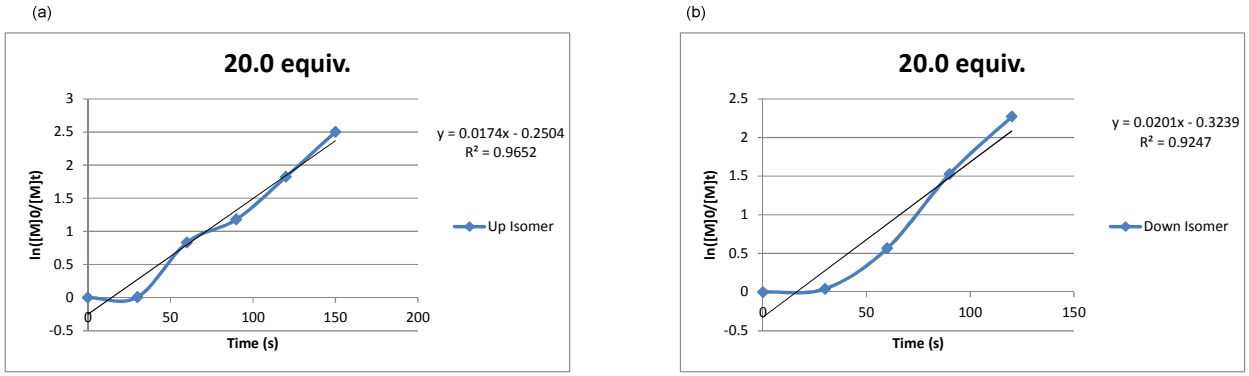

Figure S7. Initiation data for **III** using 20.0 equiv. of phenyl vinyl ether. (a) *up*-**III**. (b) *down*-**III**.

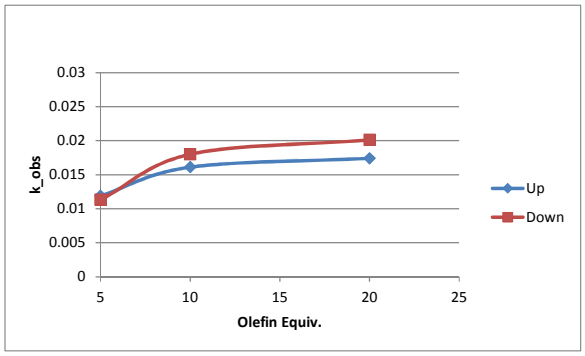

Figure S8. Initiation data for **III** comparing *up*-**III** and *down*-**III**.

Data for **IV**:

(a)

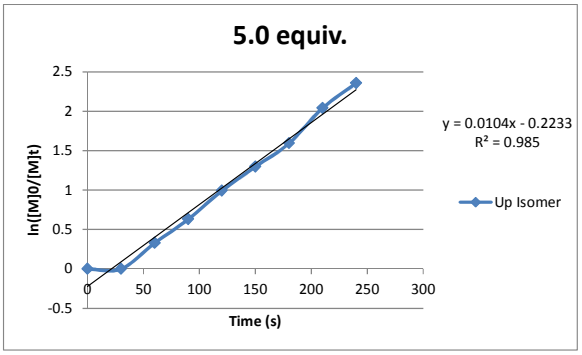

(b)

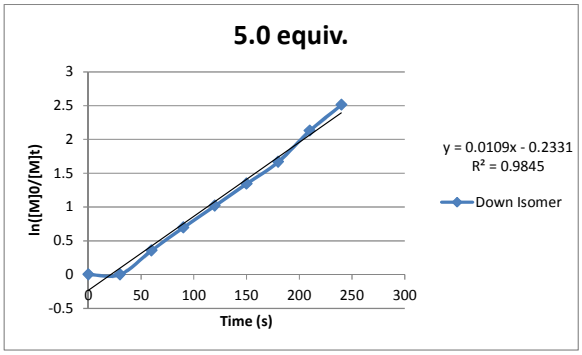

Figure S9. Initiation data for **IV** using 5.0 equiv. of phenyl vinyl ether. (a) *up*-**IV**. (b) *down*-**IV**.

(a)

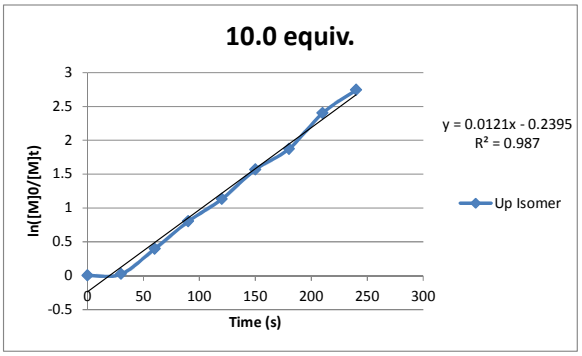

(b)

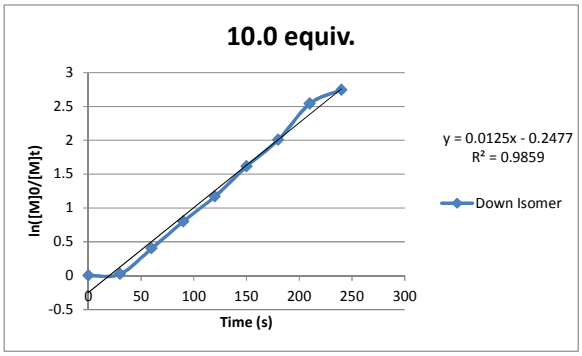

Figure S10. Initiation data for **IV** using 10.0 equiv. of phenyl vinyl ether. (a) *up*-**IV**. (b) *down*-**IV**.

(a)

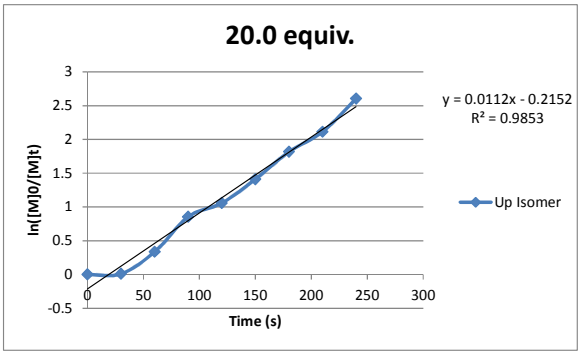

(b)

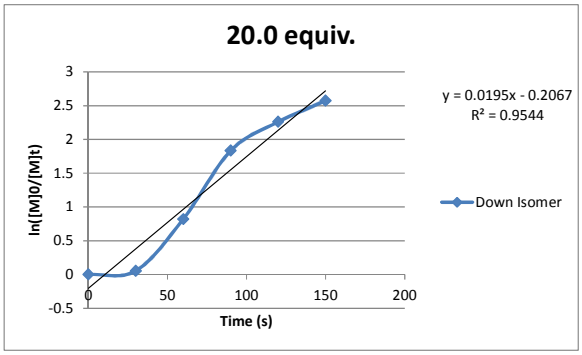

Figure S11. Initiation data for **IV** using 20.0 equiv. of phenyl vinyl ether. (a) *up*-**IV**. (b) *down*-**IV**.

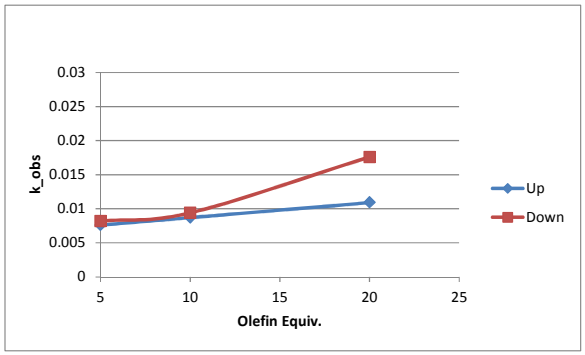

Figure S12. Initiation data for **IV** comparing *up*-**IV** and *down*-**IV**.

Data for **V**:

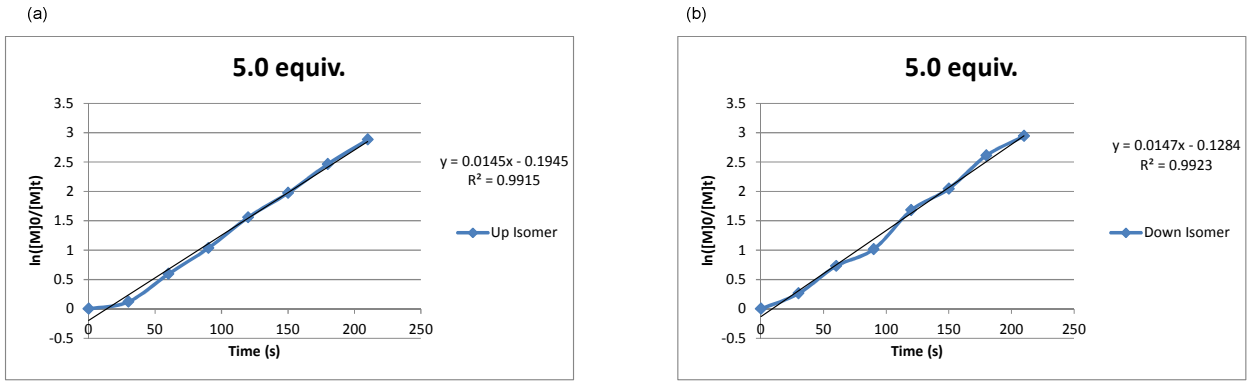

Figure S13. Initiation data for **V** using 5.0 equiv. of phenyl vinyl ether. (a) *up*-**V**. (b) *down*-**V**.

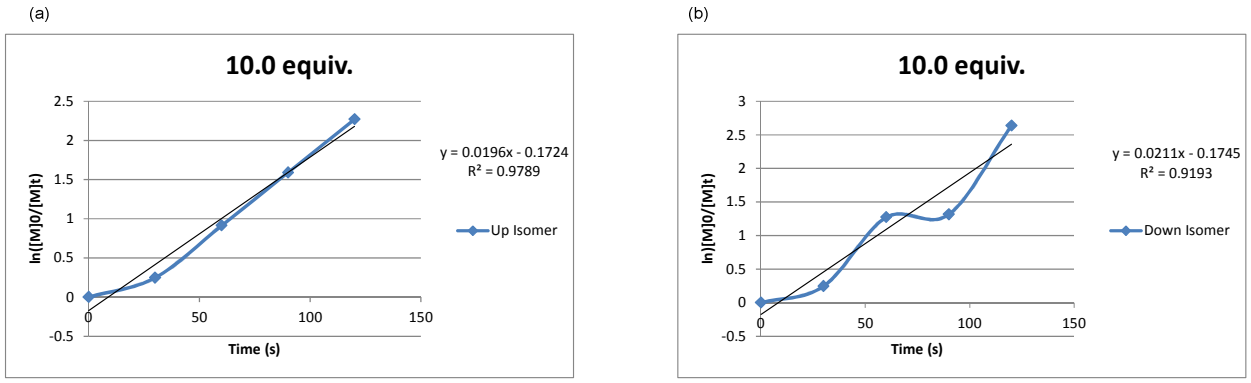

Figure S14. Initiation data for **V** using 10.0 equiv. of phenyl vinyl ether. (a) *up*-**V**. (b) *down*-**V**.

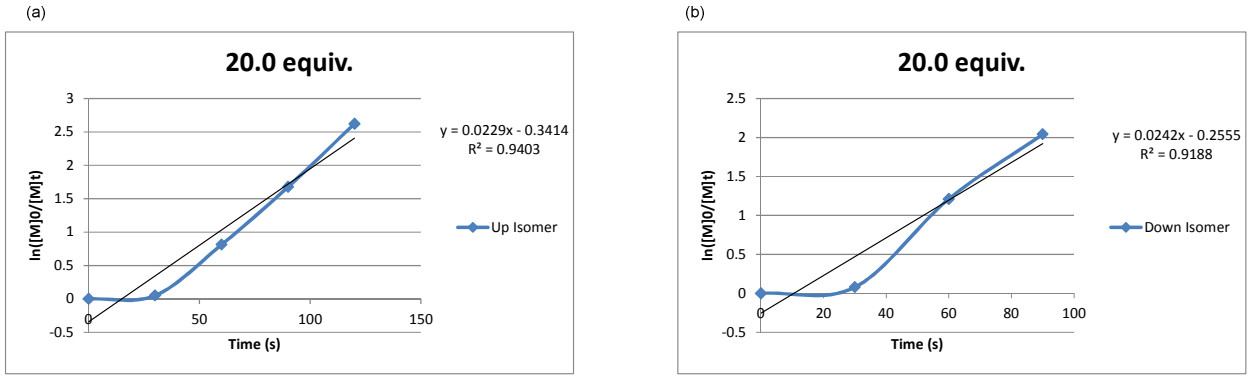

Figure S15. Initiation data for **V** using 20.0 equiv. of phenyl vinyl ether. (a) *up*-**V**. (b) *down*-**V**.

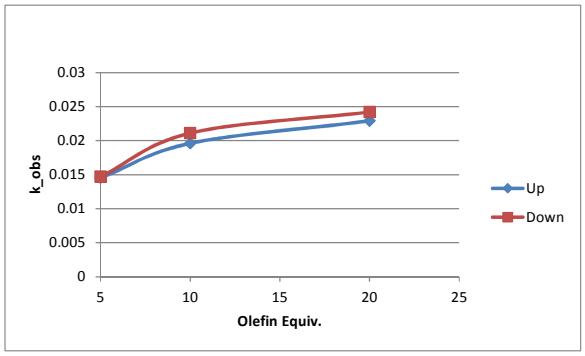

Figure S16. Initiation data for **V** comparing *up*-**V** and *down*-**V**.

Data for **VI**:

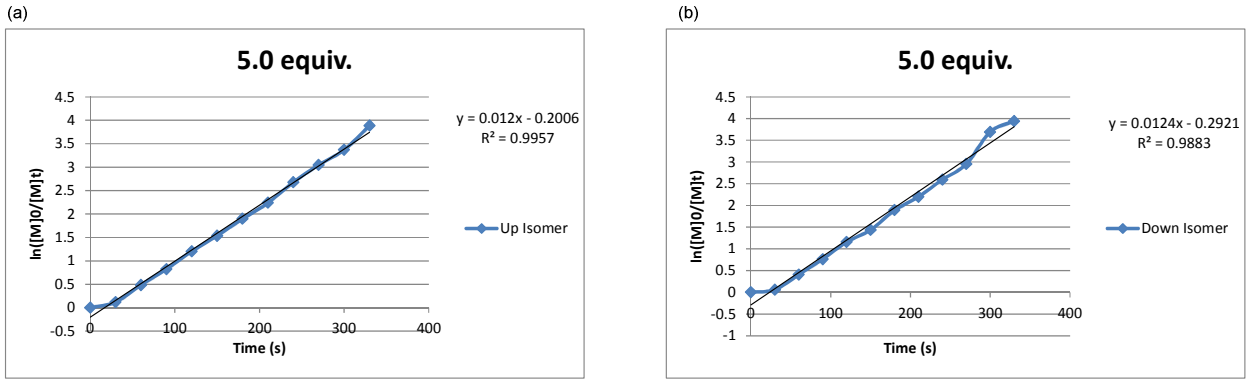

Figure S17. Initiation data for **VI** using 5.0 equiv. of phenyl vinyl ether. (a) *up*-**VI**. (b) *down*-**VI**.

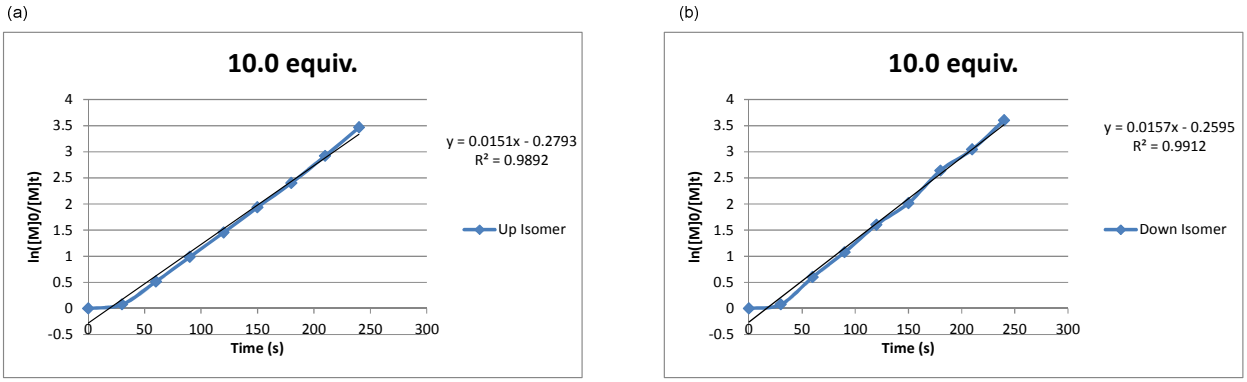

Figure S18. Initiation data for **VI** using 10.0 equiv. of phenyl vinyl ether. (a) *up*-**VI**. (b) *down*-**VI**.

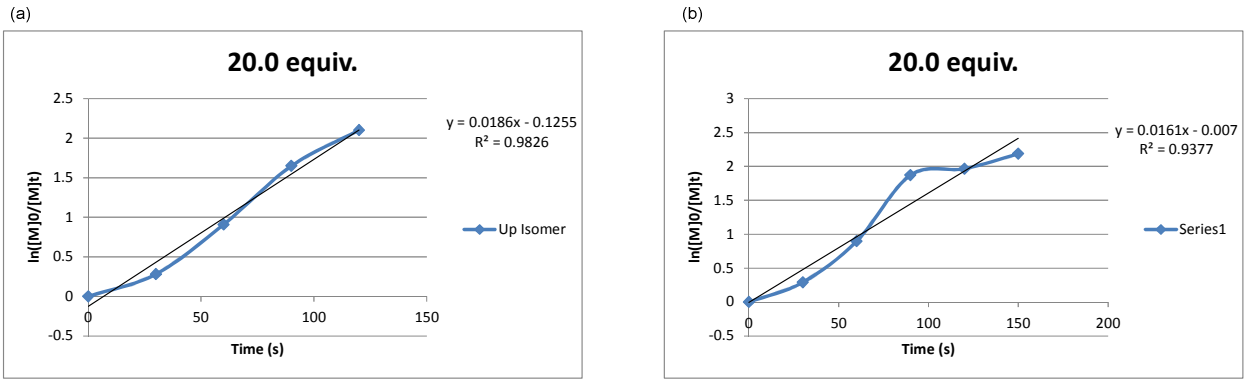

Figure S19. Initiation data for **VI** using 20.0 equiv. of phenyl vinyl ether. (a) *up*-**VI**. (b) *down*-**VI**.

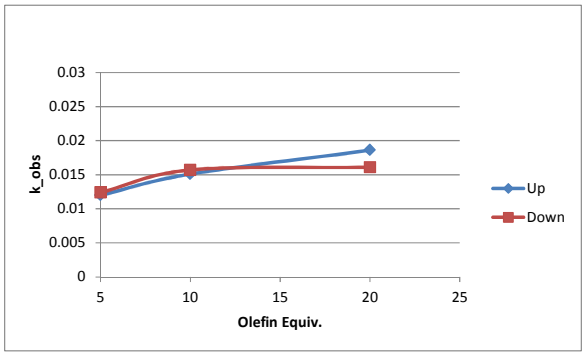

Figure S20. Initiation data for **VI** comparing *up*-**VI** and *down*-**VI**.

II–VI Comparison:

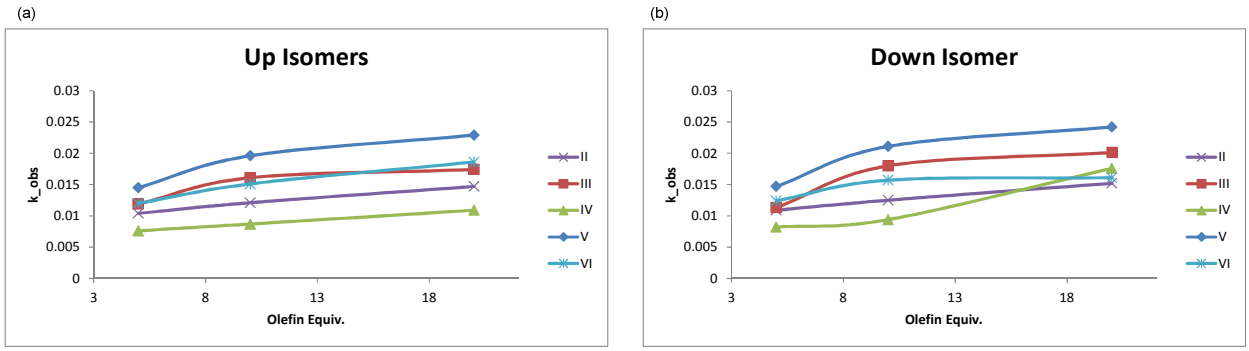

Figure S21. Initiation data comparing ruthenium dithiolates **II–VI** using phenyl vinyl ether. (a) *up*-isomers. (b) *down*-isomers.

II. GC Method

Volatile products were analyzed using an Agilent 6850 gas chromatography (GC) instrument with a flame ionization detector (FID). The following conditions and equipment were used:

Column: HP-5, 30m x 0.25mm (ID) x 0.25µm film thickness.
Manufacturer: Agilent
GC and column conditions: Injector temperature: 250 ºC, Detector temperature: 280 ºC
Oven temperature: Starting temperature: 100 ºC, hold time: 5 min
Ramp rate: Ramp 1: 10 °C/min to 170 °C, hold time: 5 min
Ramp 2: 5 °C/min to 210 °C, hold time: 10 min
Carrier gas: Helium
Average velocity: 32 cm/sec
Split ratio: 40.8:1

III. X-ray Crystal Structure of *up*-V

Slow diffusion of Et_2O from a solution of **V** into hexamethyldisiloxane provided brown, needle-like crystals which were sufficient for x-ray crystallography.

Table S1. Crystal data and structure refinement for *up*-**V**.

Identification code	*up*-**V**	
Empirical formula	C49 H56 N2 O2 Ru S2	
Formula weight	870.14	
Temperature	100 K	
Wavelength	0.71073 Å	
Crystal system	Monoclinic	
Space group	P 1 21/c 1	
Unit cell dimensions	a = 16.195(5) Å	a= 90°
	b = 15.811(3) Å	b= 110.260(12)°

	c = 18.013(4) Å	g = 90°
Volume	4327.3(19) Å^3	
Z	4	
Density (calculated)	1.336 Mg/m^3	
Absorption coefficient	0.500 mm^{-1}	
F(000)	1824	
Crystal size	0.18 x 0.17 x 0.08 mm^3	
Theta range for data collection	2.576 to 38.713°.	
Index ranges	-27<=h<=27, -26<=k<=26, -31<=l<=30	
Reflections collected	346920	
Independent reflections	23300 [R(int) = 0.0569]	
Completeness to theta = 25.000°	99.9 %	
Absorption correction	Semi-empirical from equivalents	
Max. and min. transmission	1.0000 and 0.9649	
Refinement method	Full-matrix least-squares on F^2	
Data / restraints / parameters	23300 / 0 / 515	
Goodness-of-fit on F^2	1.067	
Final R indices [I>2sigma(I)]	R1 = 0.0440, wR2 = 0.0959	
R indices (all data)	R1 = 0.0697, wR2 = 0.1049	
Extinction coefficient	n/a	
Largest diff. peak and hole	2.871 and -0.809 e.Å^{-3}	

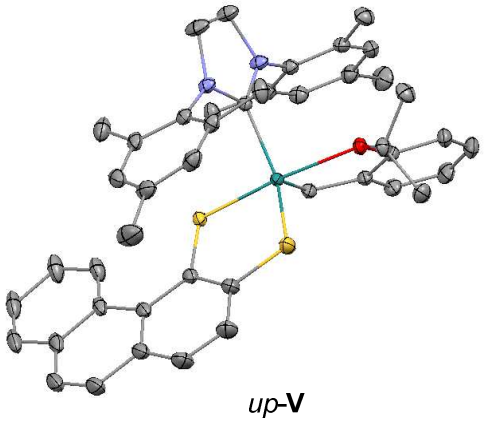

up-**V**

Figure S22. X-ray crystal structure of *up*-**V**.

IV. NOE Spectrum of V

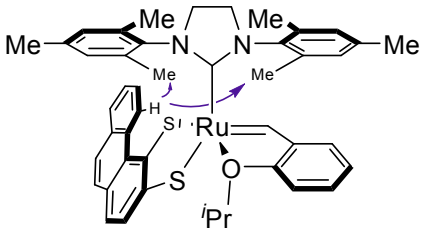

Proton at the 5-position of the phenanthrene dithiolate is at 11.72 ppm for the up isomer and 10.83 for the down isomer.

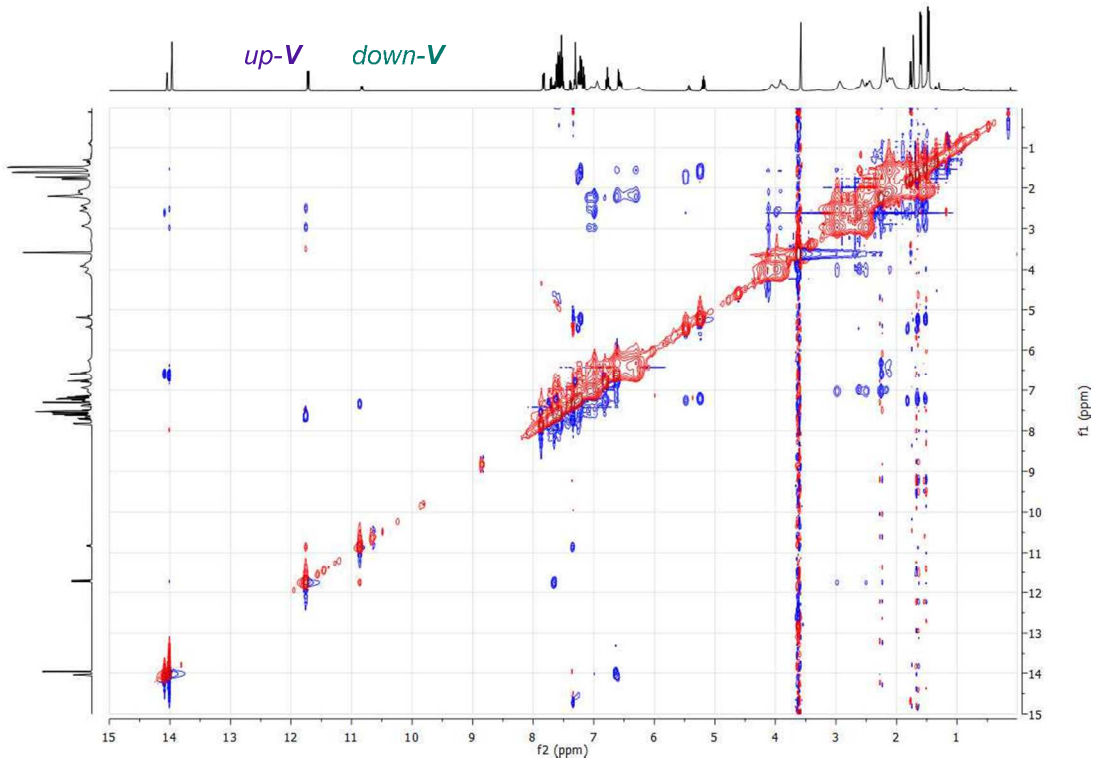

Figure S23. NOE spectrum of **V**.

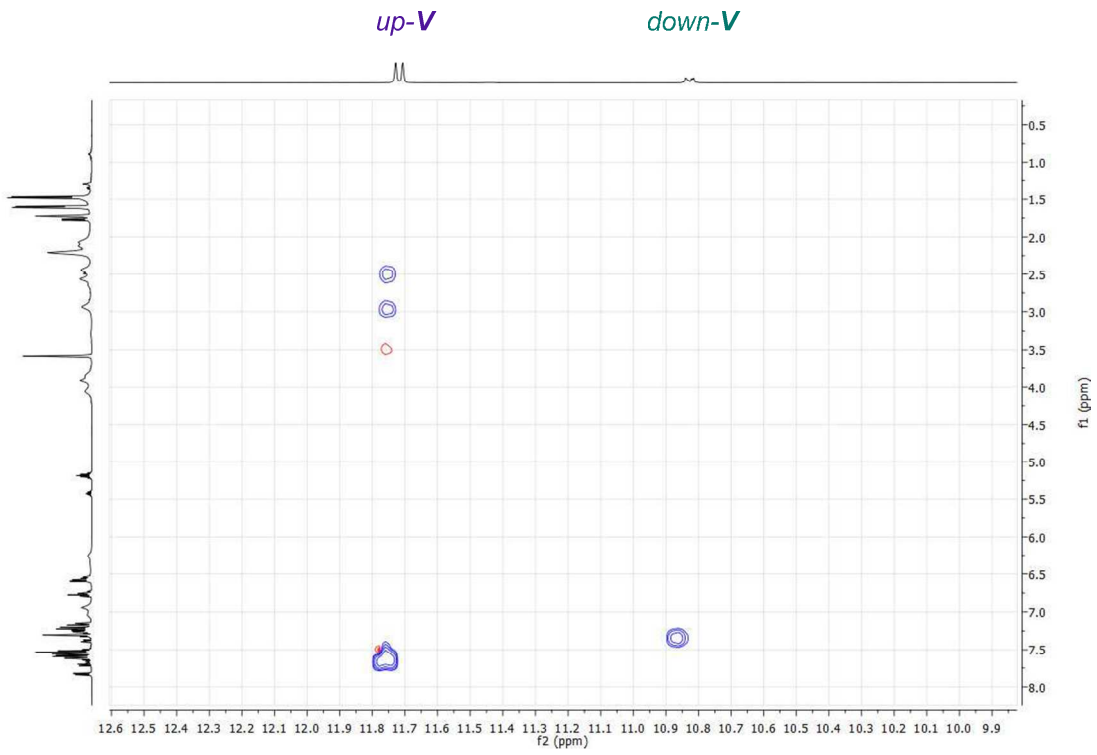

Figure S24. Expanded portion of NOE of **V** indicating some interaction between the proton at the 5-position of the phenanthrene system and the aryl methyl groups in *up*-**V.**

V. ^{1}H NMR of III at 100 °C for 15 h.

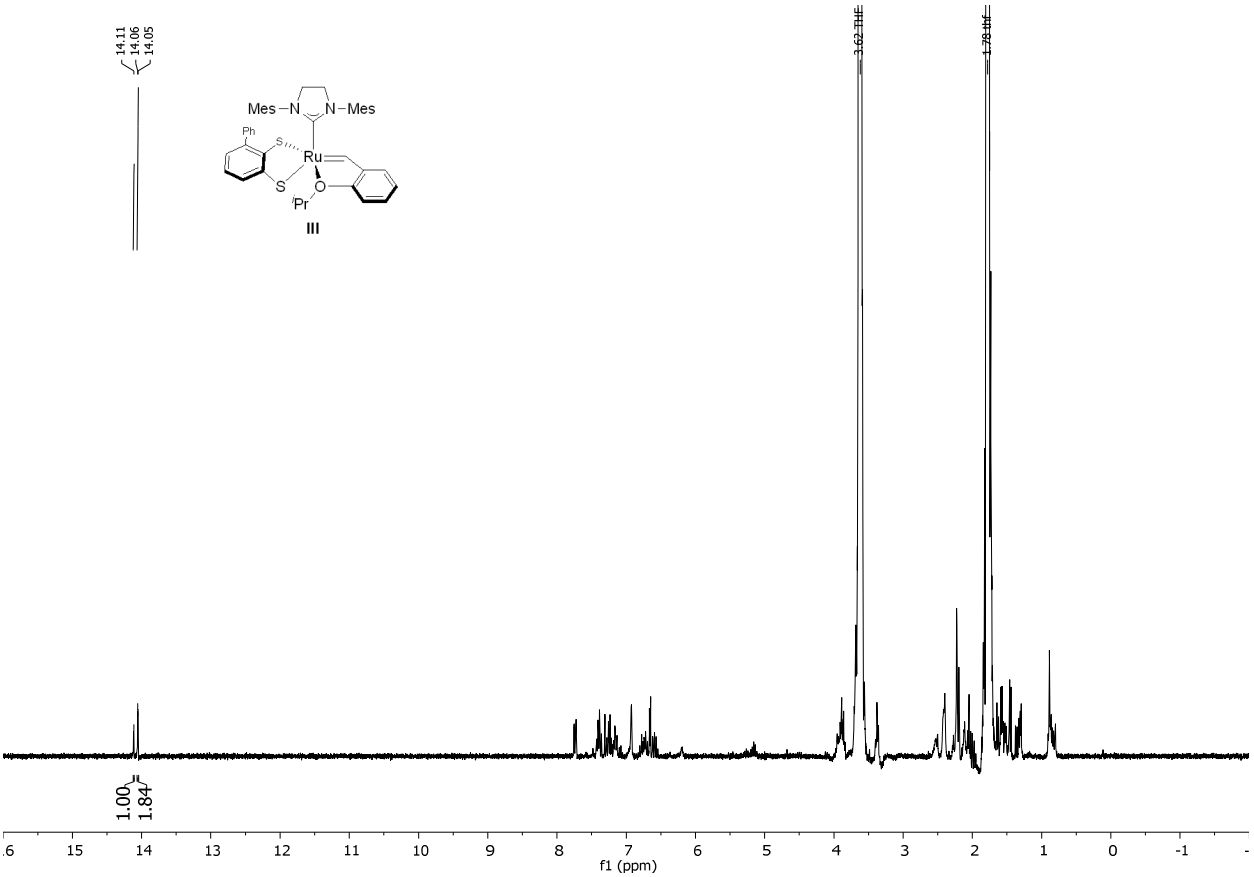

Figure S25. ^{1}H NMR spectrum (300 MHz, THF-d_8) of **III** after stirring overnight at 100 °C.

VI. Computational Details

All calculations were performed using Gaussian 09.[1] Geometry optimizations and frequency calculations were performed at the B3LYP[2–4] level using LANL2DZ for ruthenium and 6-31G(d) for all other atoms. Zero point vibrational energies, thermal corrections, and entropies were computed from frequency calculations with a standard state of 298 K and 1 atm. Quasiharmonic oscillator approximations were used to compute the entropic contributions to the Gibbs free energies, as discussed by Truhlar.[5,6] Single point energy calculations were performed at the M06[7,8] level using SDD for ruthenium and 6-311+G(d,p) for other atoms with the SMD[9] continuum solvent model for THF.

VII. References

(1) Gaussian 09 Citation | Gaussian.com http://gaussian.com/g09citation/ (accessed Jul 18, 2017).
(2) Becke, A. D. *Phys. Rev. A* **1988**, *38* (6), 3098.
(3) Becke, A. D. *J. Chem. Phys.* **1993**, *98* (7), 5648.
(4) Lee, C.; Yang, W.; Parr, R. G. *Phys. Rev. B* **1988**, *37* (2), 785.
(5) Zhao, Y.; Truhlar, D. G. *Phys. Chem. Chem. Phys.* **2008**, *10* (19), 2813.
(6) Ribeiro, R. F.; Marenich, A. V.; Cramer, C. J.; Truhlar, D. G. *J. Phys. Chem. B* **2011**, *115* (49), 14556.
(7) Zhao, Y.; Truhlar, D. G. *Theor. Chem. Acc.* **2008**, *120* (1–3), 215.
(8) Zhao, Y.; Truhlar, D. G. *Acc. Chem. Res.* **2008**, *41* (2), 157.
(9) Marenich, A. V.; Cramer, C. J.; Truhlar, D. G. *J. Phys. Chem. B* **2009**, *113* (18), 6378.

VIII. Spectra

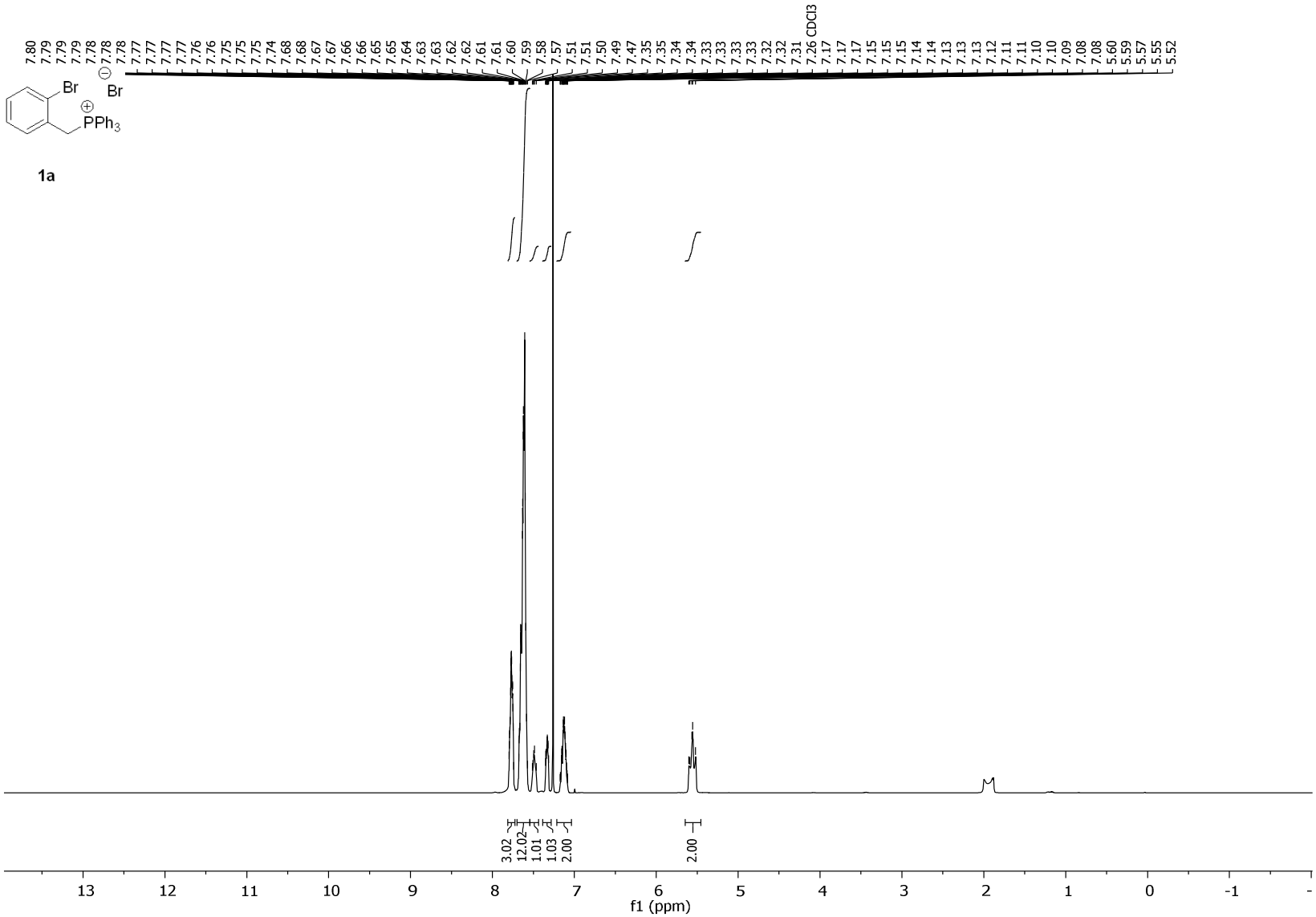

Figure S26. ^{1}H NMR spectrum (400 MHz, $CDCl_3$) of **1a**.

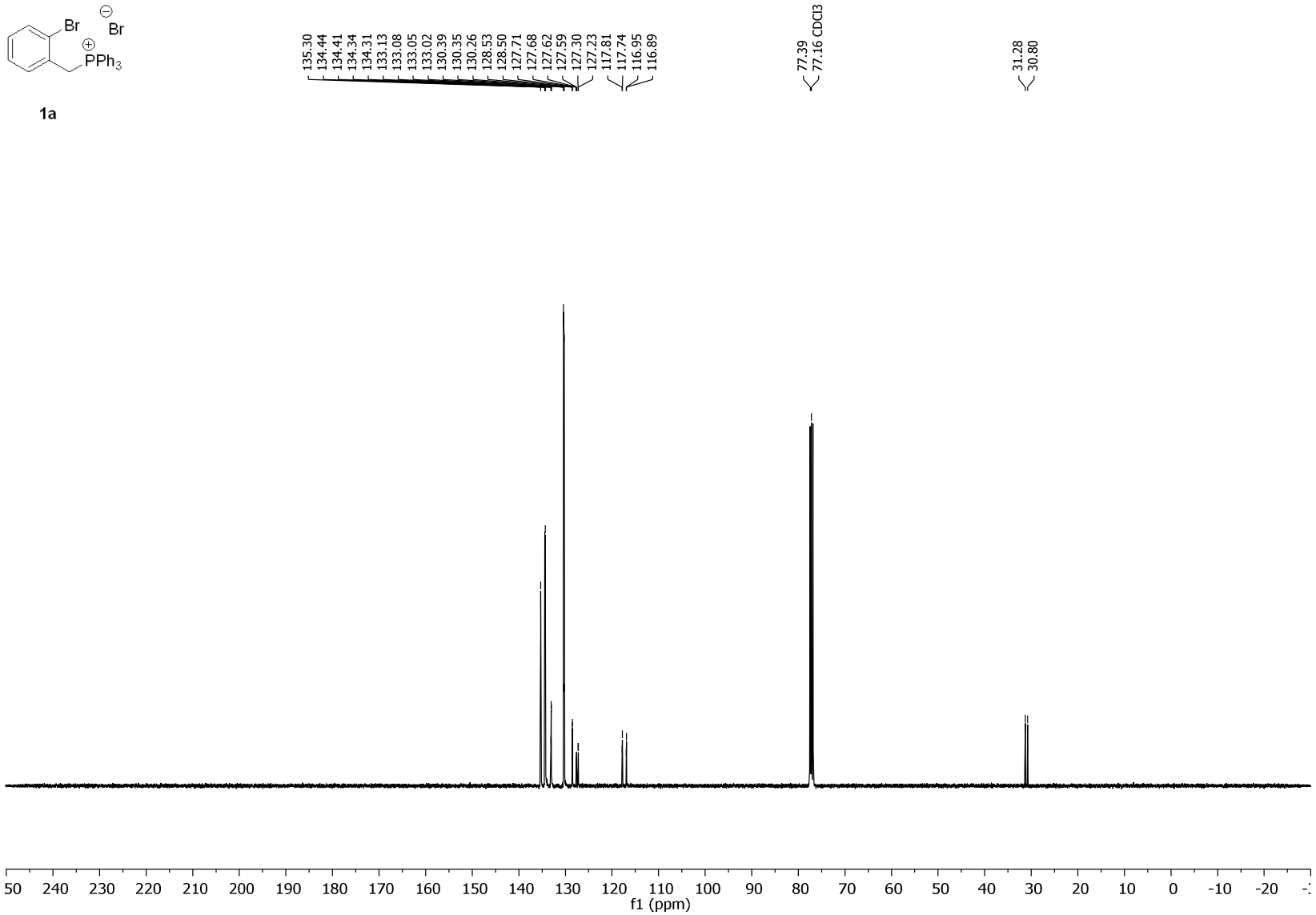

Figure S27. $^{13}C\{^{1}H\}$ NMR spectrum (101 MHz, $CDCl_3$) of **1a**.

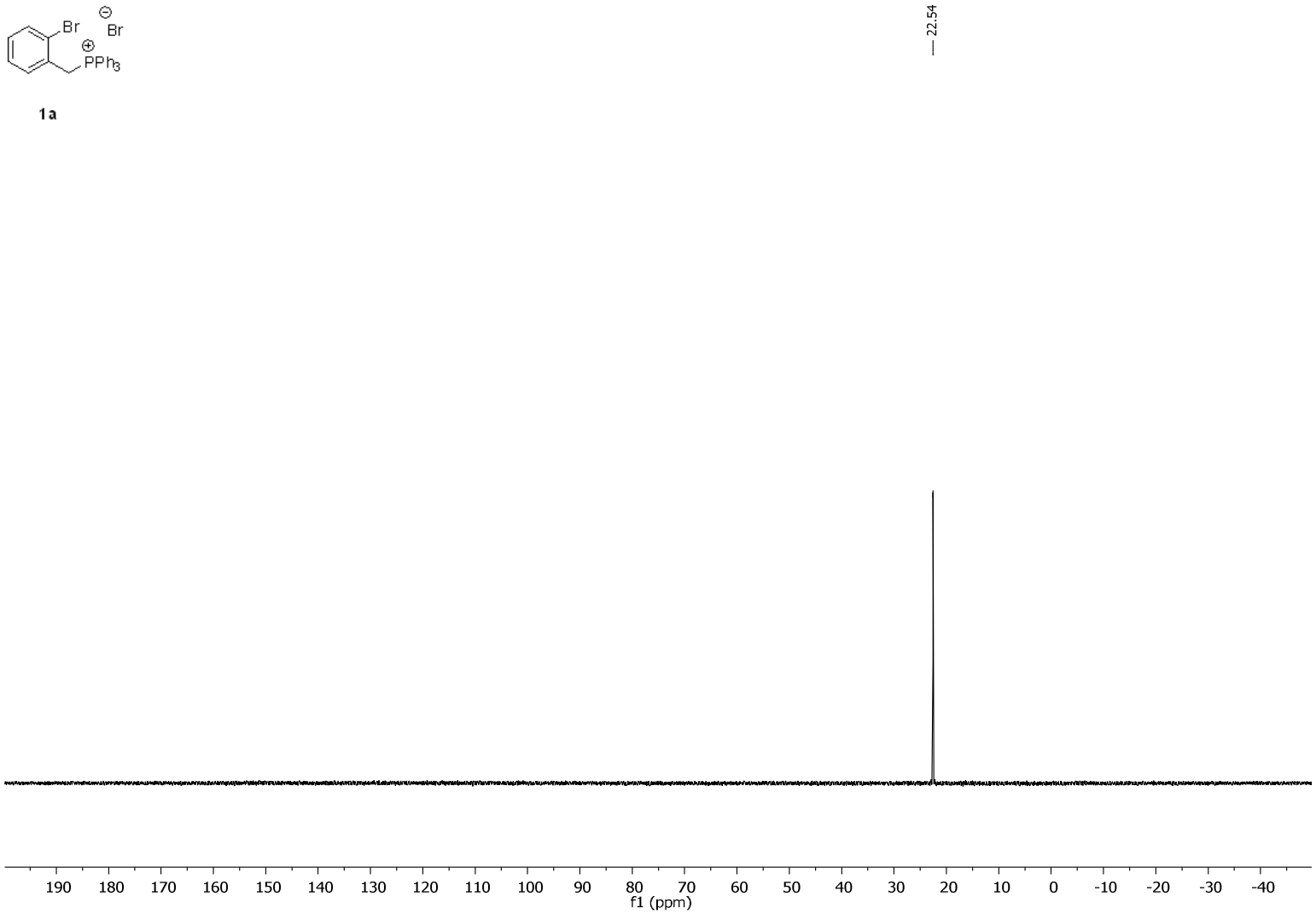

Figure S28. $^{13}P\{^{1}H\}$ NMR spectrum (121 MHz, $CDCl_3$) of **1a**.

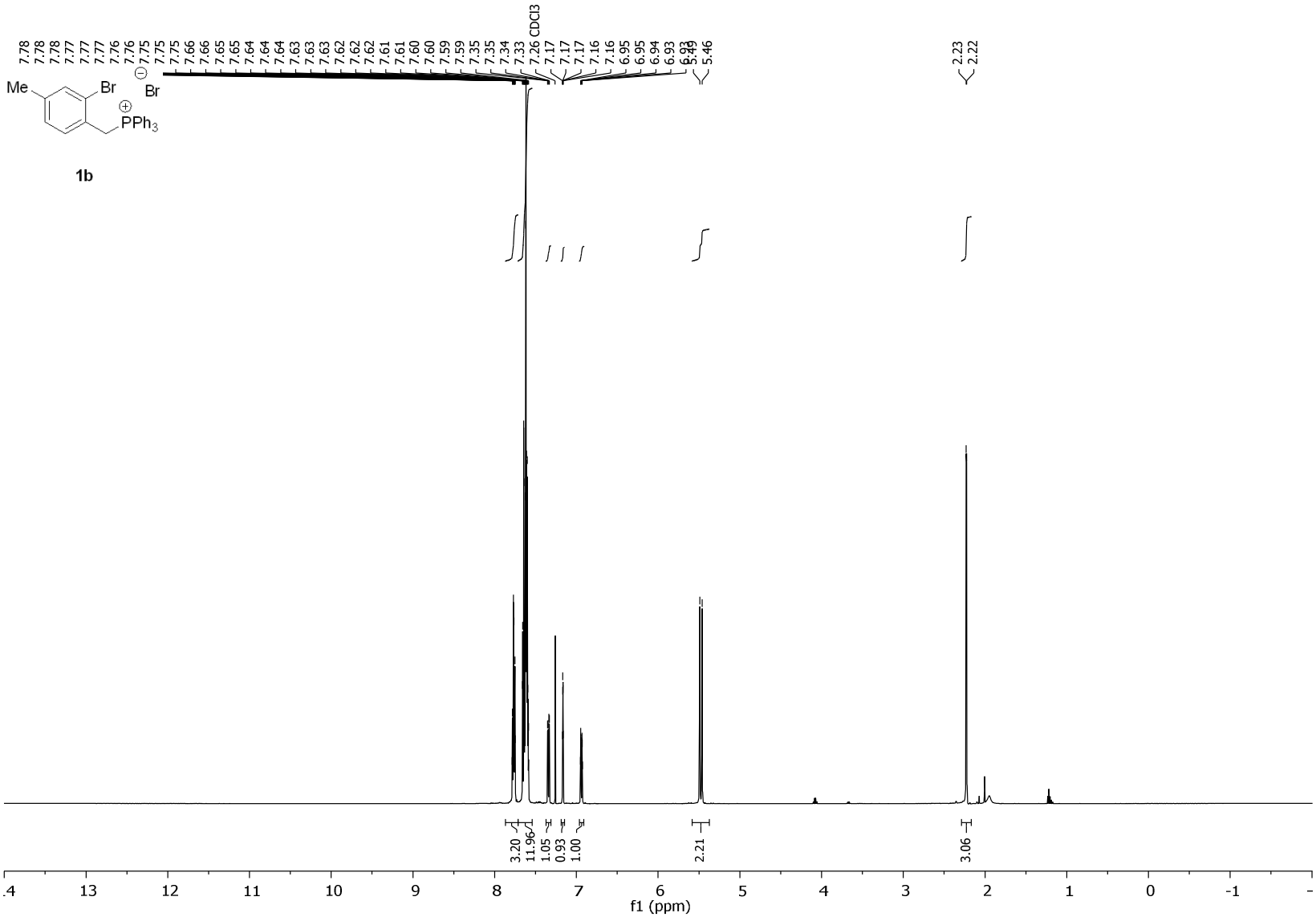

Figure S29. ^{1}H NMR spectrum (500 MHz, $CDCl_3$) of **1b**.

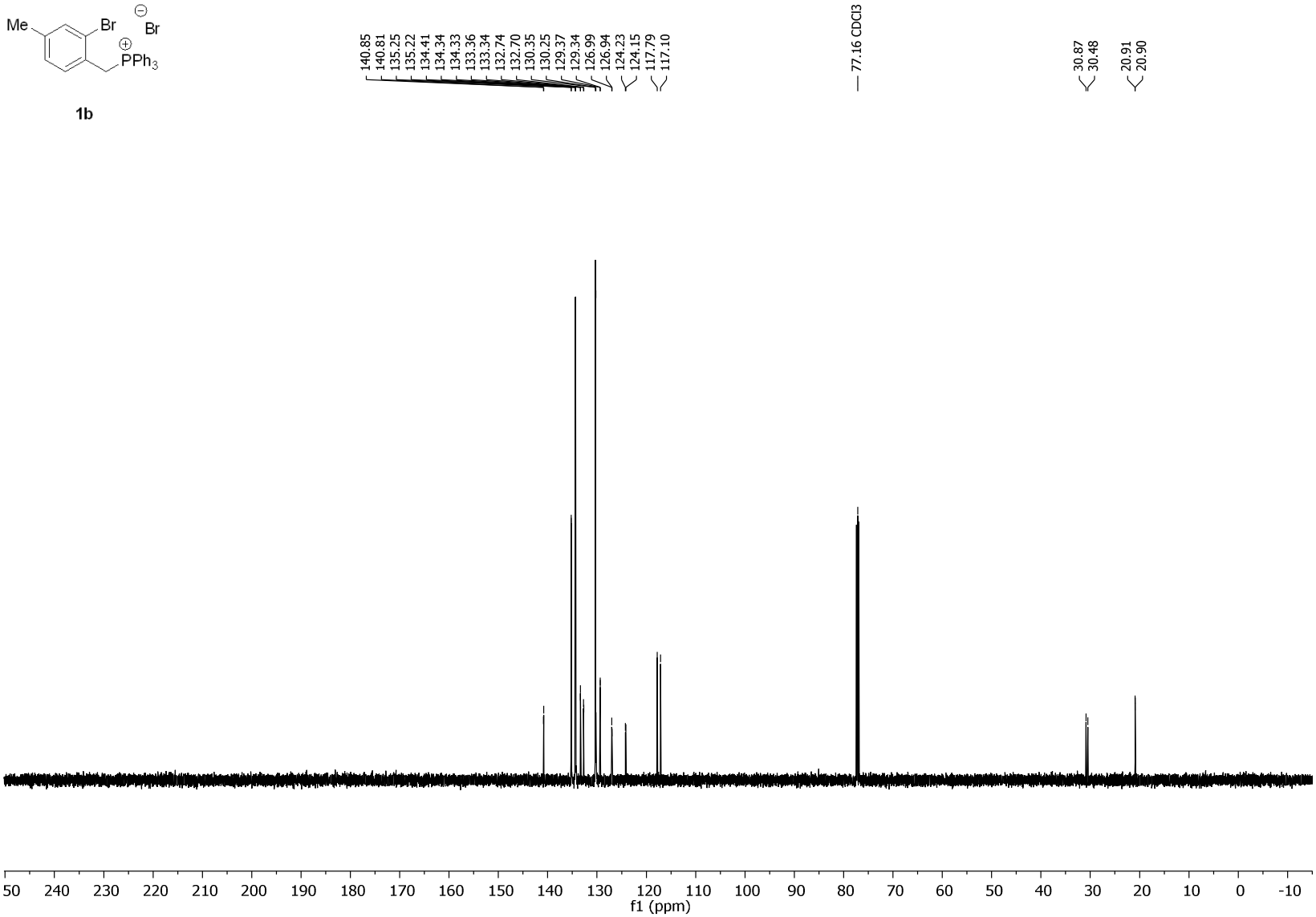

Figure S30. $^{13}C\{^{1}H\}$ NMR spectrum (126 MHz, $CDCl_3$) of **1b**.

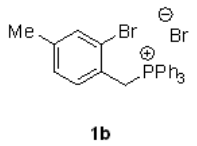

1b

Figure S31. $^{13}P\{^{1}H\}$ NMR spectrum (121 MHz, $CDCl_3$) of **1b**.

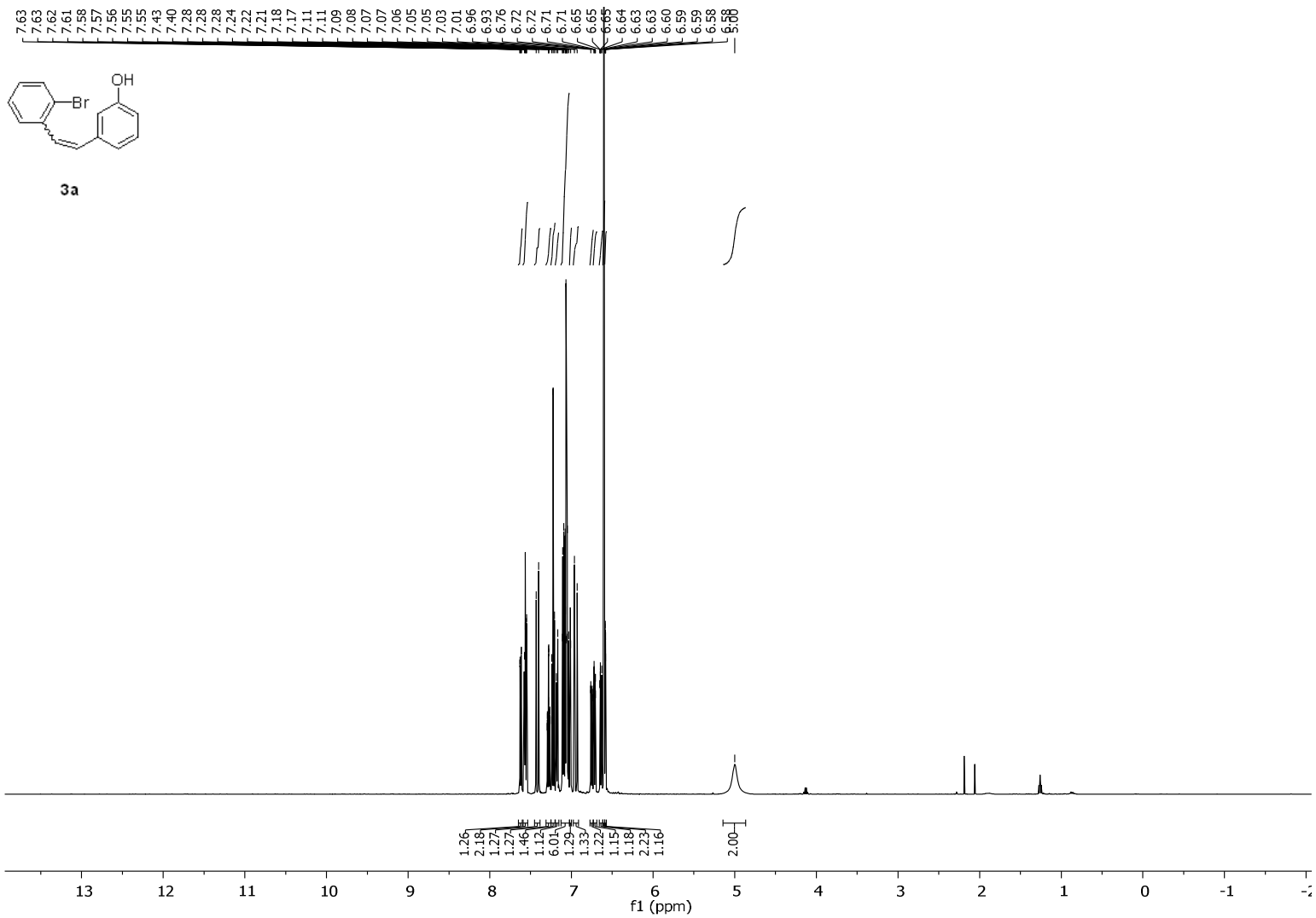

Figure S32. ^{1}H NMR spectrum (500 MHz, $CDCl_3$) of **3a**.

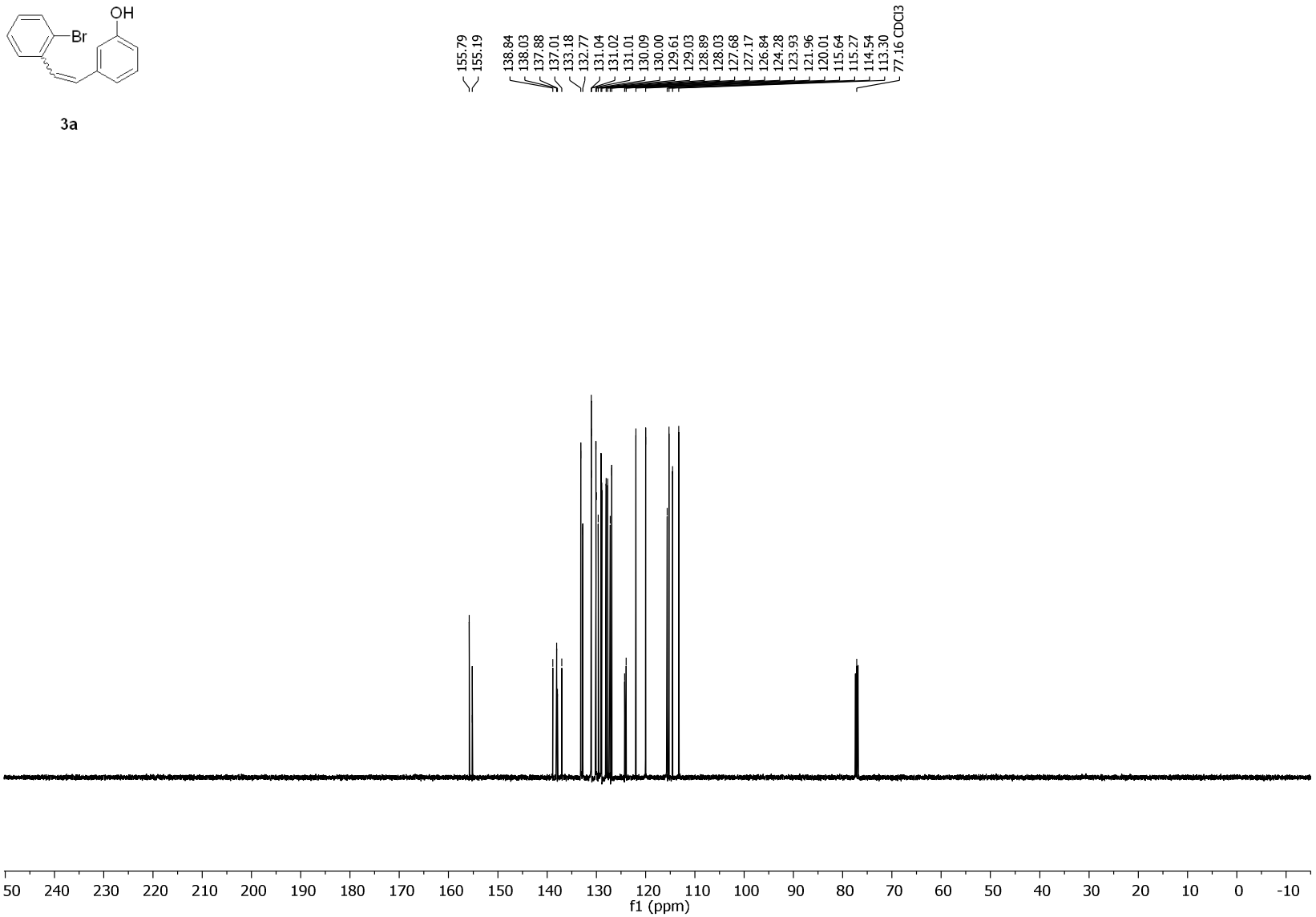

Figure S33. $^{13}C\{^{1}H\}$ NMR spectrum (126 MHz, $CDCl_3$) of **3a**.

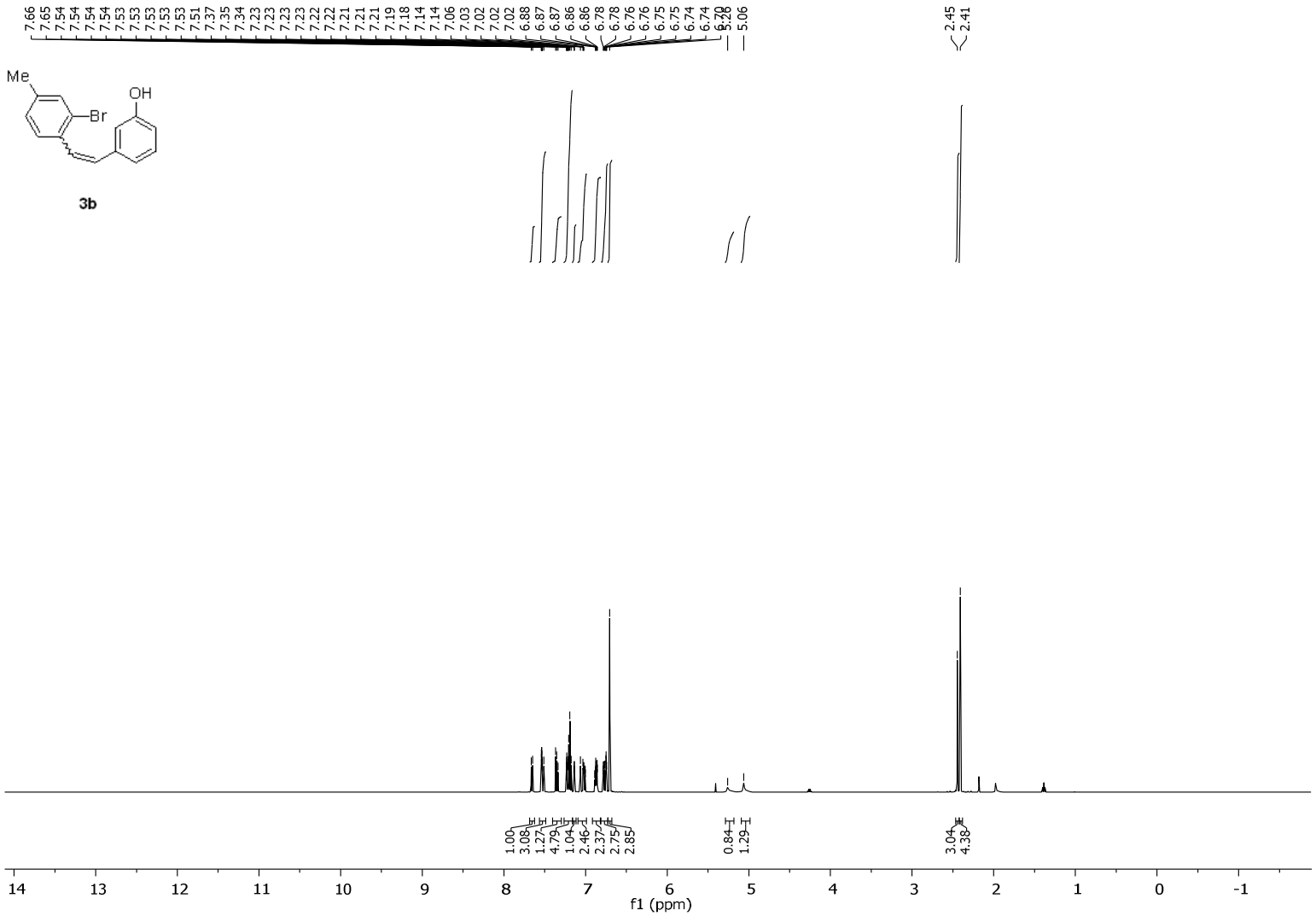

Figure S34. ^{1}H NMR spectrum (500 MHz, $CDCl_3$) of **3b**.

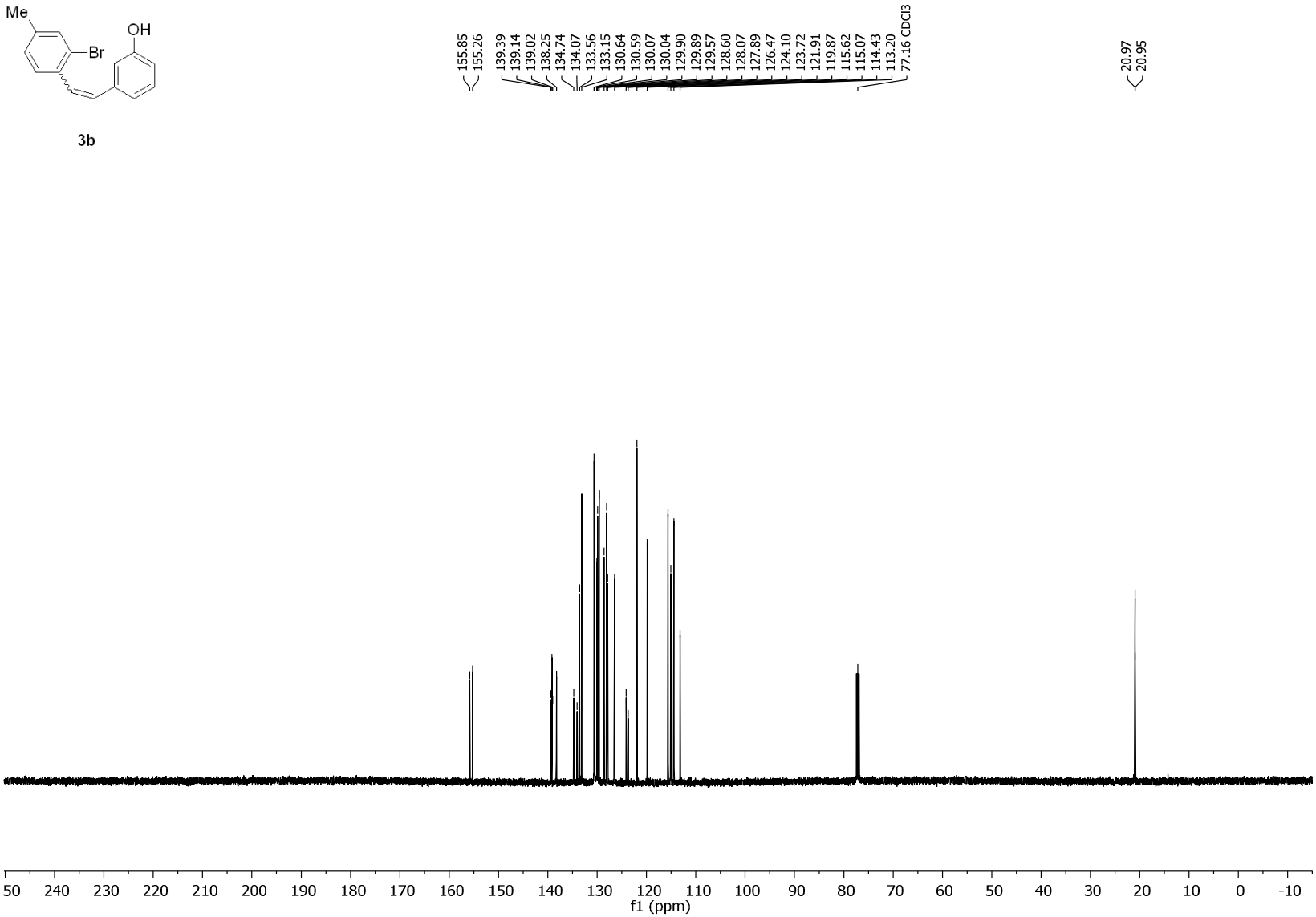

Figure S35. $^{13}C\{^{1}H\}$ NMR spectrum (126 MHz, $CDCl_3$) of **3b**.

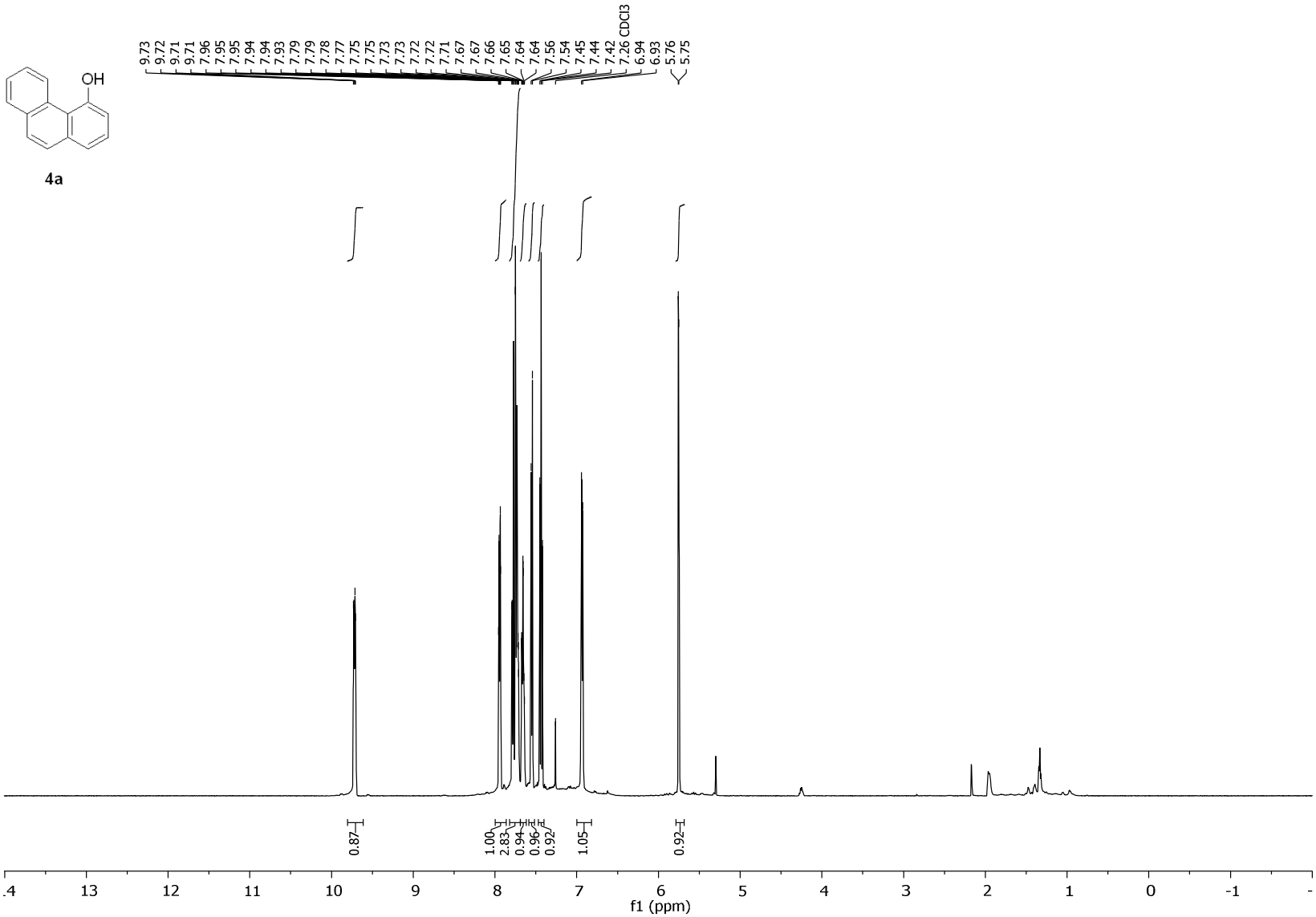

Figure S36. ^{1}H NMR spectrum (500 MHz, $CDCl_3$) of **4a**.

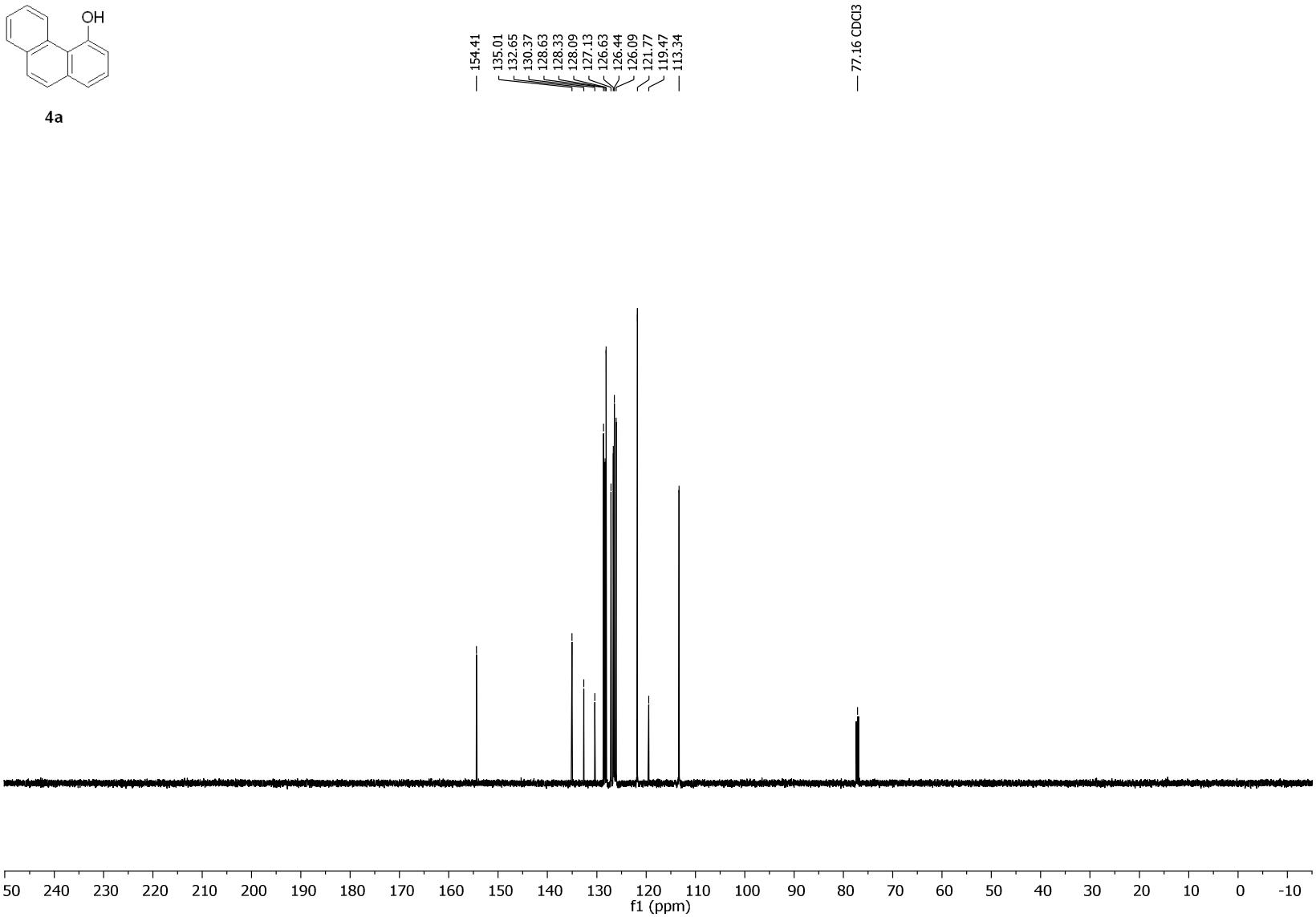

Figure S37. $^{13}C\{^{1}H\}$ NMR spectrum (126 MHz, $CDCl_3$) of **4a**.

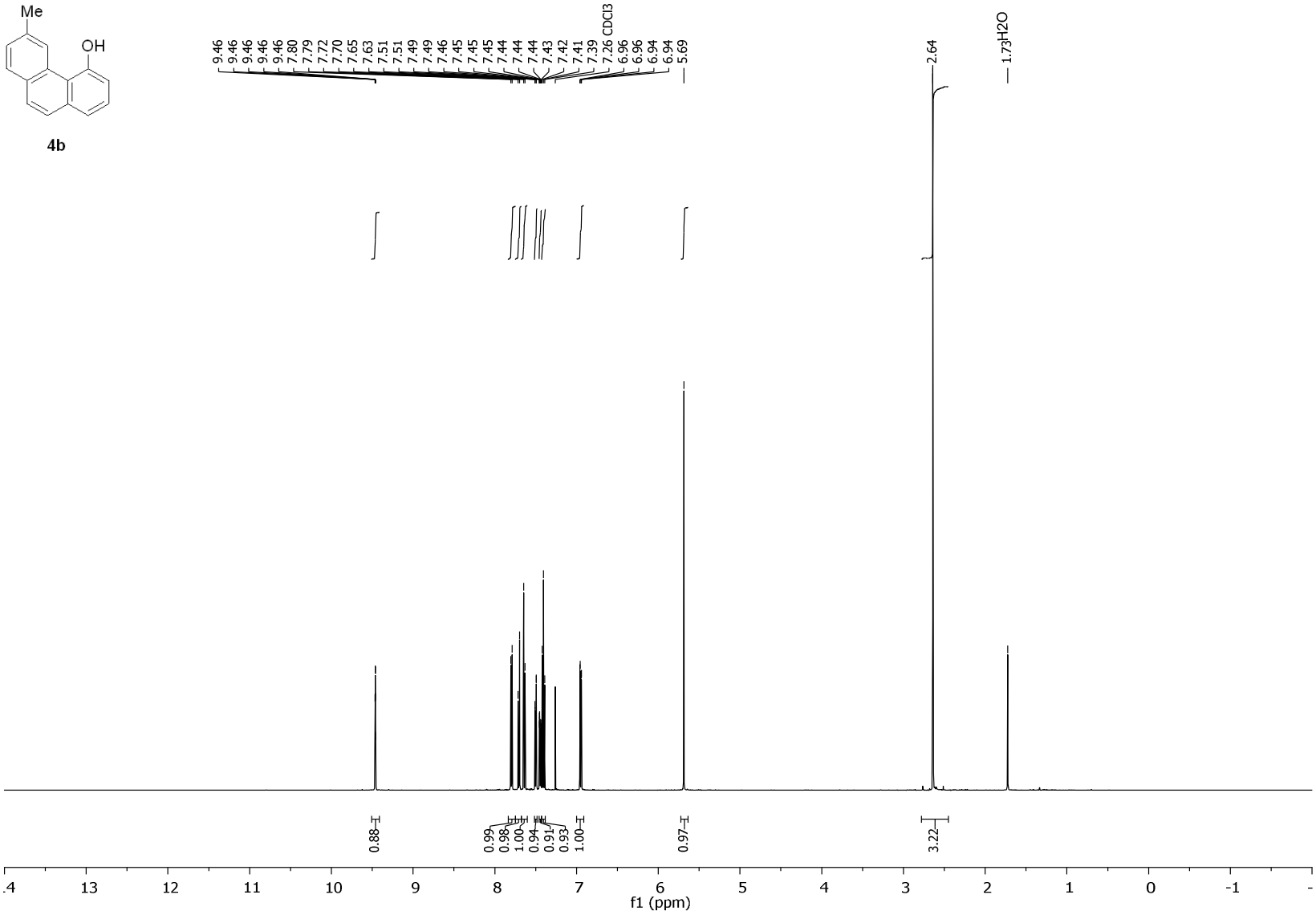

Figure S38. ^{1}H NMR spectrum (500 MHz, $CDCl_3$) of **4b**.

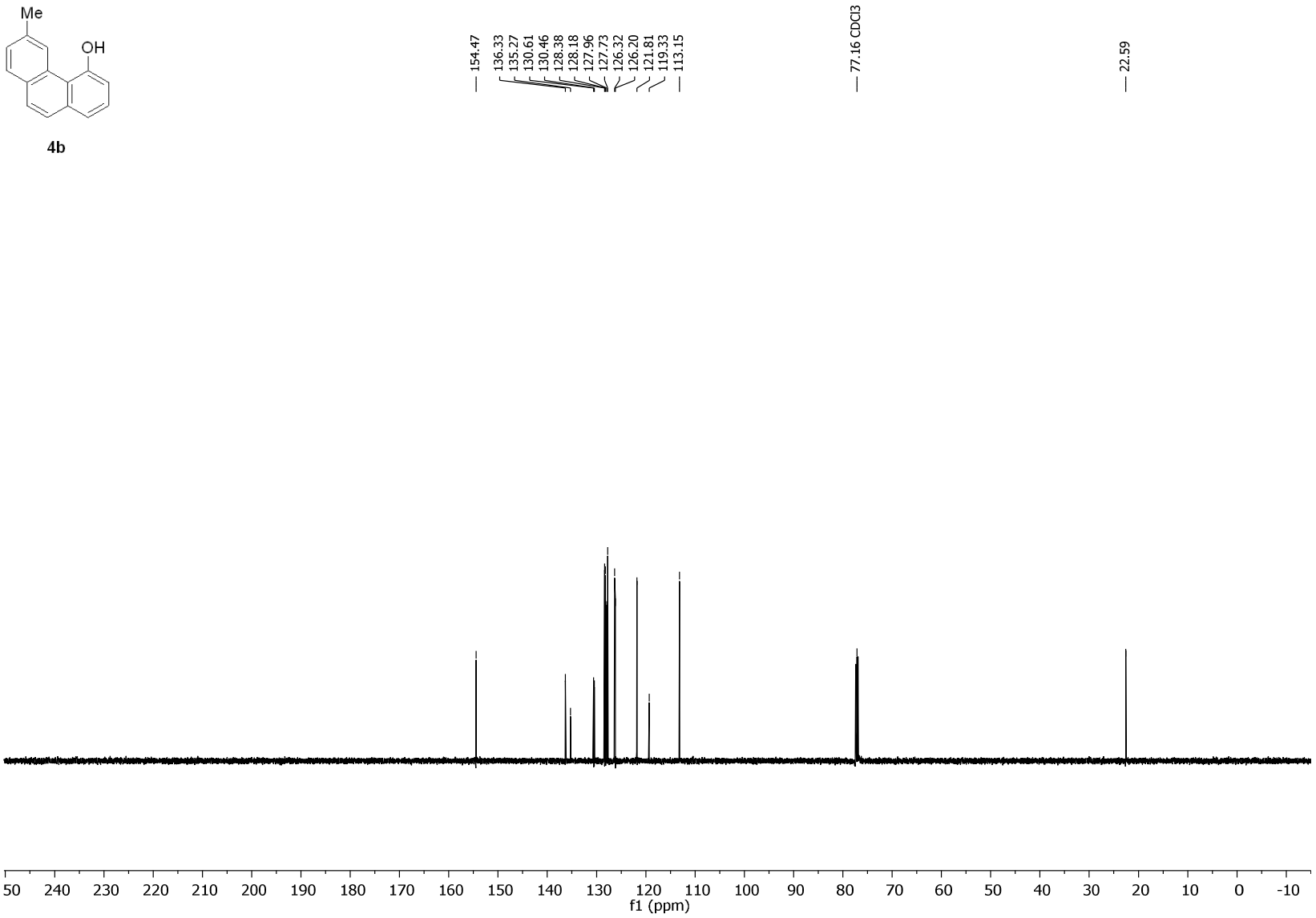

Figure S39. $^{13}C\{^{1}H\}$ NMR spectrum (126 MHz, $CDCl_3$) of **4b**.

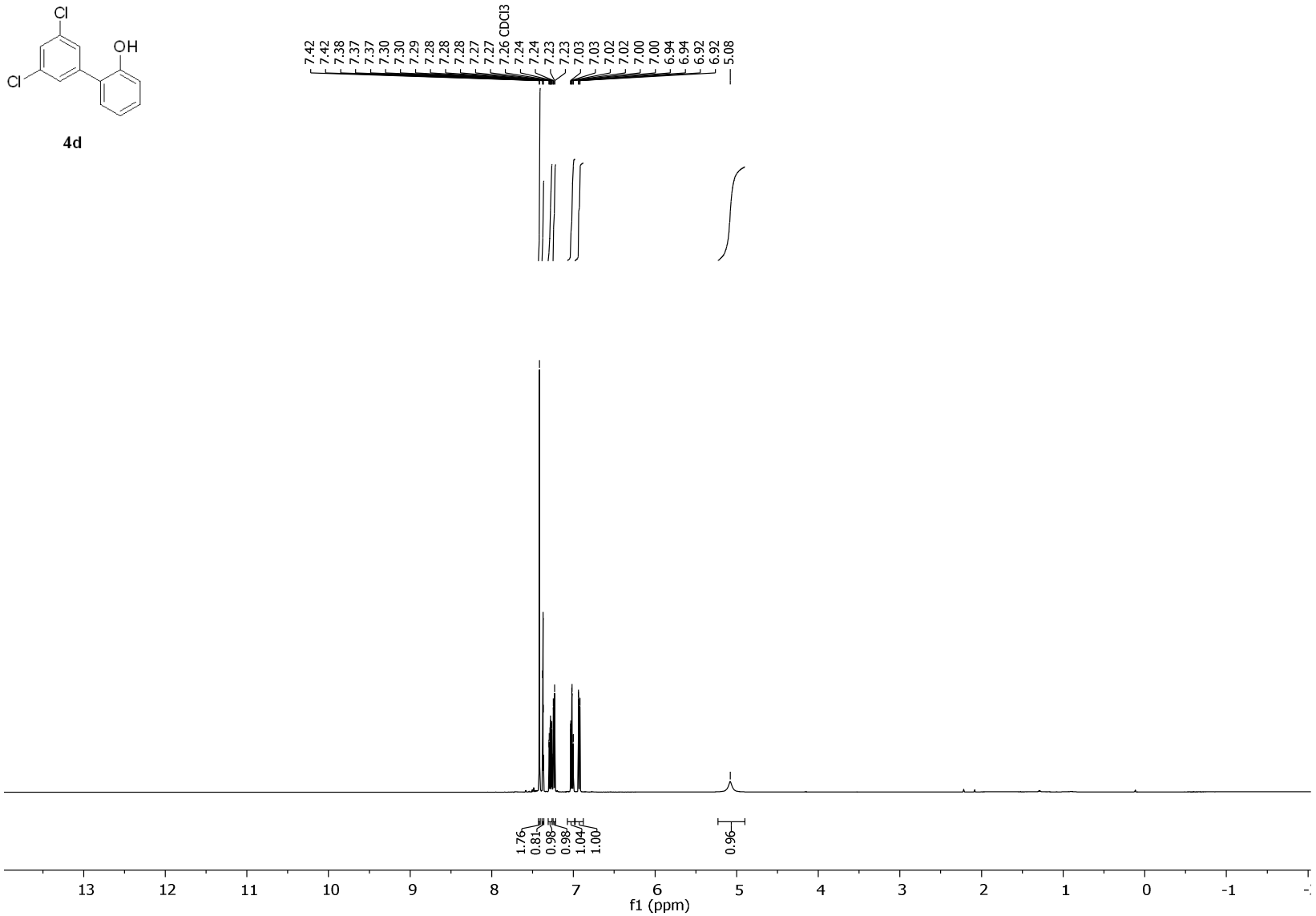

Figure S40. ^{1}H NMR spectrum (500 MHz, $CDCl_3$) of **4d**.

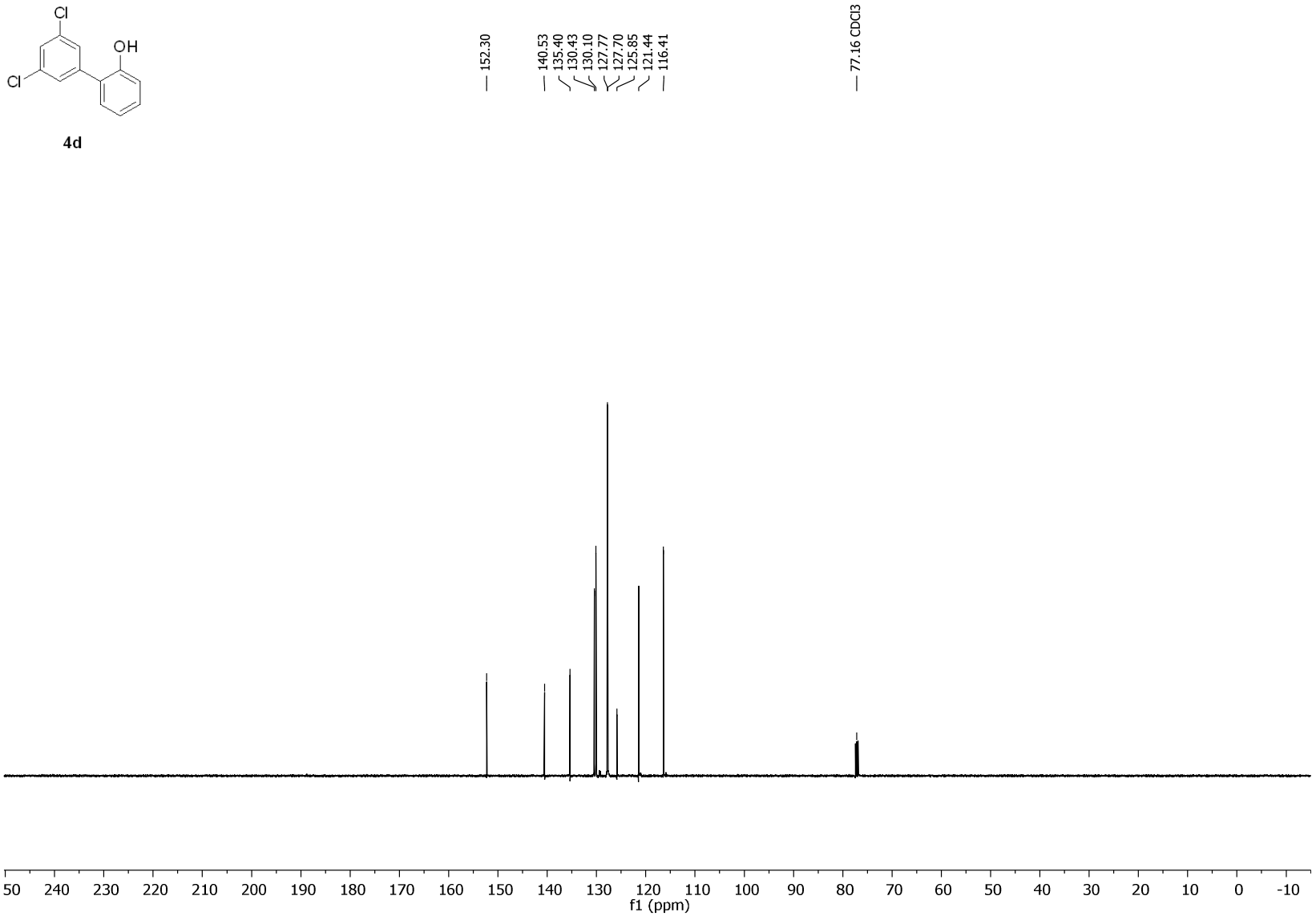

Figure S41. $^{13}C\{^{1}H\}$ NMR spectrum (126 MHz, $CDCl_3$) of **4d**.

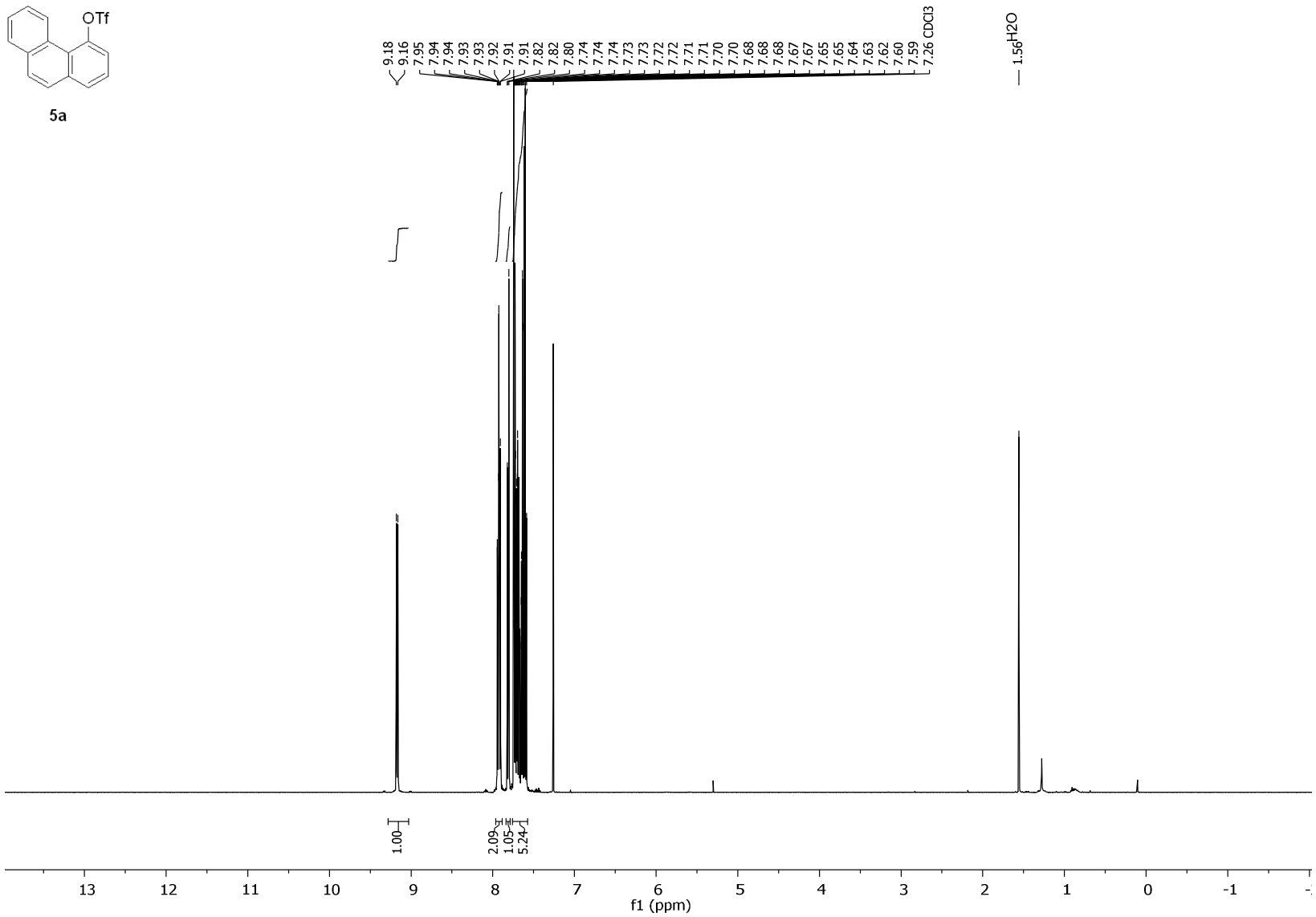

Figure S42. ^{1}H NMR spectrum (500 MHz, $CDCl_3$) of **5a**.

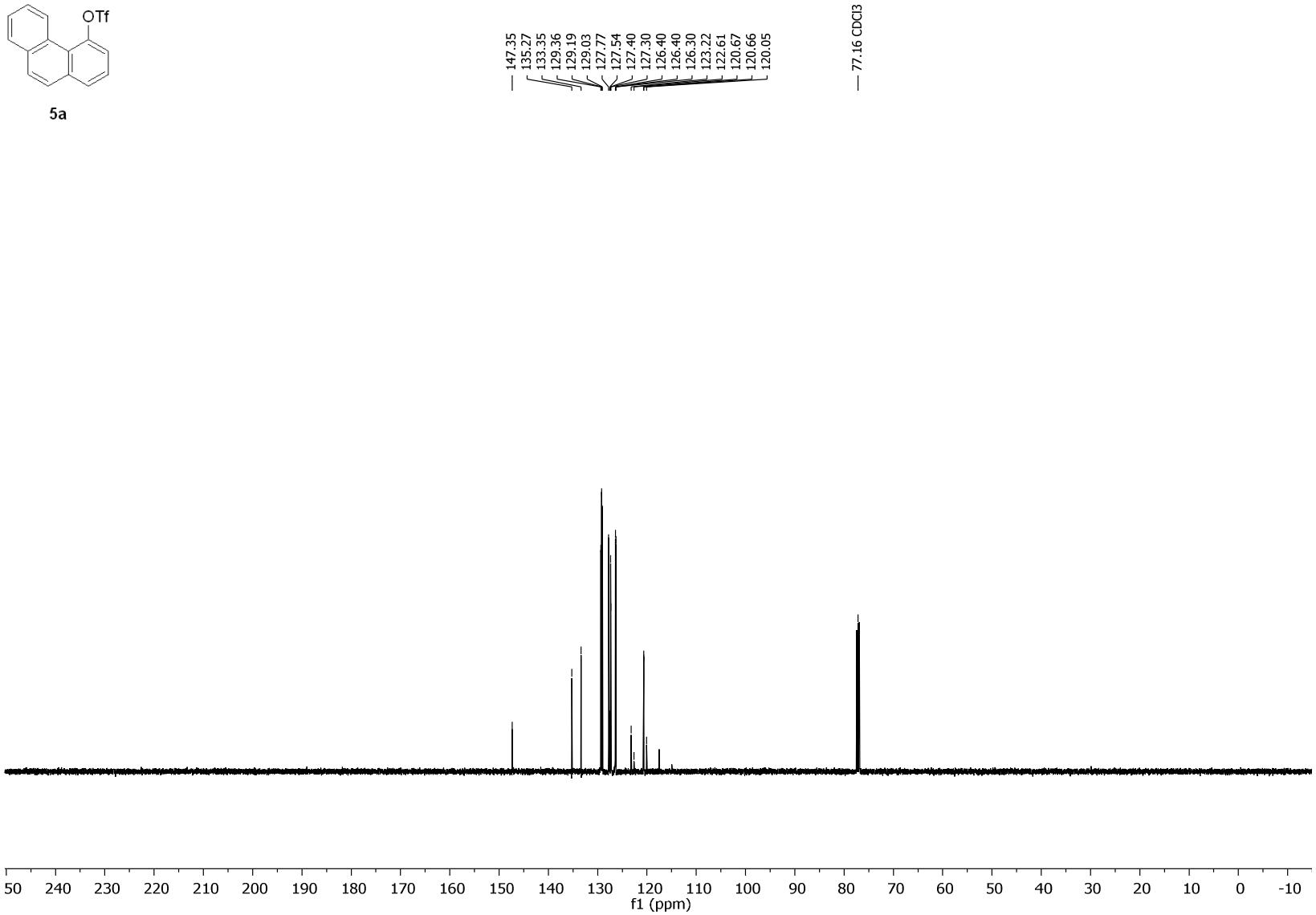

Figure S43. $^{13}C\{^{1}H\}$ NMR spectrum (126 MHz, $CDCl_3$) of **5a**.

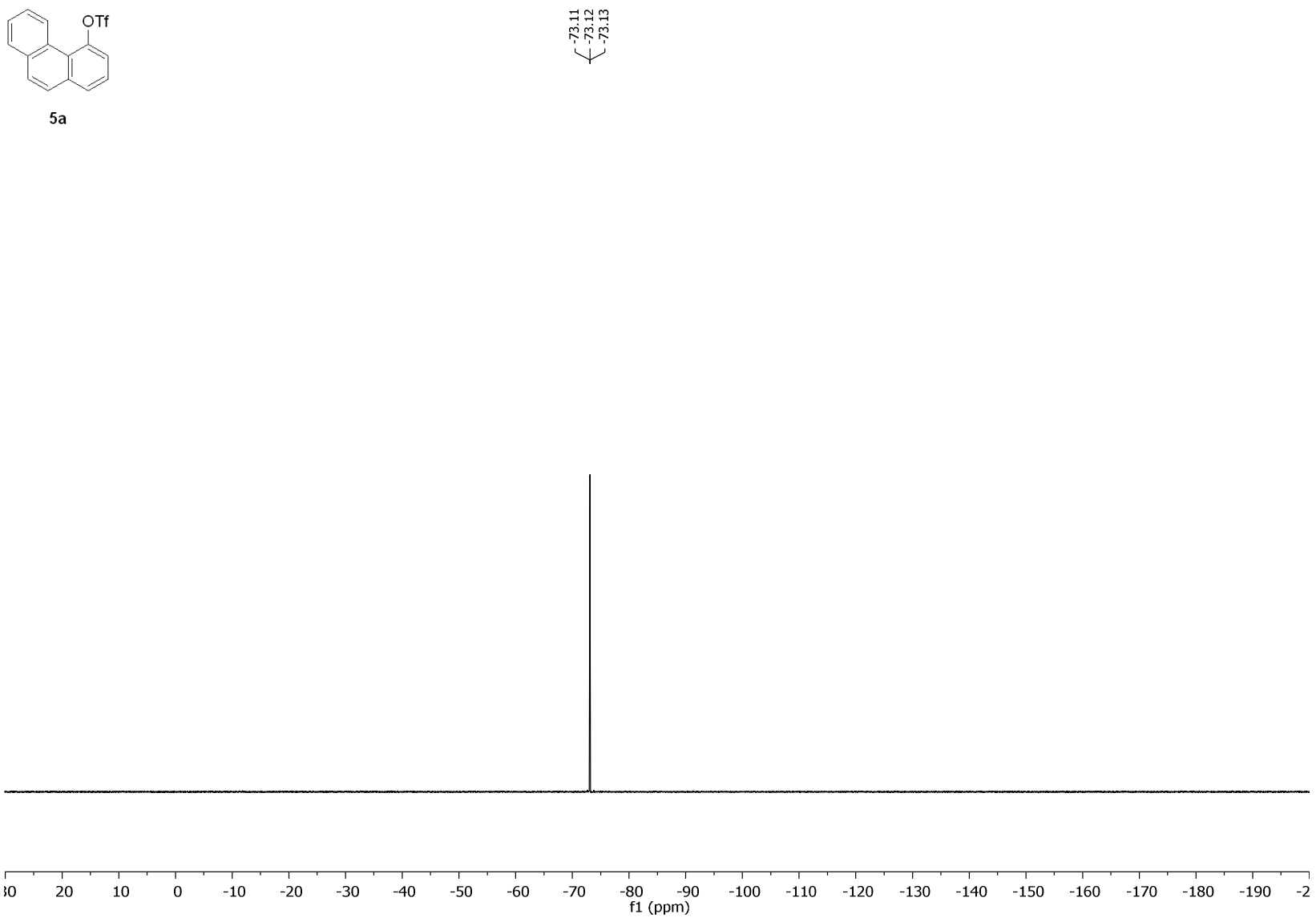

Figure S44. ^{19}F NMR spectrum (282 MHz, $CDCl_3$) of **5a**.

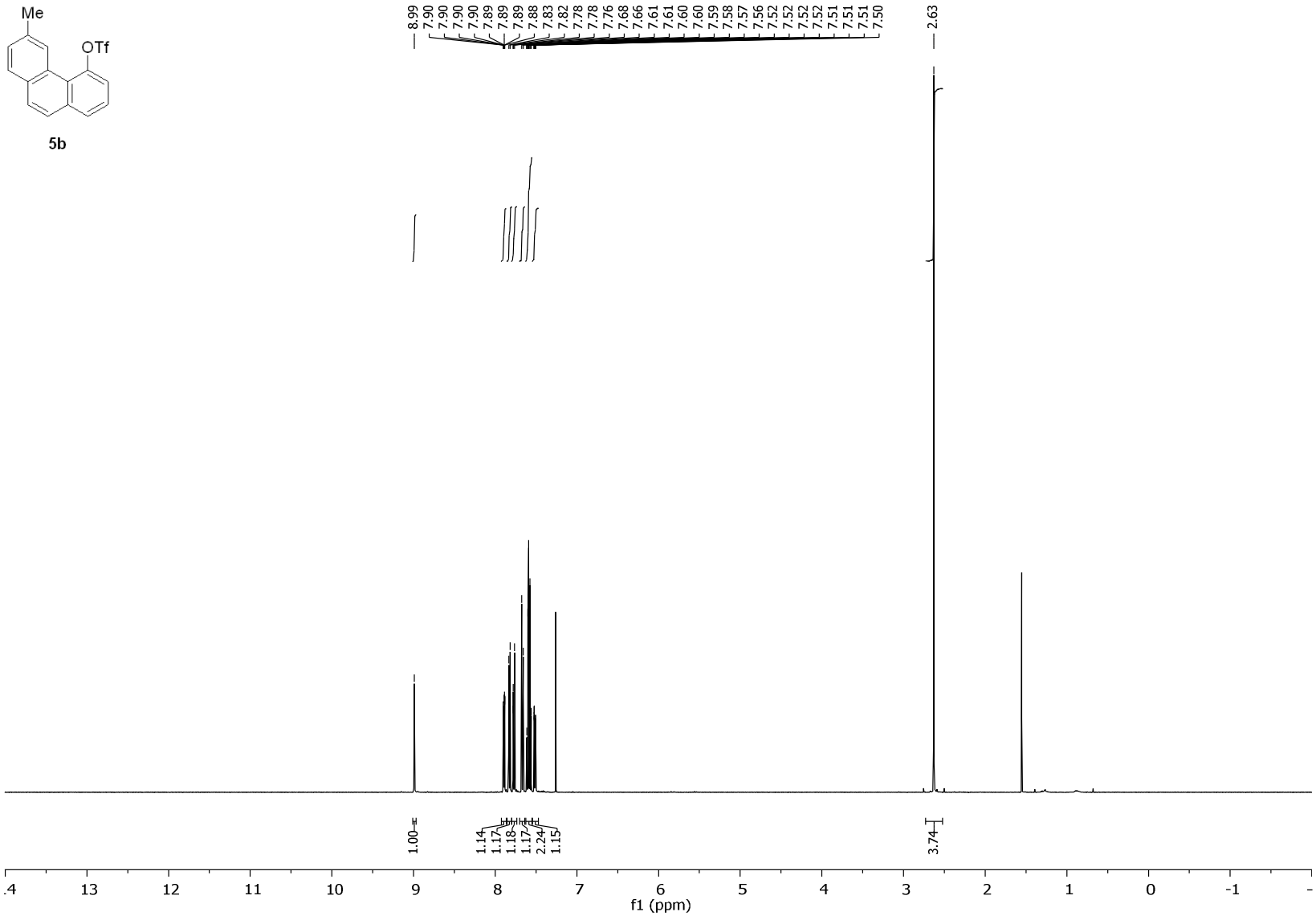

Figure S45. ^{1}H NMR spectrum (500 MHz, $CDCl_3$) of **5b**.

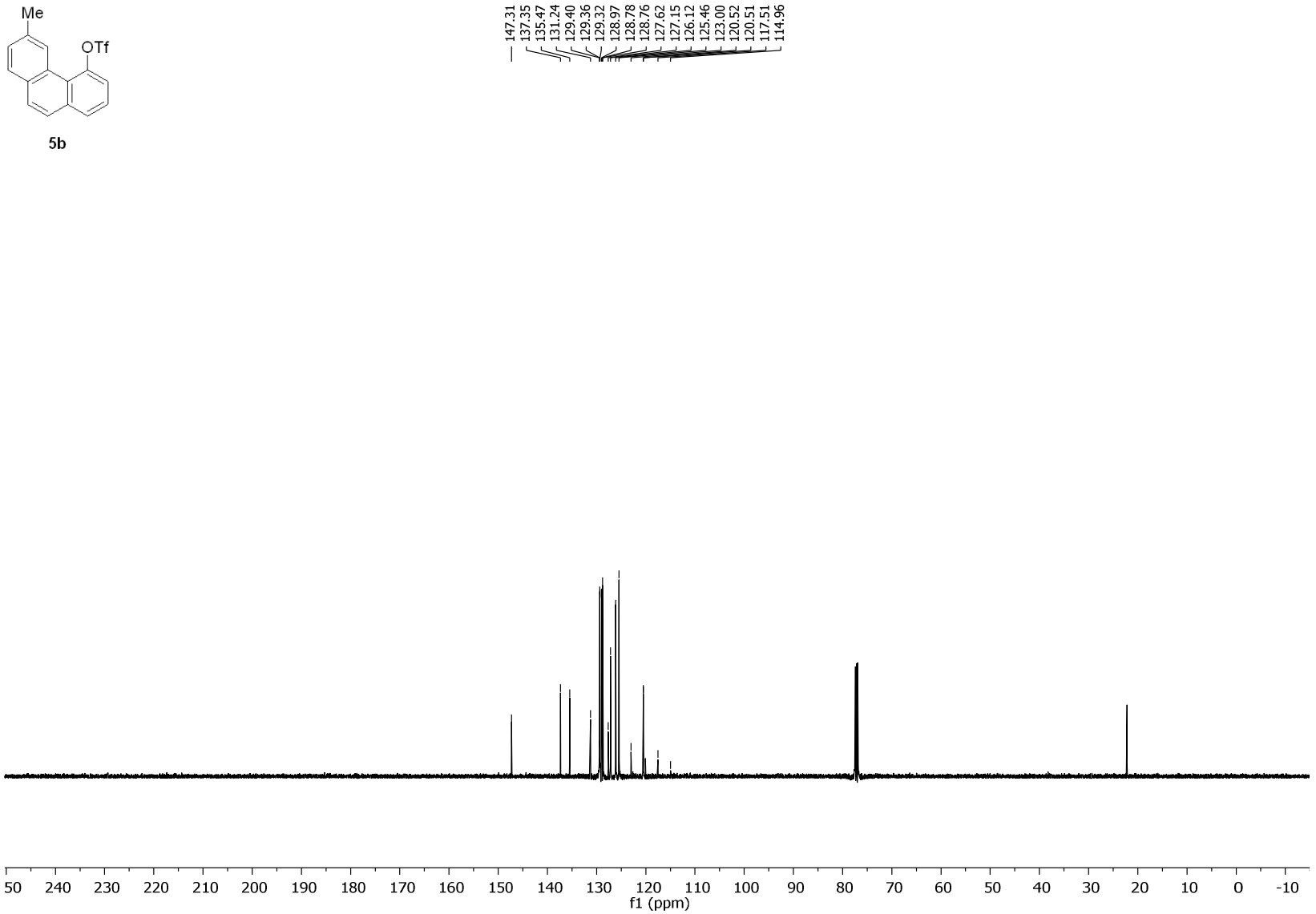

Figure S46. $^{13}C\{^{1}H\}$ NMR spectrum (126 MHz, $CDCl_3$) of **5b**.

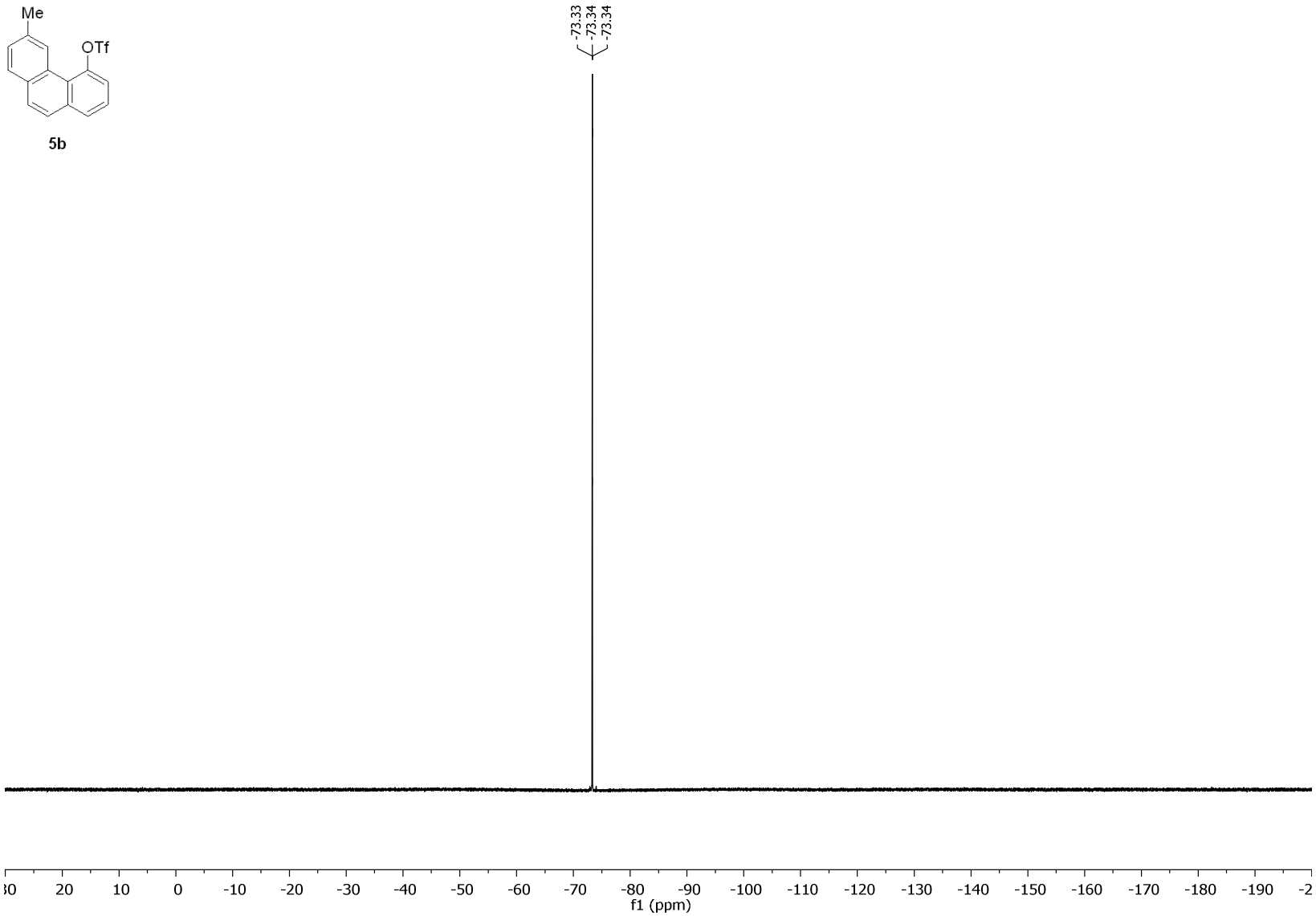

Figure S47. ^{19}F NMR spectrum (282 MHz, $CDCl_3$) of **5b**.

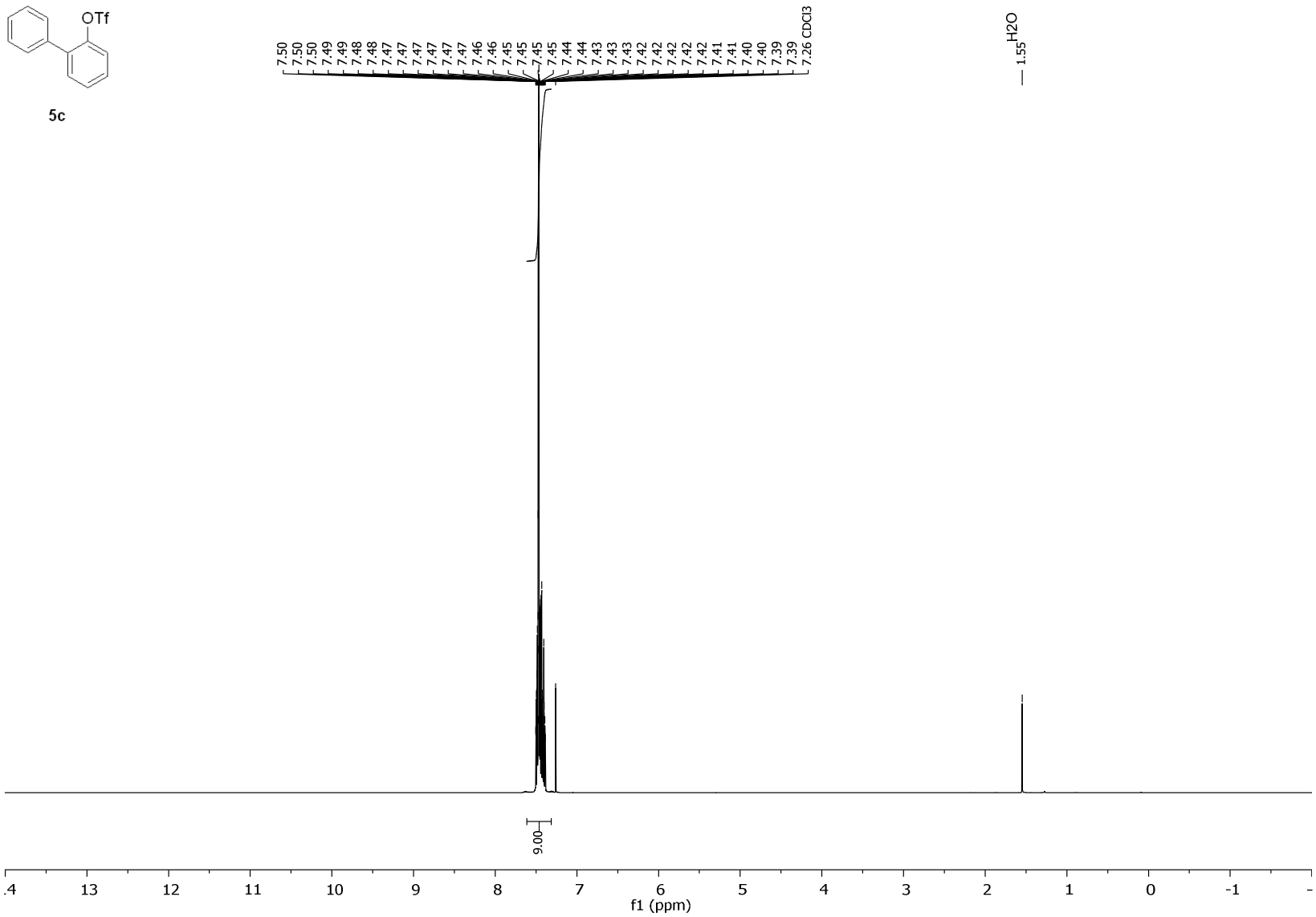

Figure S48. ^{1}H NMR spectrum (500 MHz, $CDCl_3$) of **5c**.

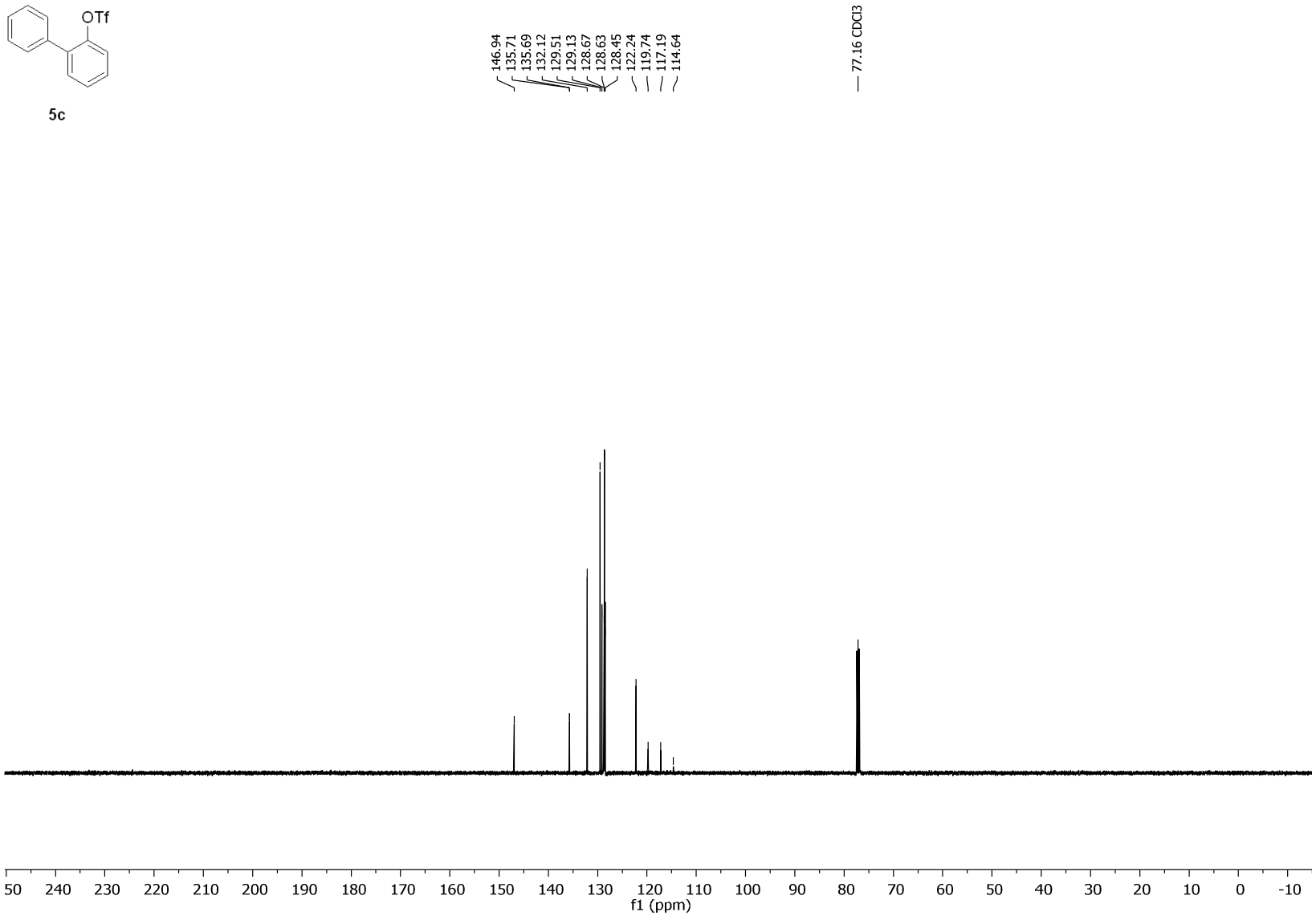

Figure S49. $^{13}C\{^{1}H\}$ NMR spectrum (126 MHz, $CDCl_3$) of **5c**.

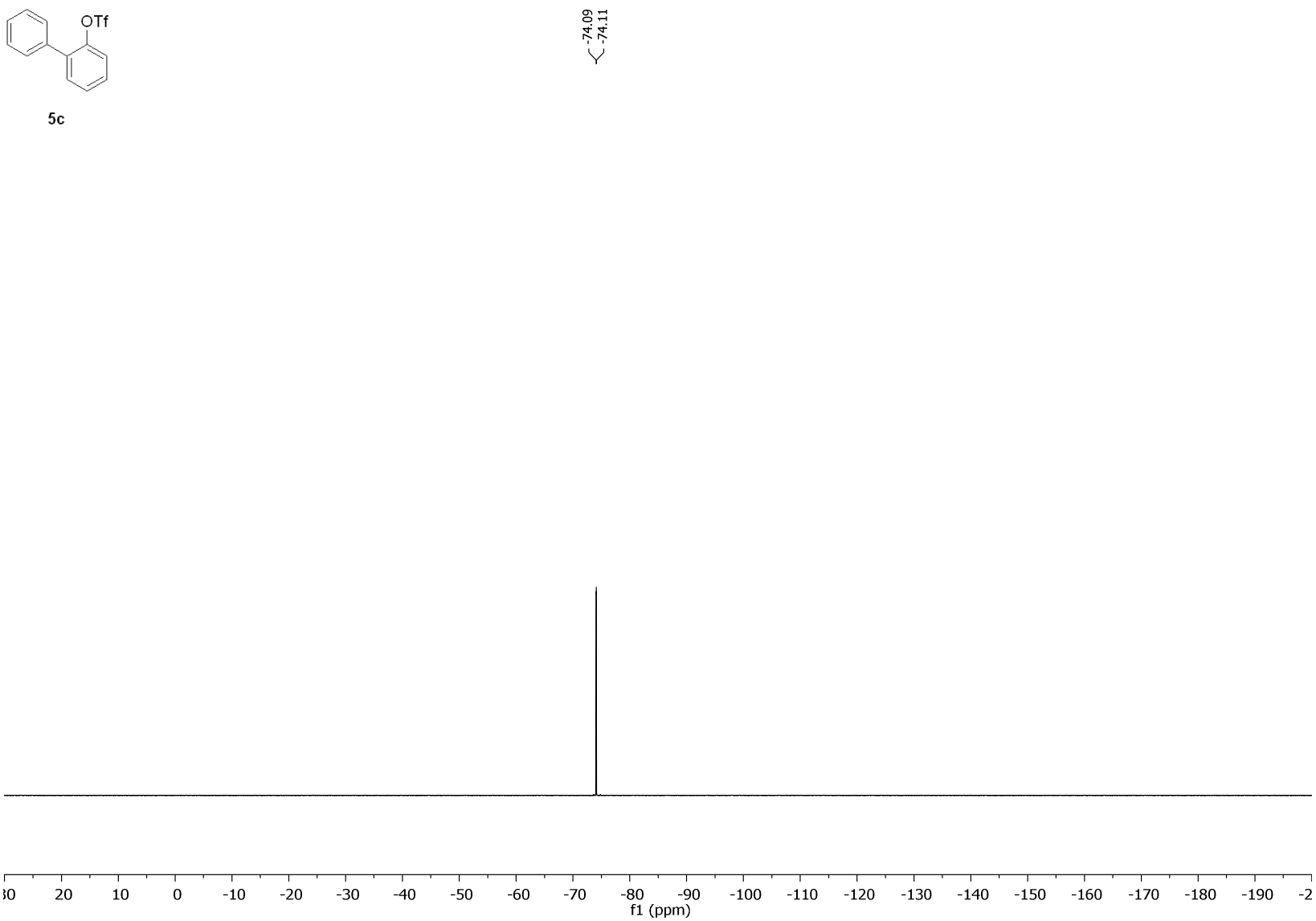

Figure S50. ^{19}F NMR spectrum (282 MHz, $CDCl_3$) of **5c**.

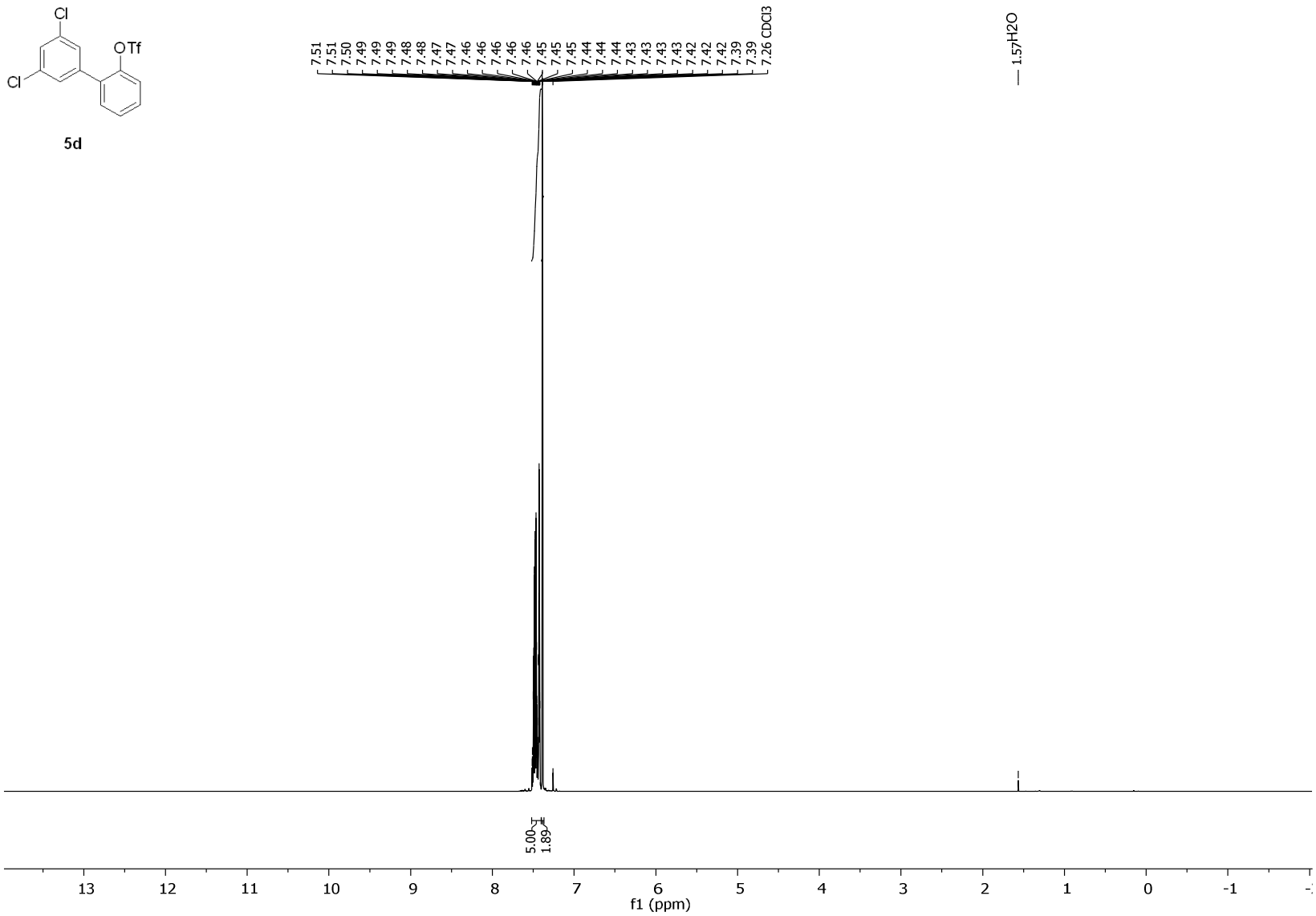

Figure S51. ^{1}H NMR spectrum (500 MHz, $CDCl_3$) of **5d**.

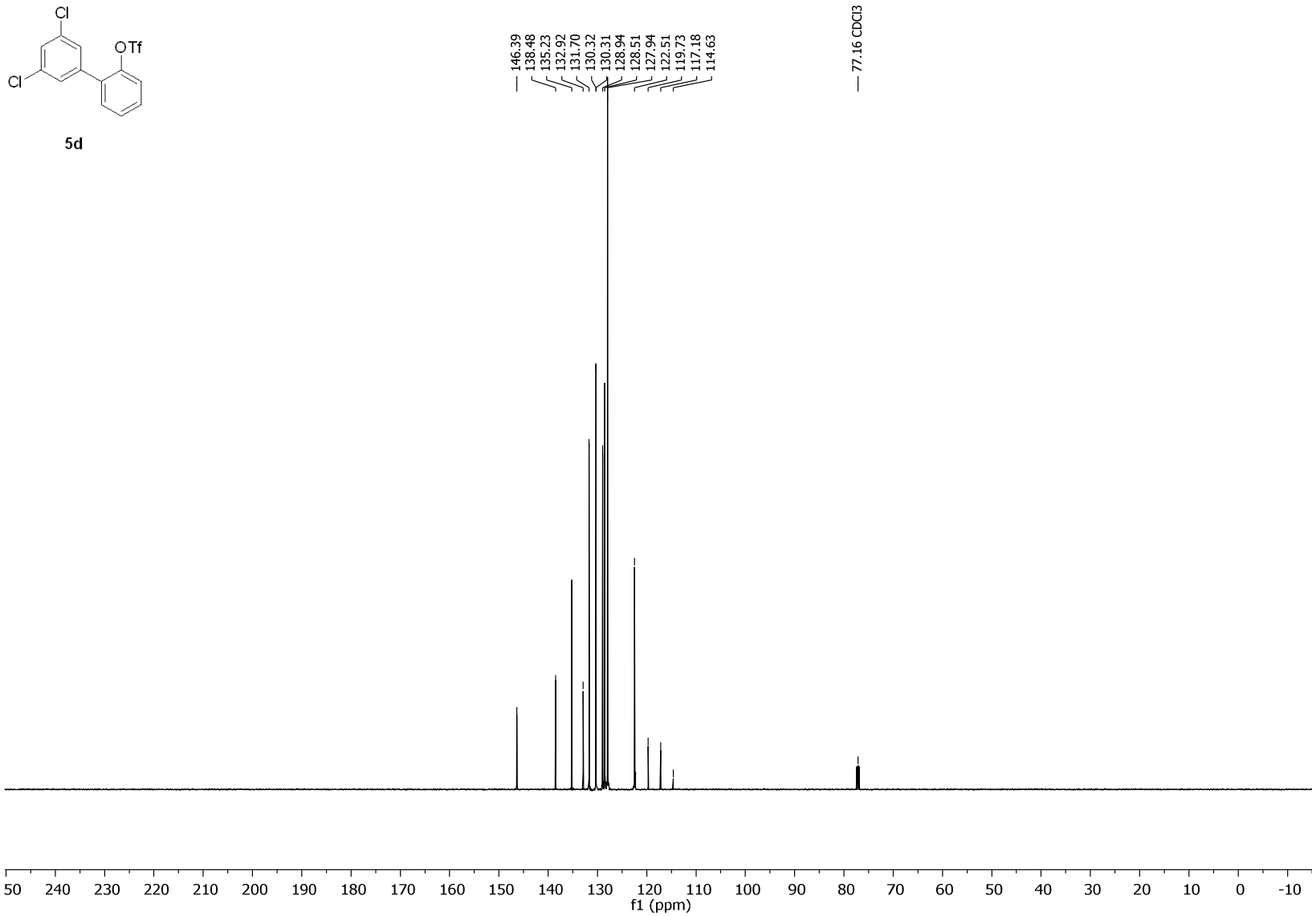

Figure S52. $^{13}C\{^{1}H\}$ NMR spectrum (126 MHz, $CDCl_3$) of **5d**.

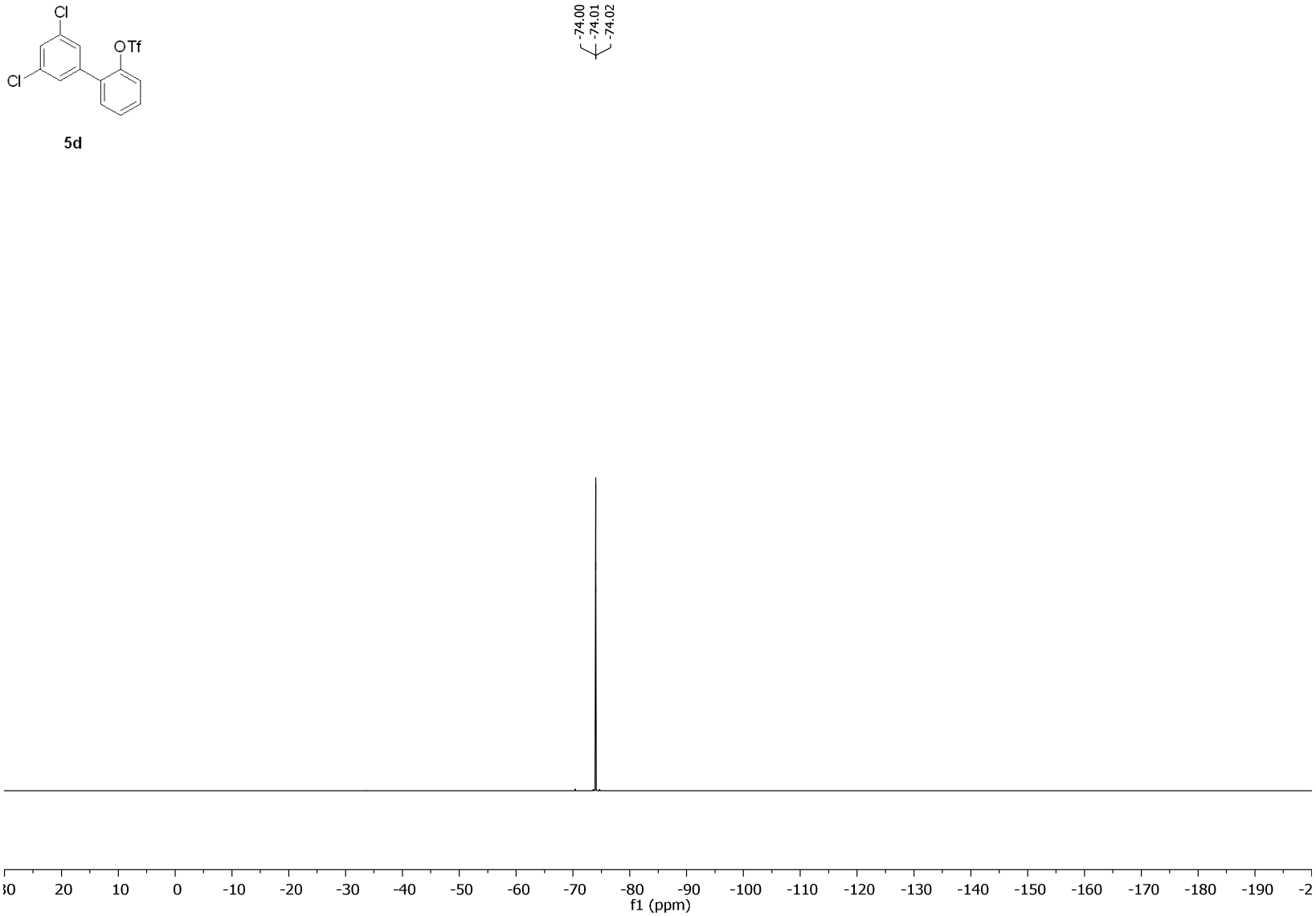

Figure S53. ^{19}F NMR spectrum (282 MHz, $CDCl_3$) of **5d**.

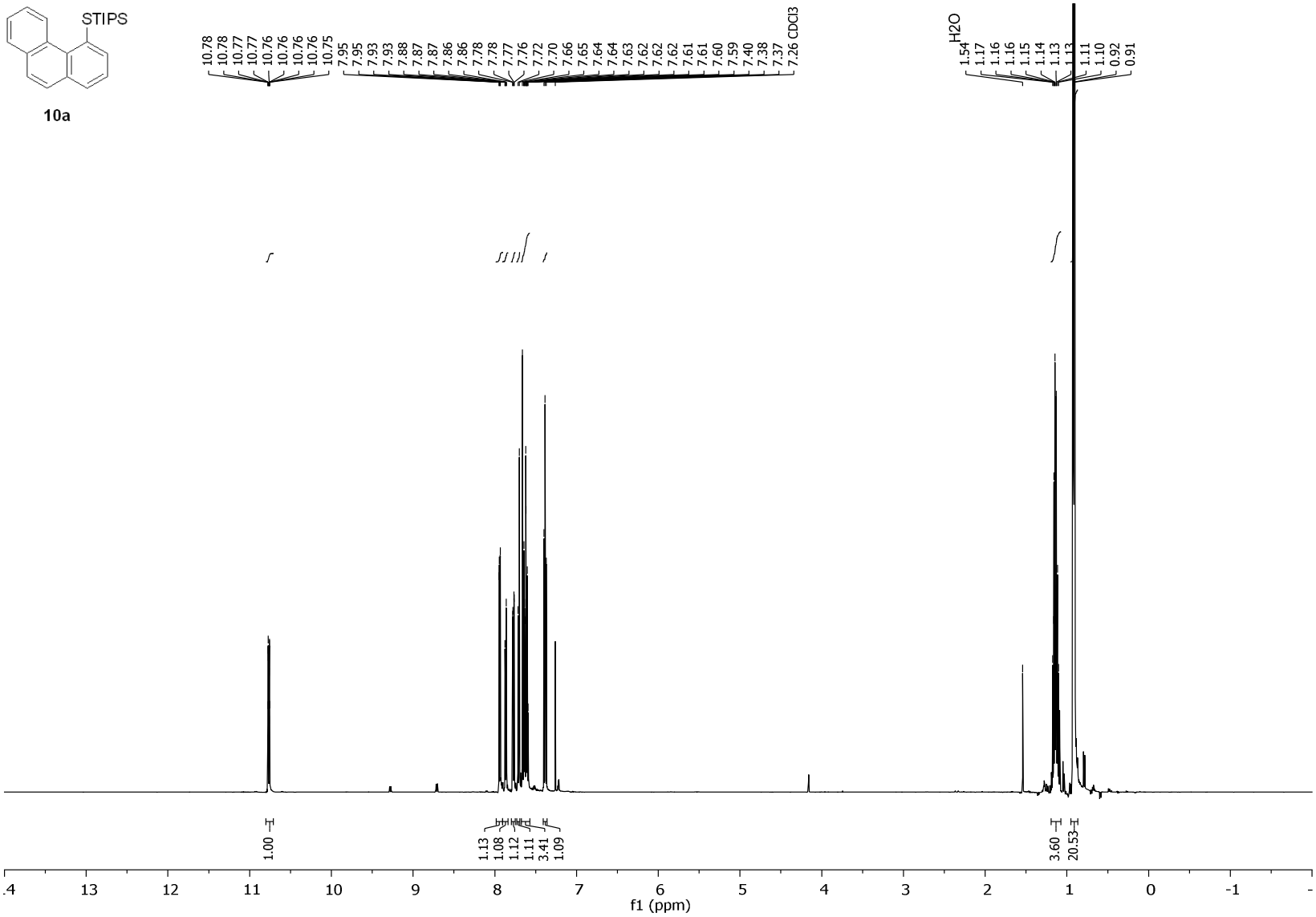

Figure S54. ^{1}H NMR spectrum (500 MHz, $CDCl_3$) of **10a**.

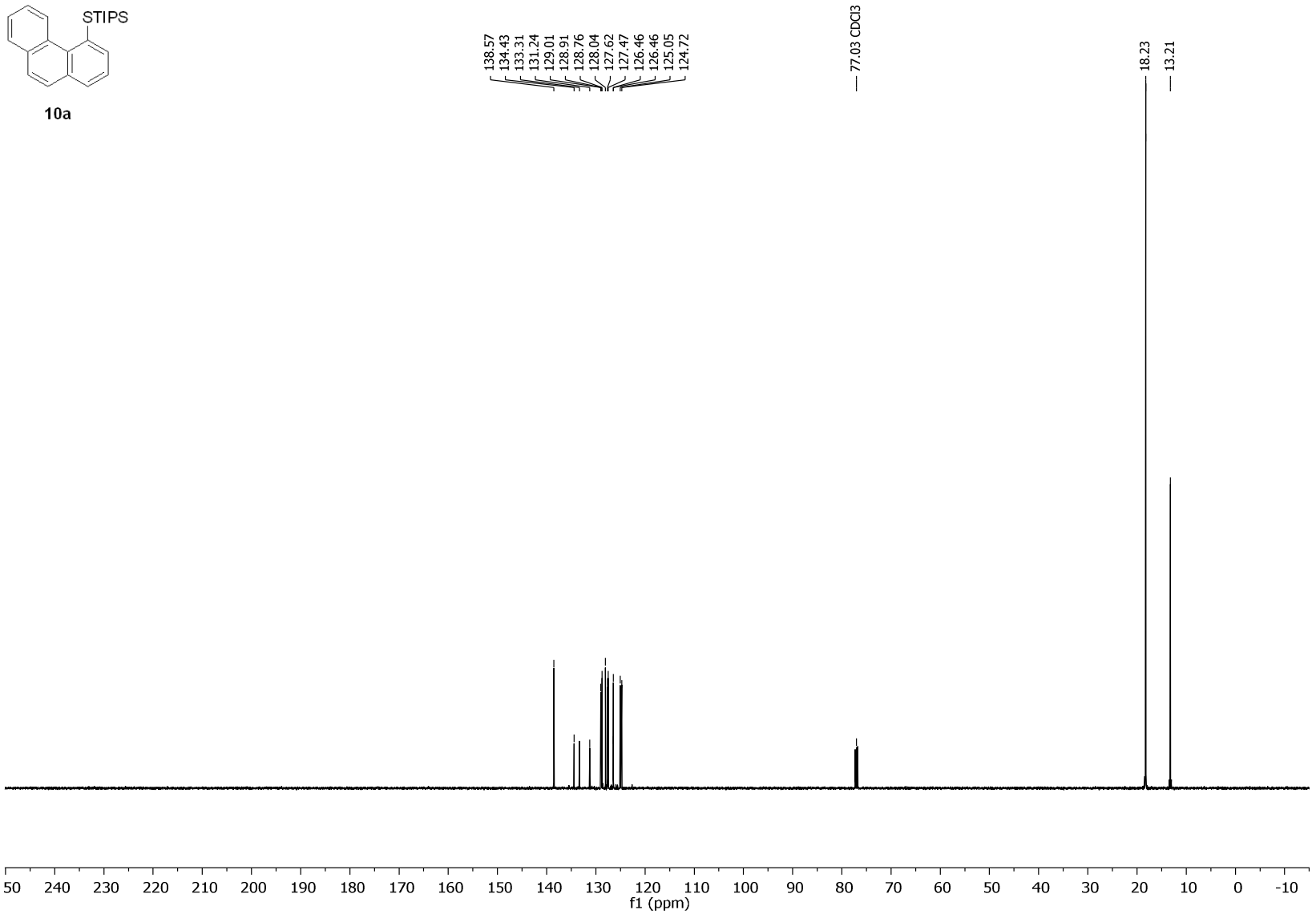

Figure S55. $^{13}C\{^{1}H\}$ NMR spectrum (126 MHz, $CDCl_3$) of **10a**.

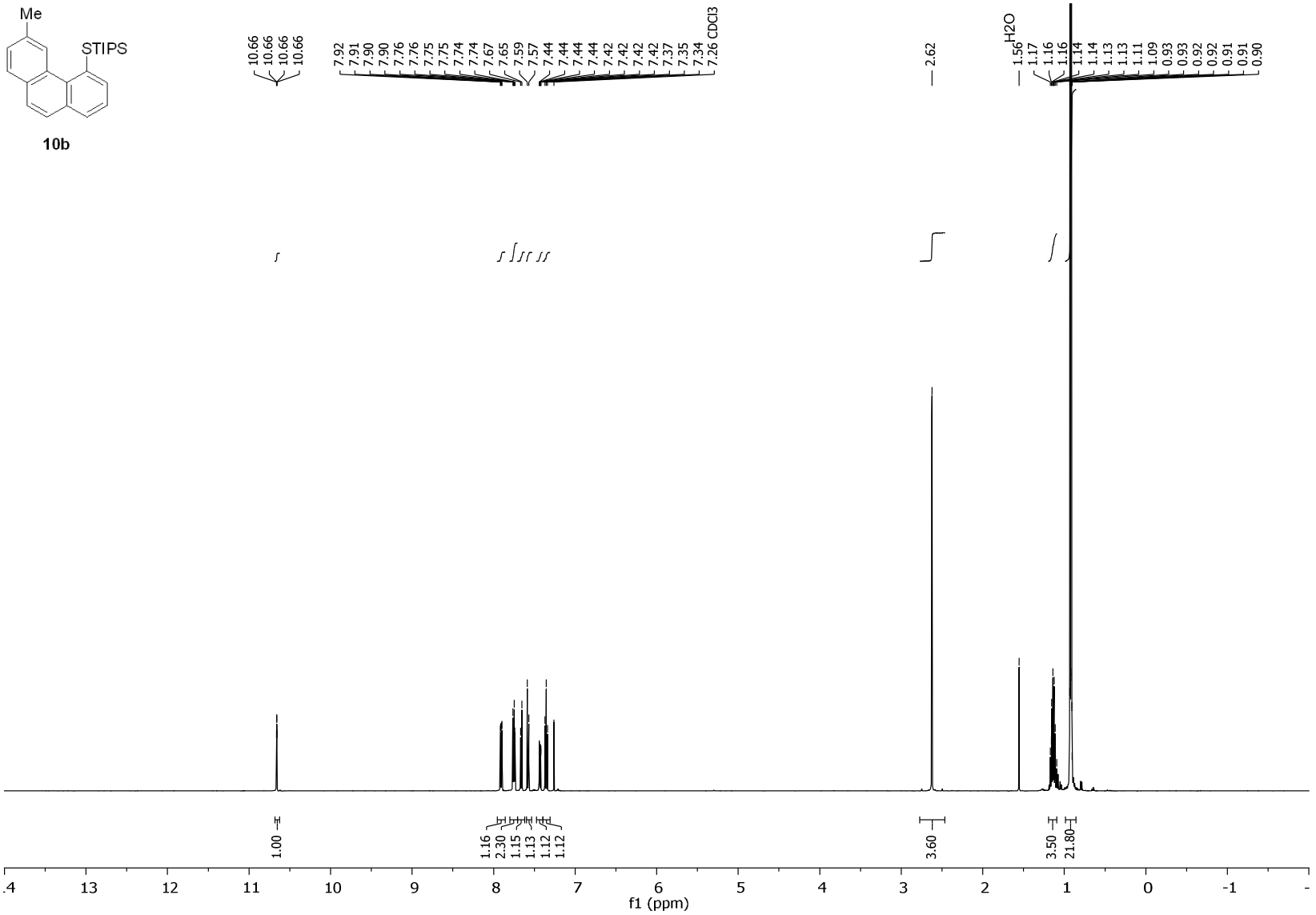

Figure S56. ^{1}H NMR spectrum (500 MHz, $CDCl_3$) of **10b**.

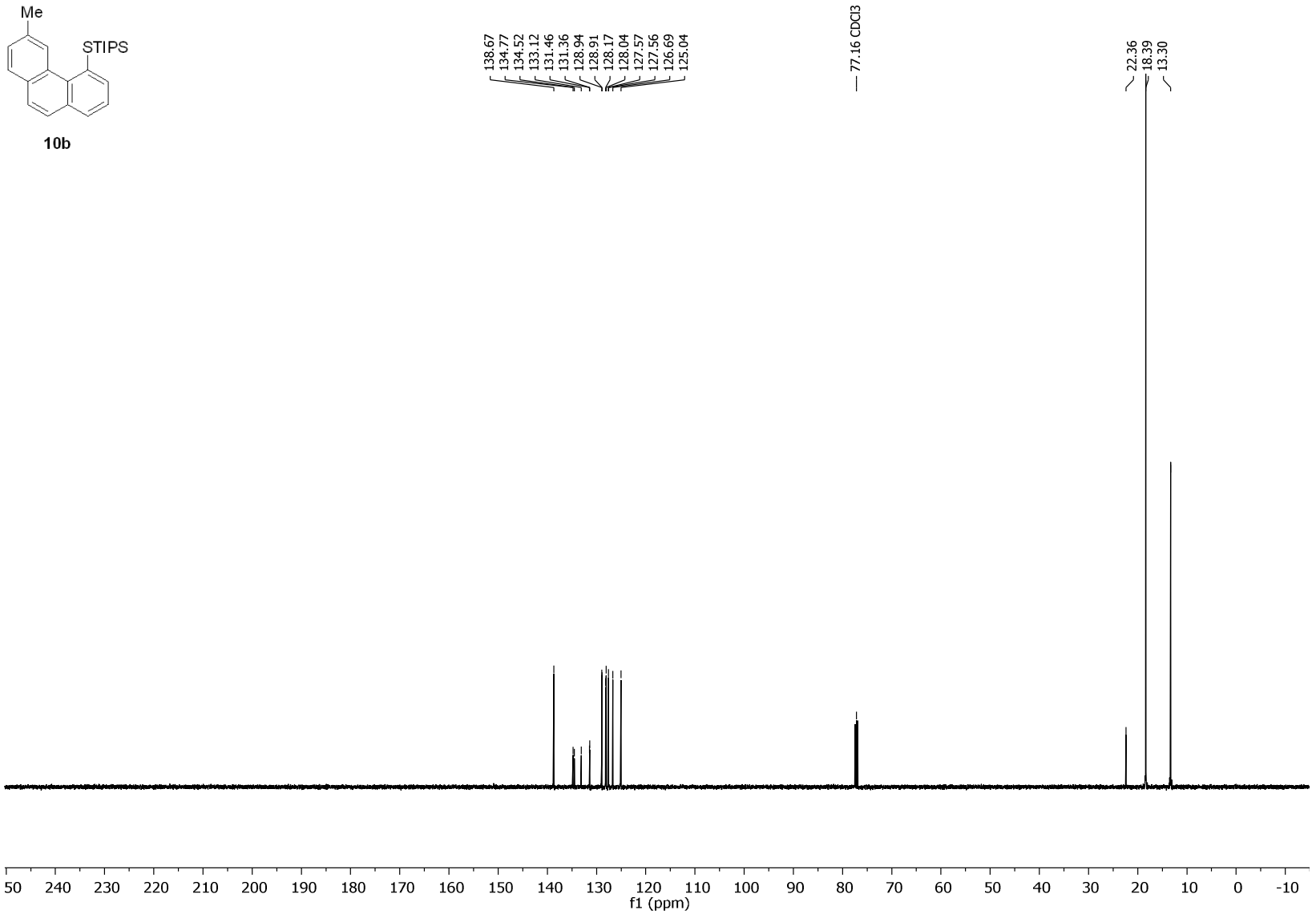

Figure S57. $^{13}C\{^{1}H\}$ NMR spectrum (126 MHz, $CDCl_3$) of **10b**.

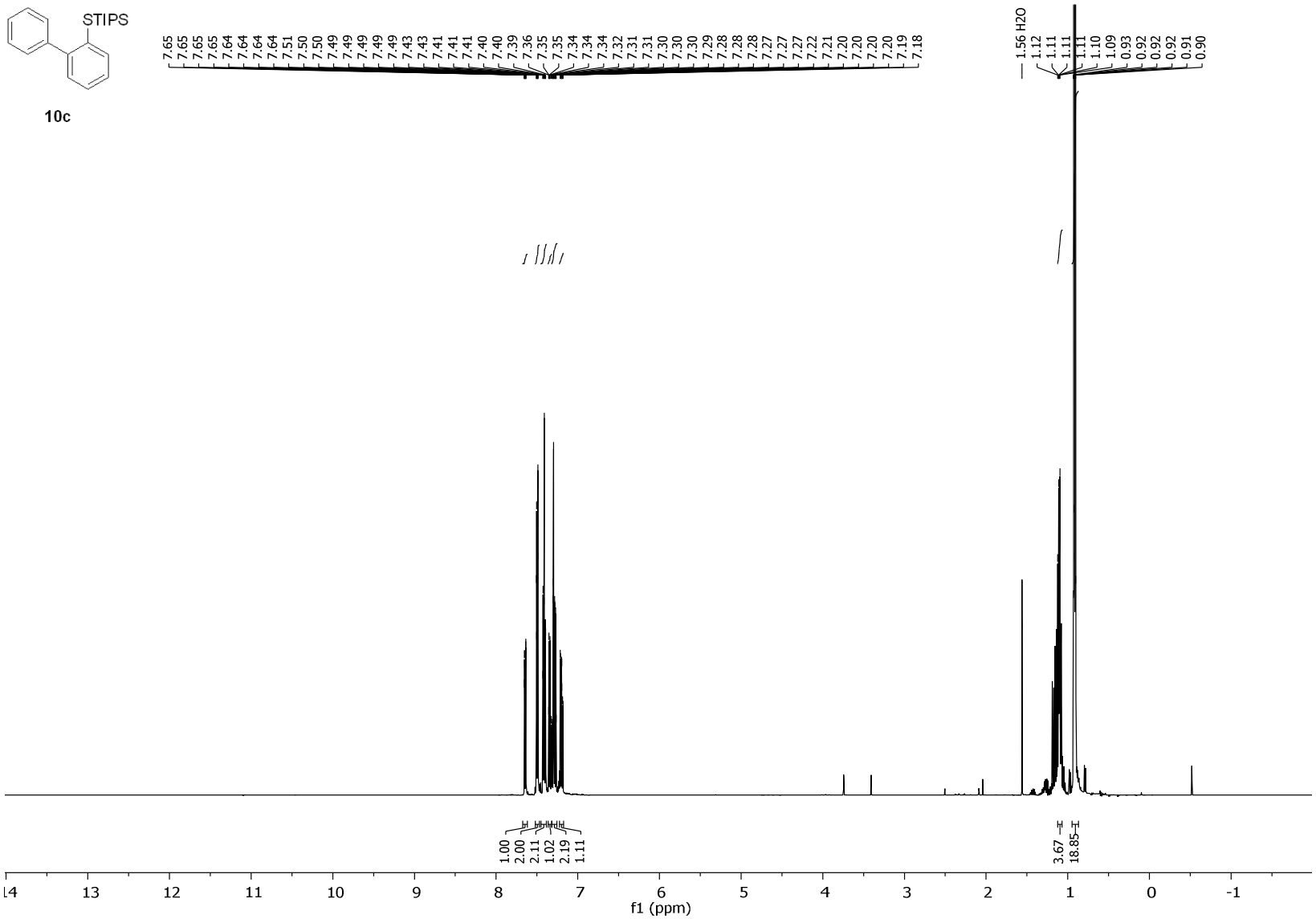

Figure S58. ^{1}H NMR spectrum (500 MHz, $CDCl_3$) of **10c**.

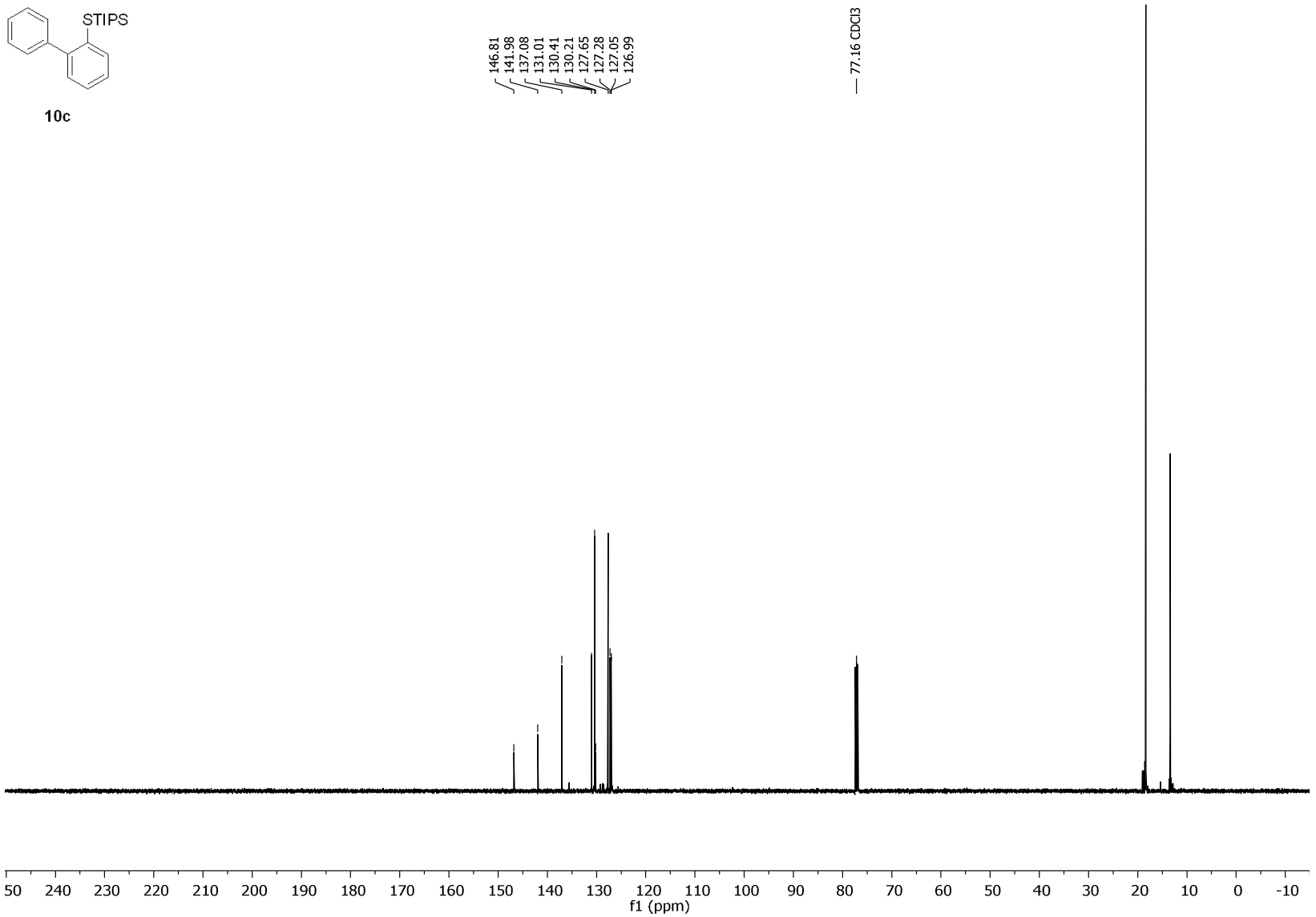

Figure S59. $^{13}C\{^{1}H\}$ NMR spectrum (126 MHz, $CDCl_3$) of **10c**.

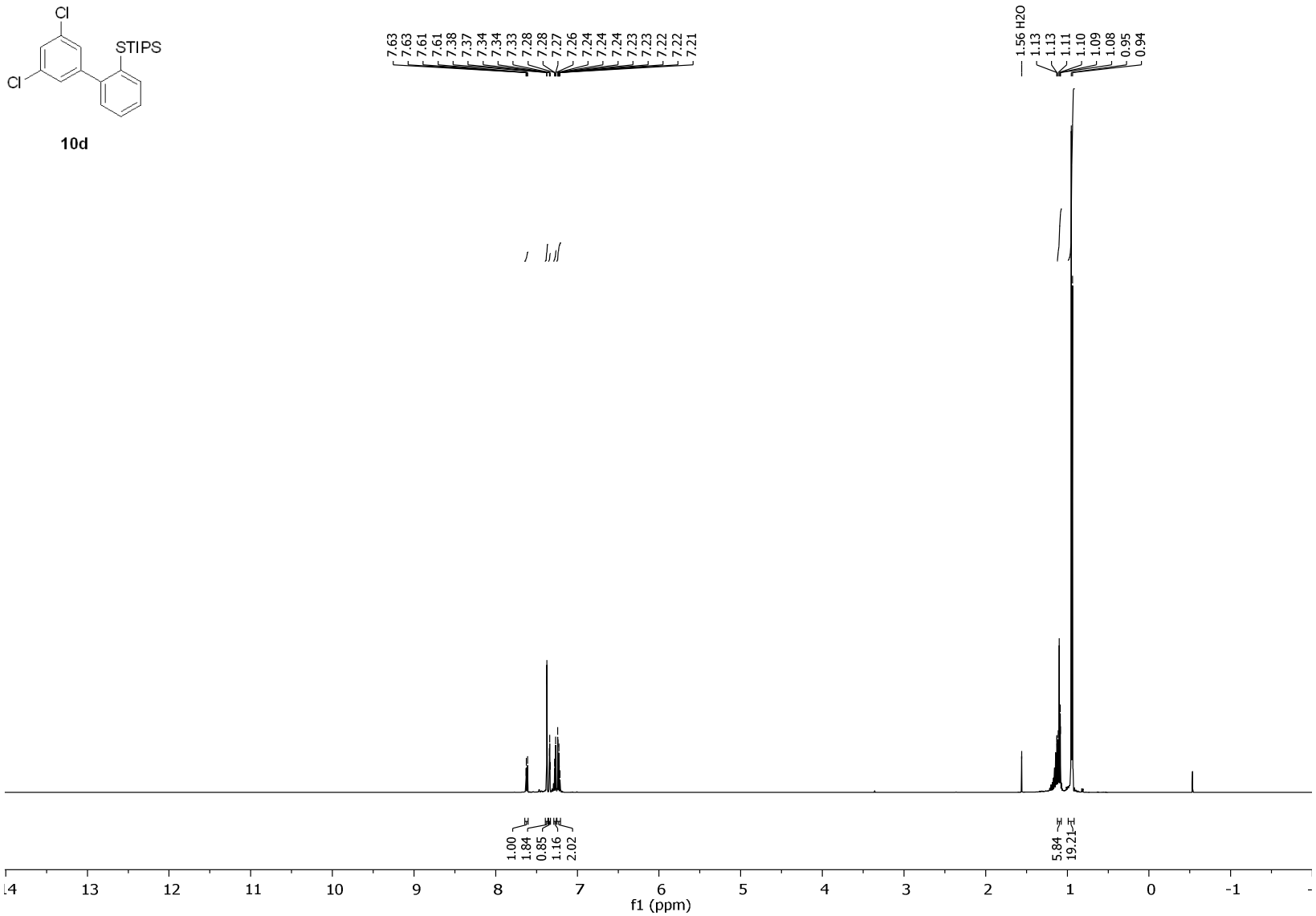

Figure S60. ^{1}H NMR spectrum (500 MHz, $CDCl_3$) of **10d**.

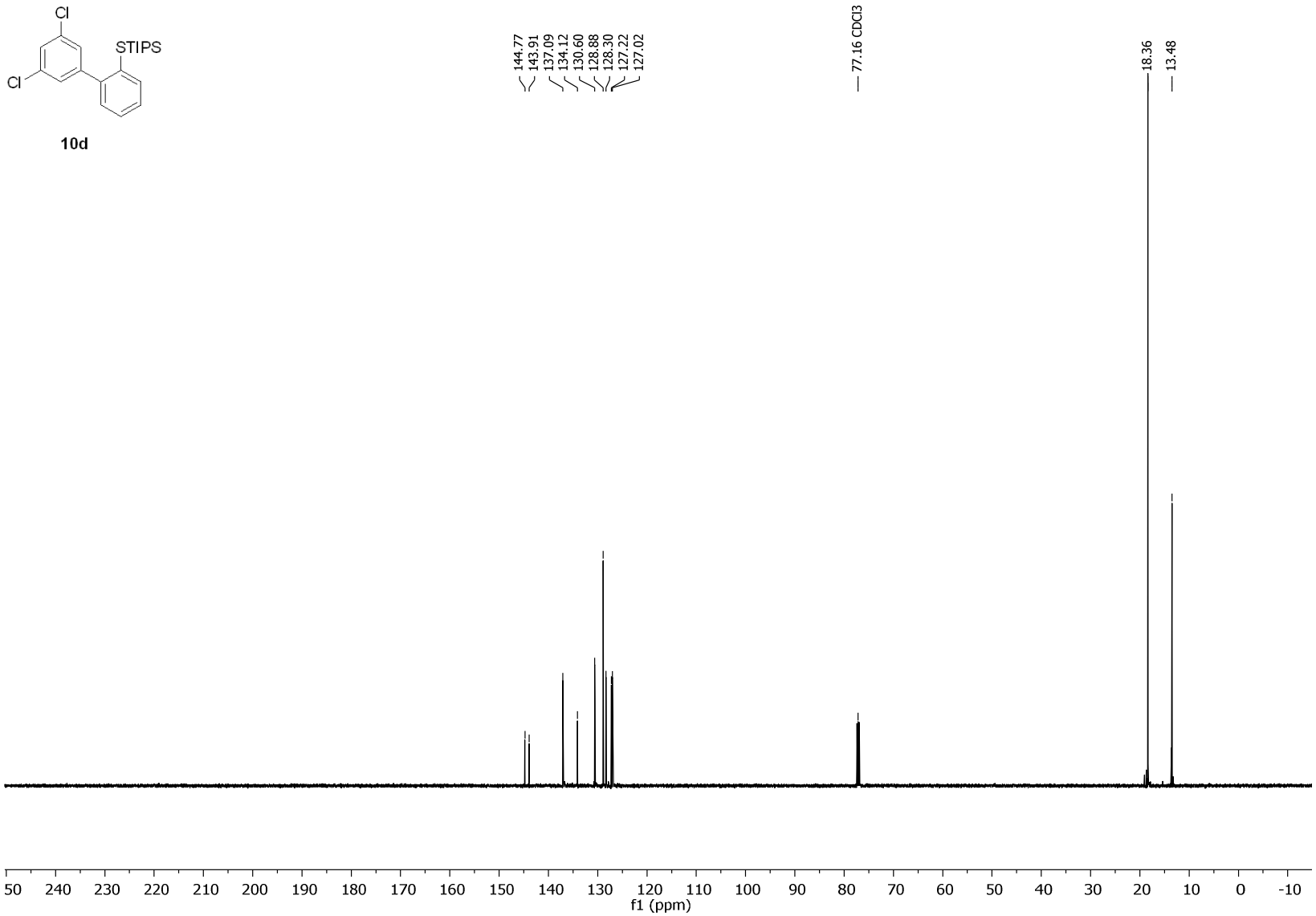

Figure S61. $^{13}C\{^{1}H\}$ NMR spectrum (126 MHz, $CDCl_3$) of **10d**.

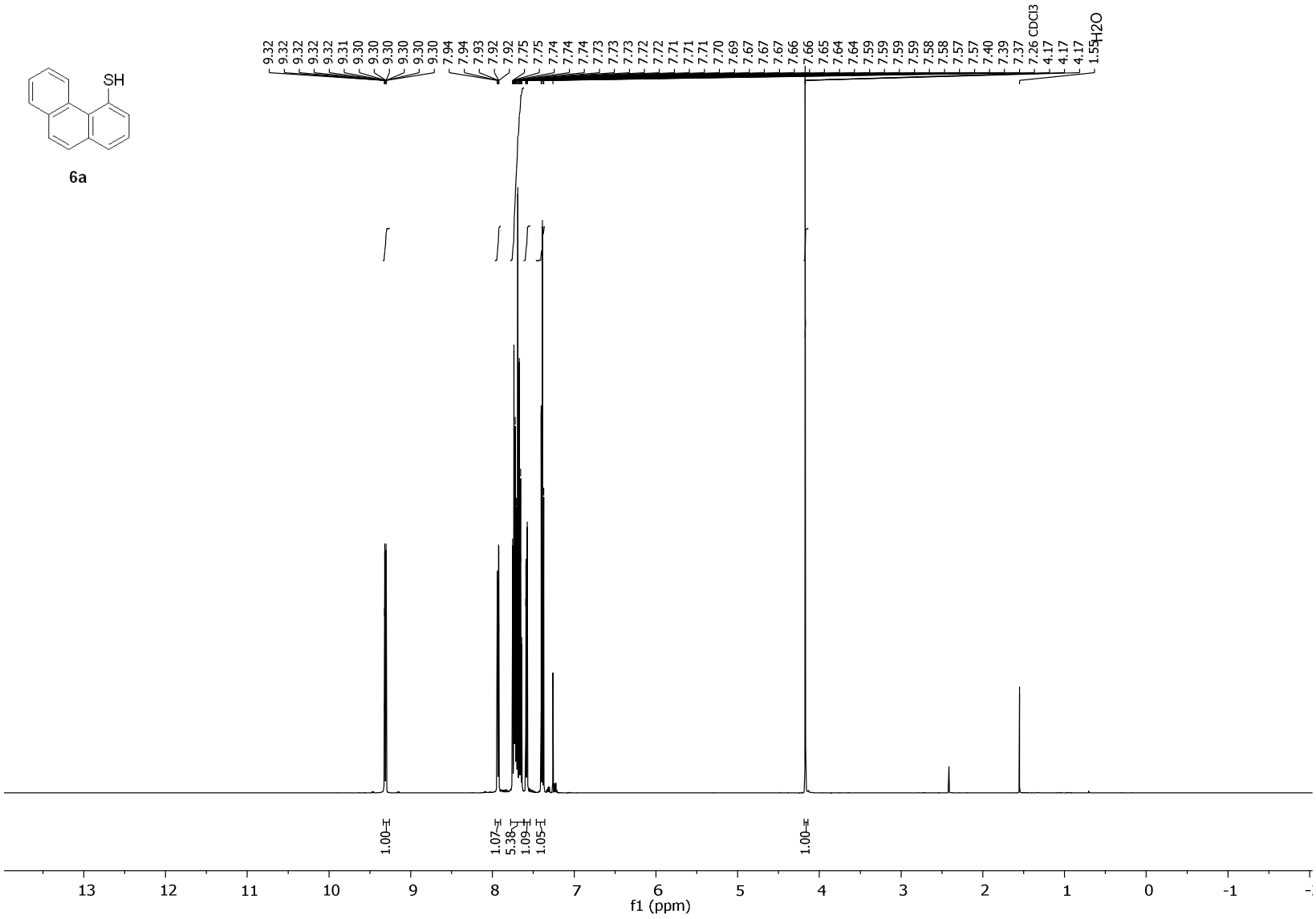

Figure S62. ^{1}H NMR spectrum (500 MHz, $CDCl_3$) of **6a**.

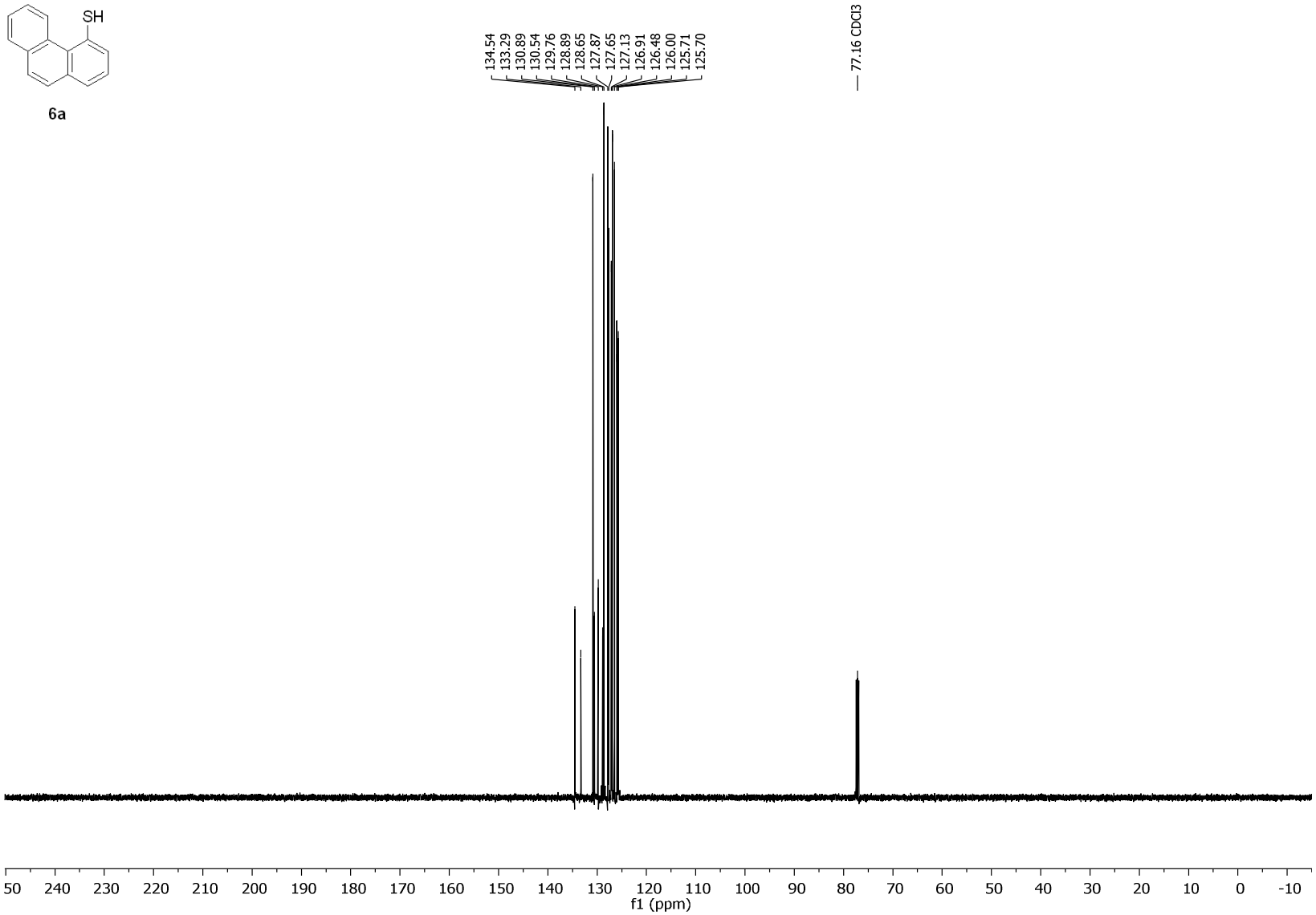

Figure S63. $^{13}C\{^{1}H\}$ NMR spectrum (126 MHz, $CDCl_3$) of **6a**.

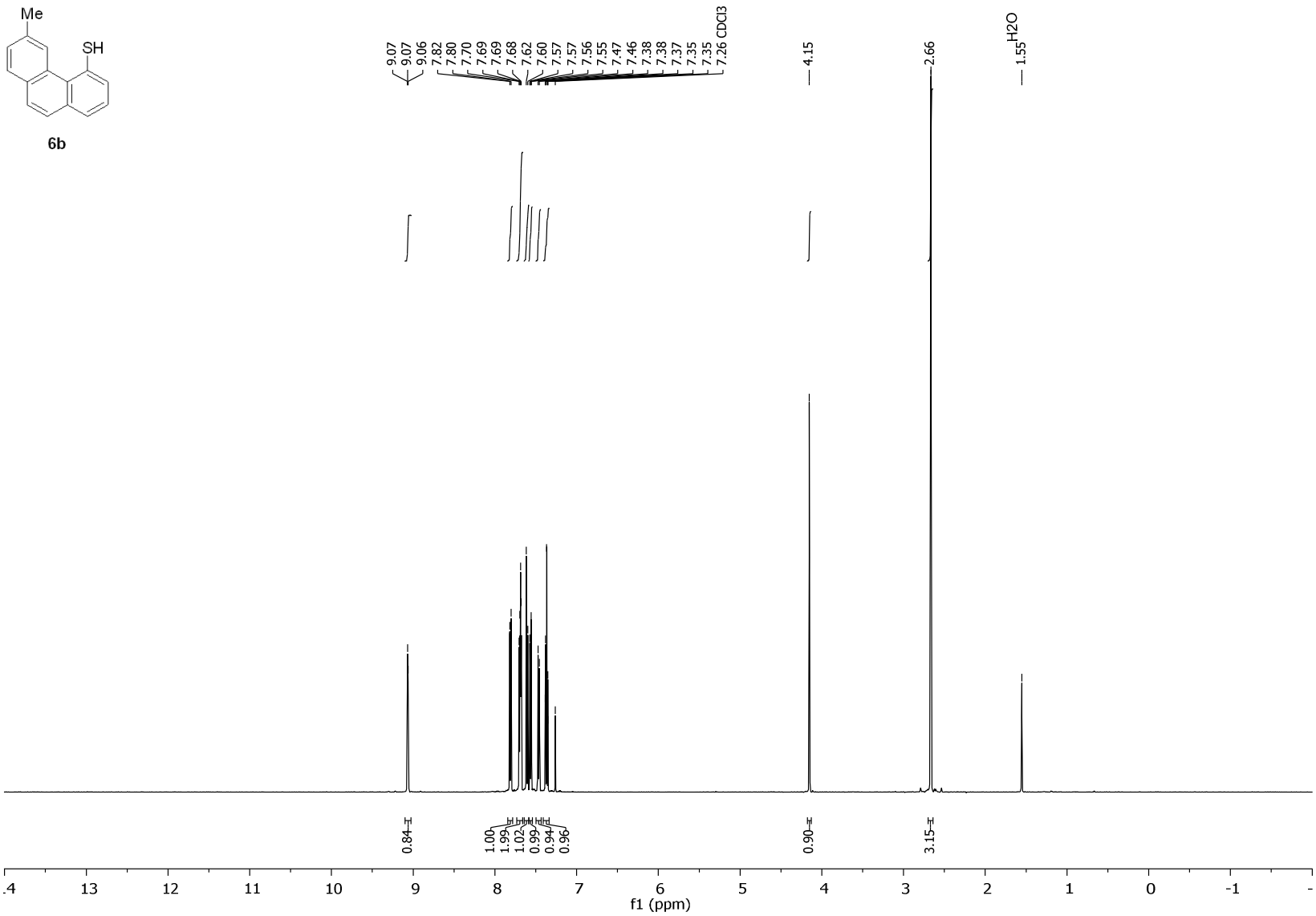

Figure S64. ^{1}H NMR spectrum (500 MHz, $CDCl_3$) of **6b**.

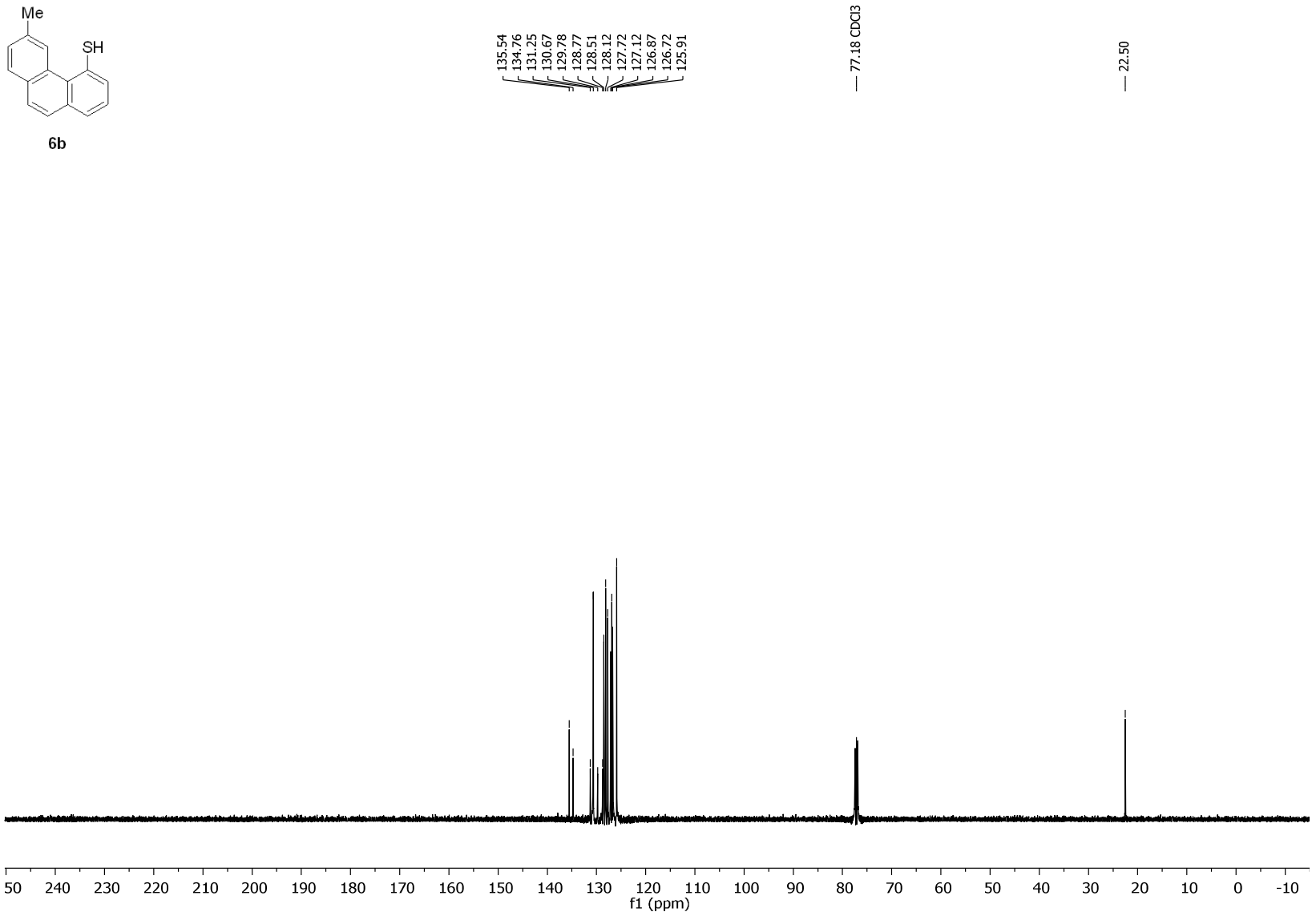

Figure S65. $^{13}C\{^{1}H\}$ NMR spectrum (126 MHz, $CDCl_3$) of **6b**.

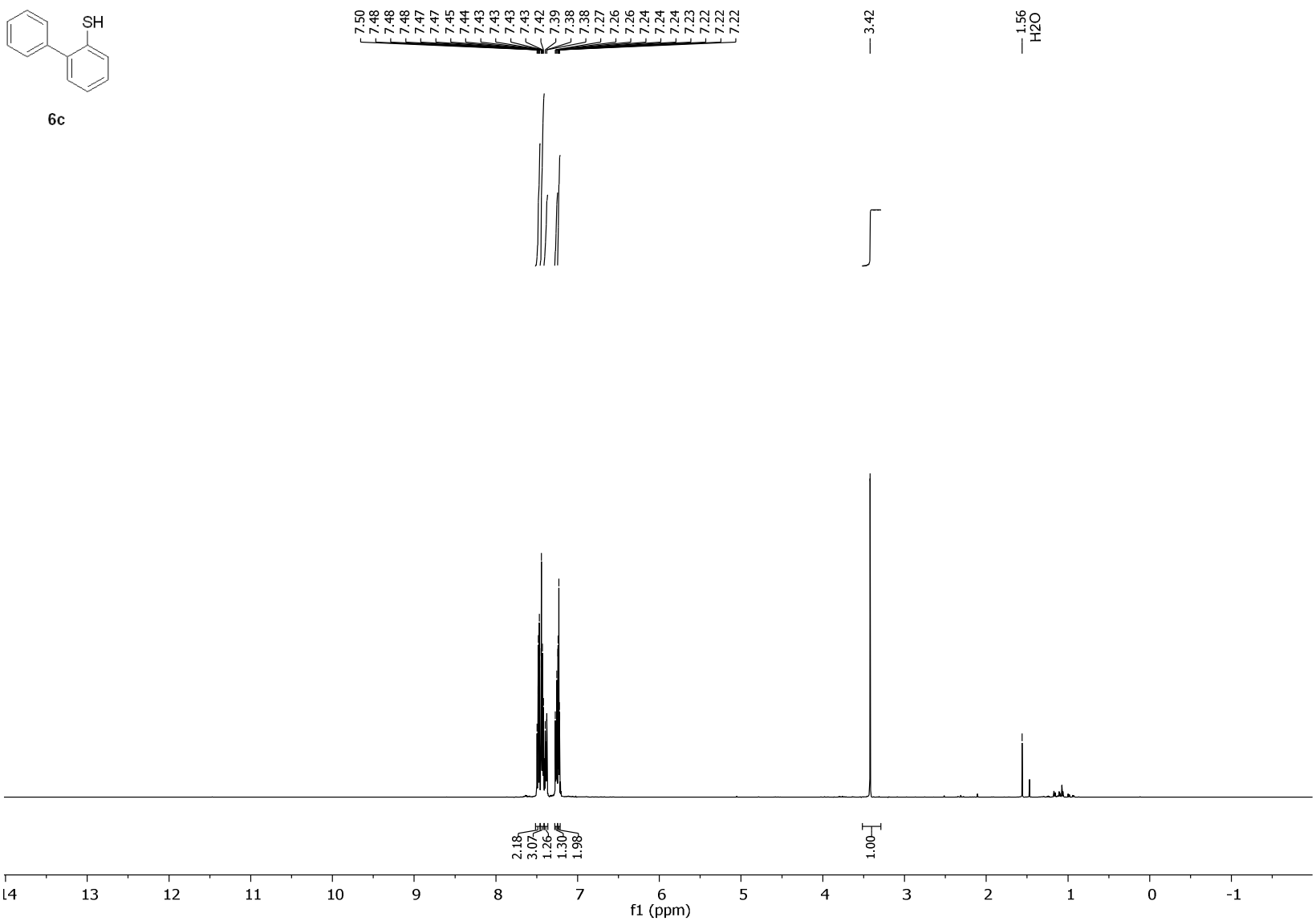

Figure S66. ^{1}H NMR spectrum (500 MHz, $CDCl_3$) of **6c**.

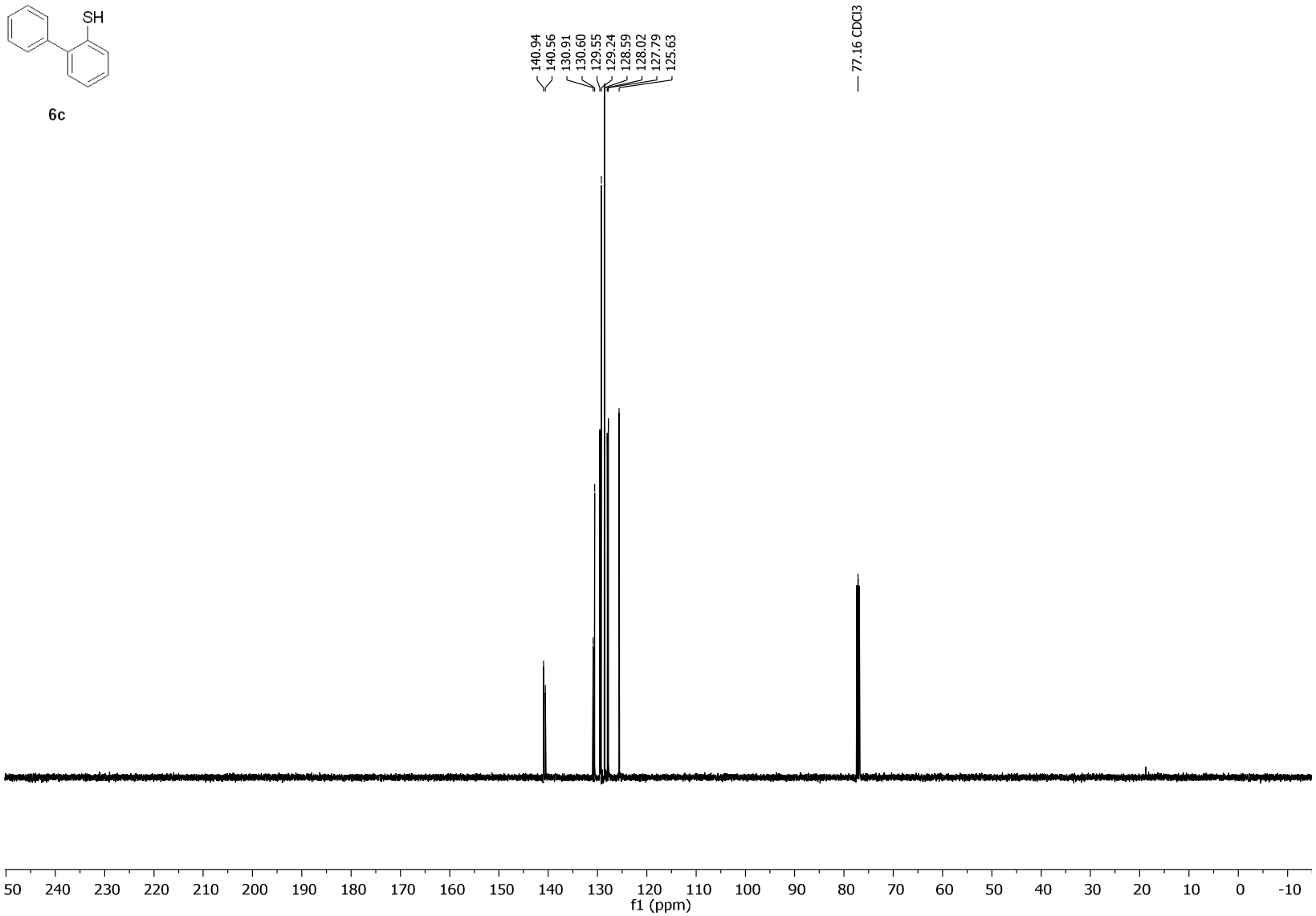

Figure S67. $^{13}C\{^{1}H\}$ NMR spectrum (126 MHz, $CDCl_3$) of **6c**.

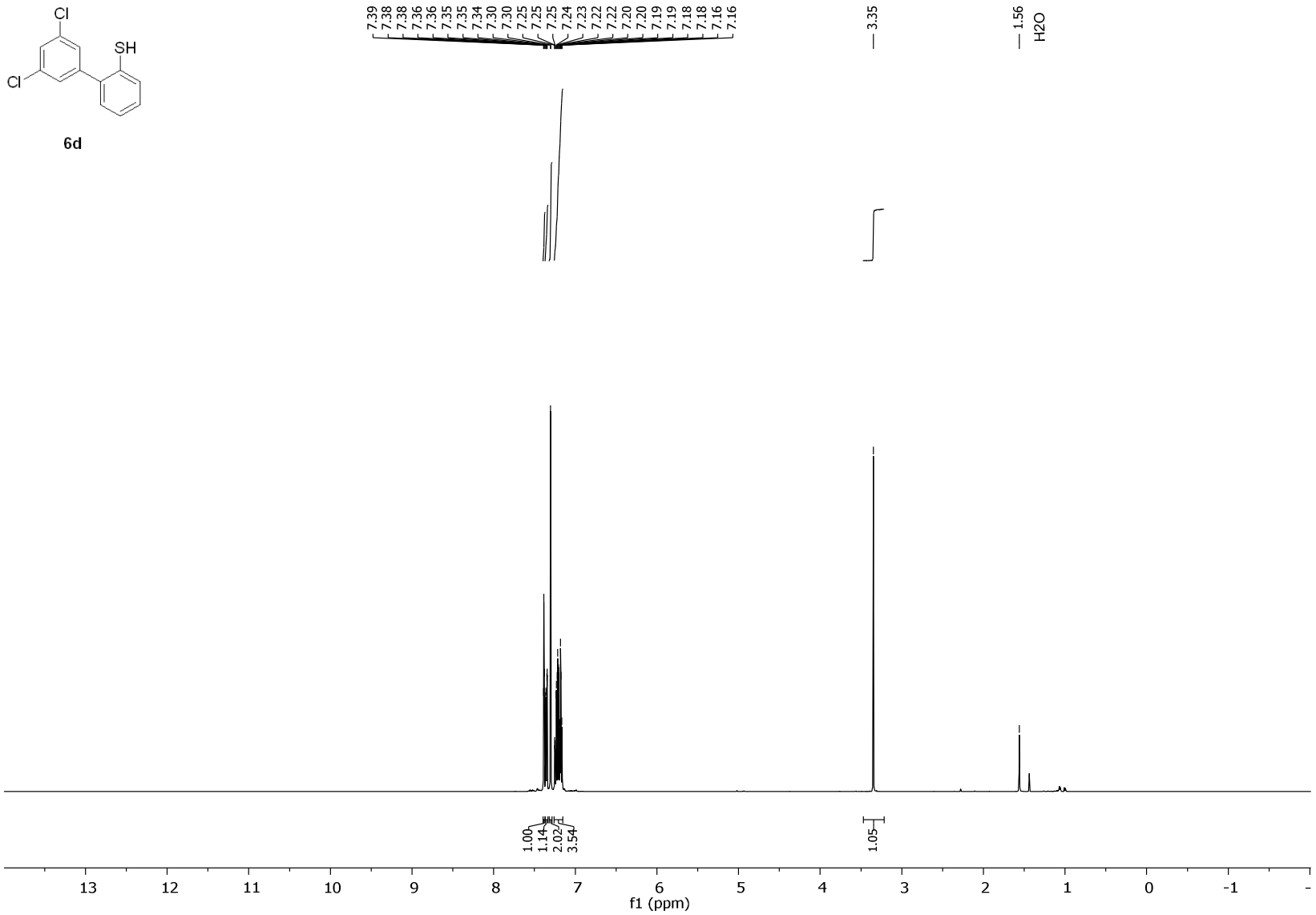

Figure S68. ^{1}H NMR spectrum (500 MHz, $CDCl_3$) of **6d**.

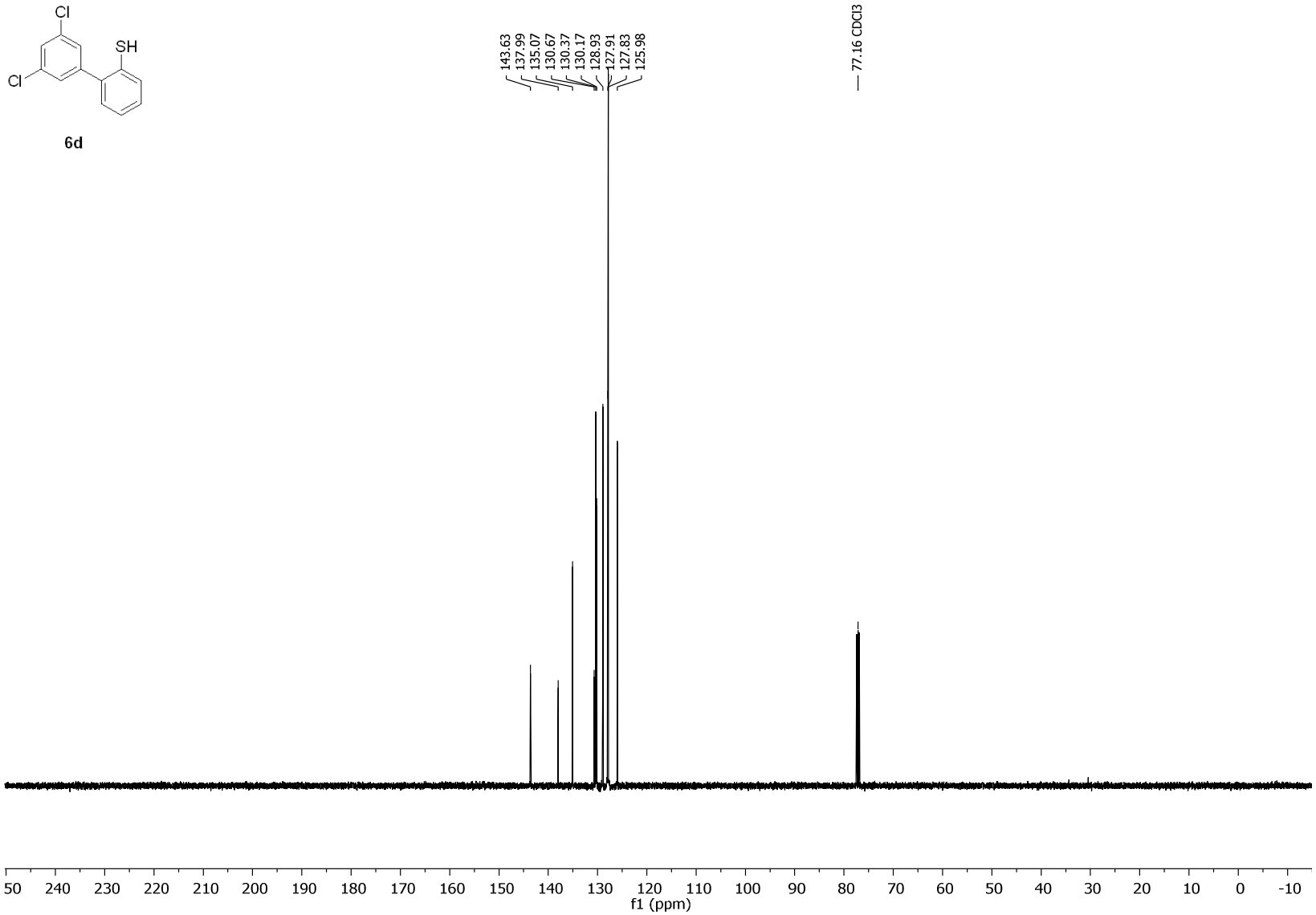

Figure S69. $^{13}C\{^{1}H\}$ NMR spectrum (126 MHz, $CDCl_3$) of **6d**.

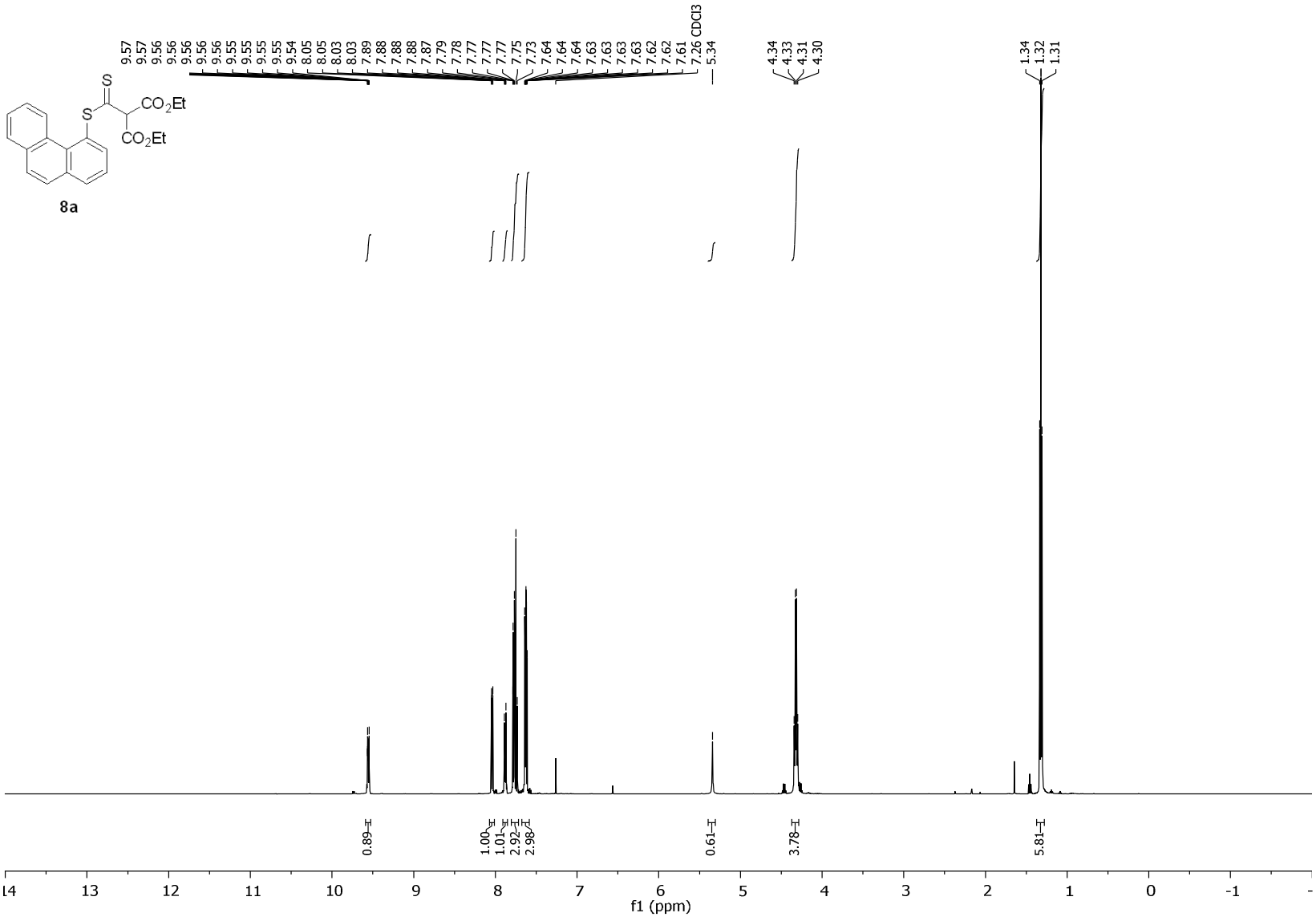

Figure S70. ^{1}H NMR spectrum (500 MHz, $CDCl_3$) of **8a**.

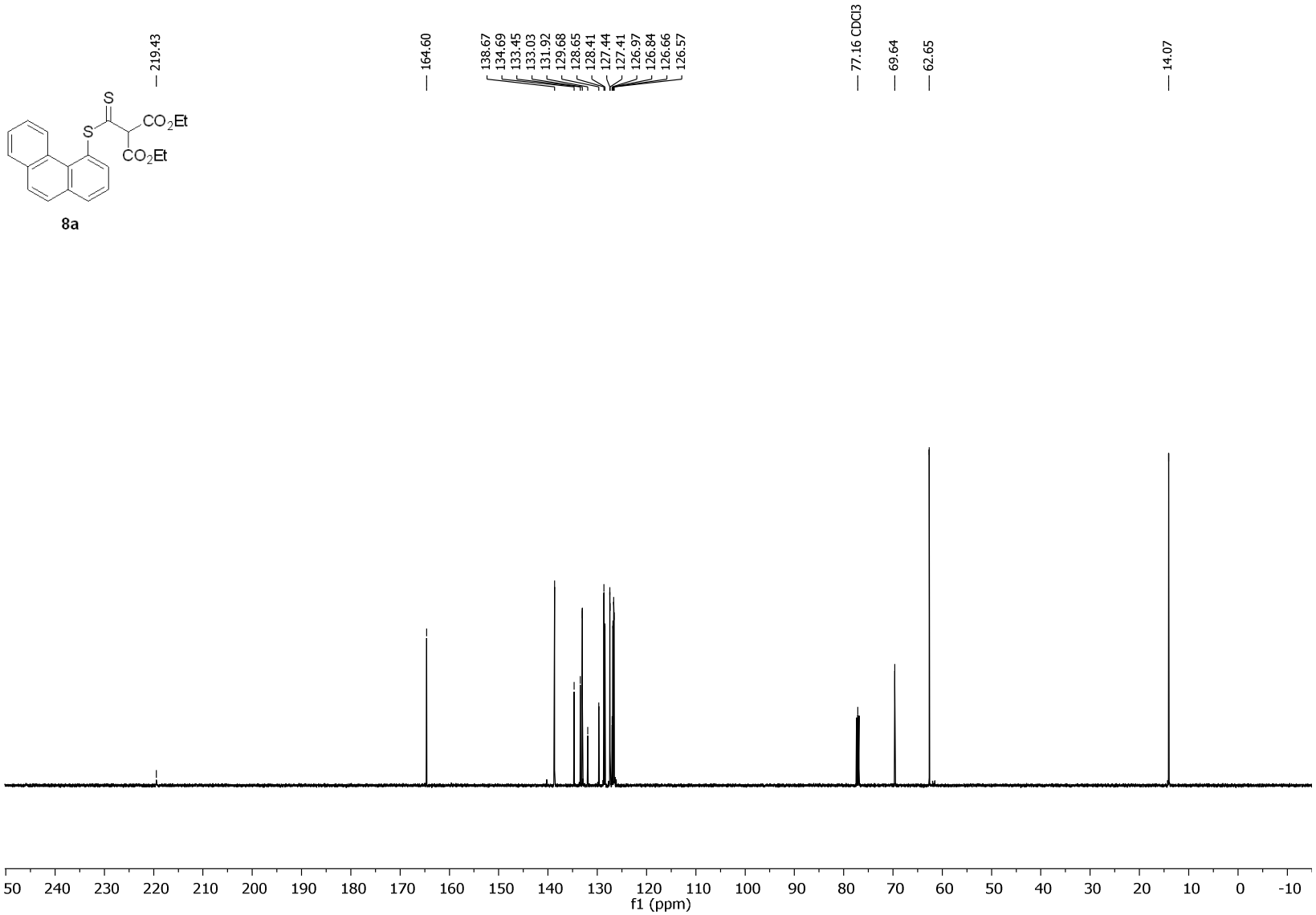

Figure S71. $^{13}C\{^{1}H\}$ NMR spectrum (126 MHz, $CDCl_3$) of **8a**.

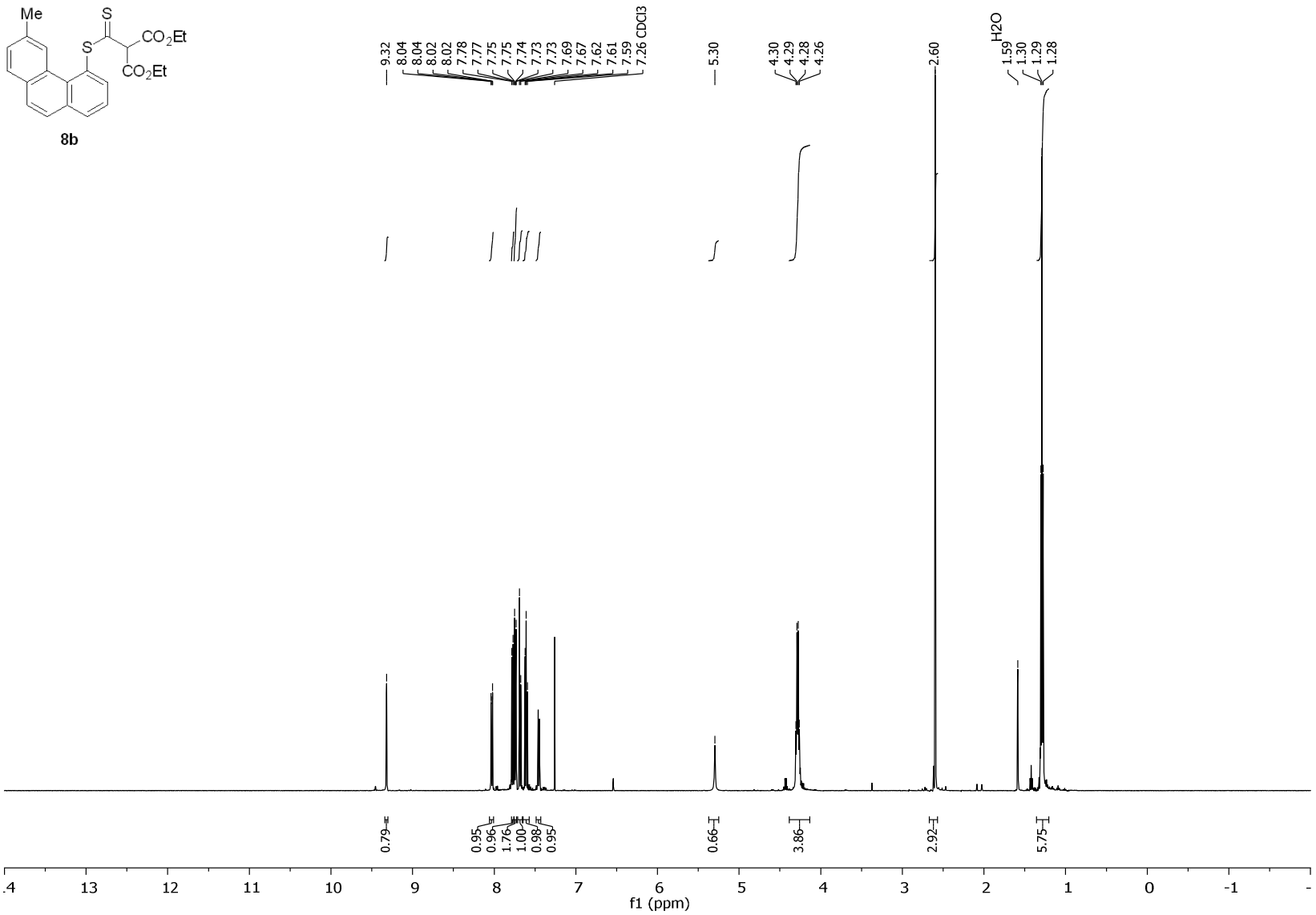

Figure S72. ^{1}H NMR spectrum (500 MHz, $CDCl_3$) of **8b**.

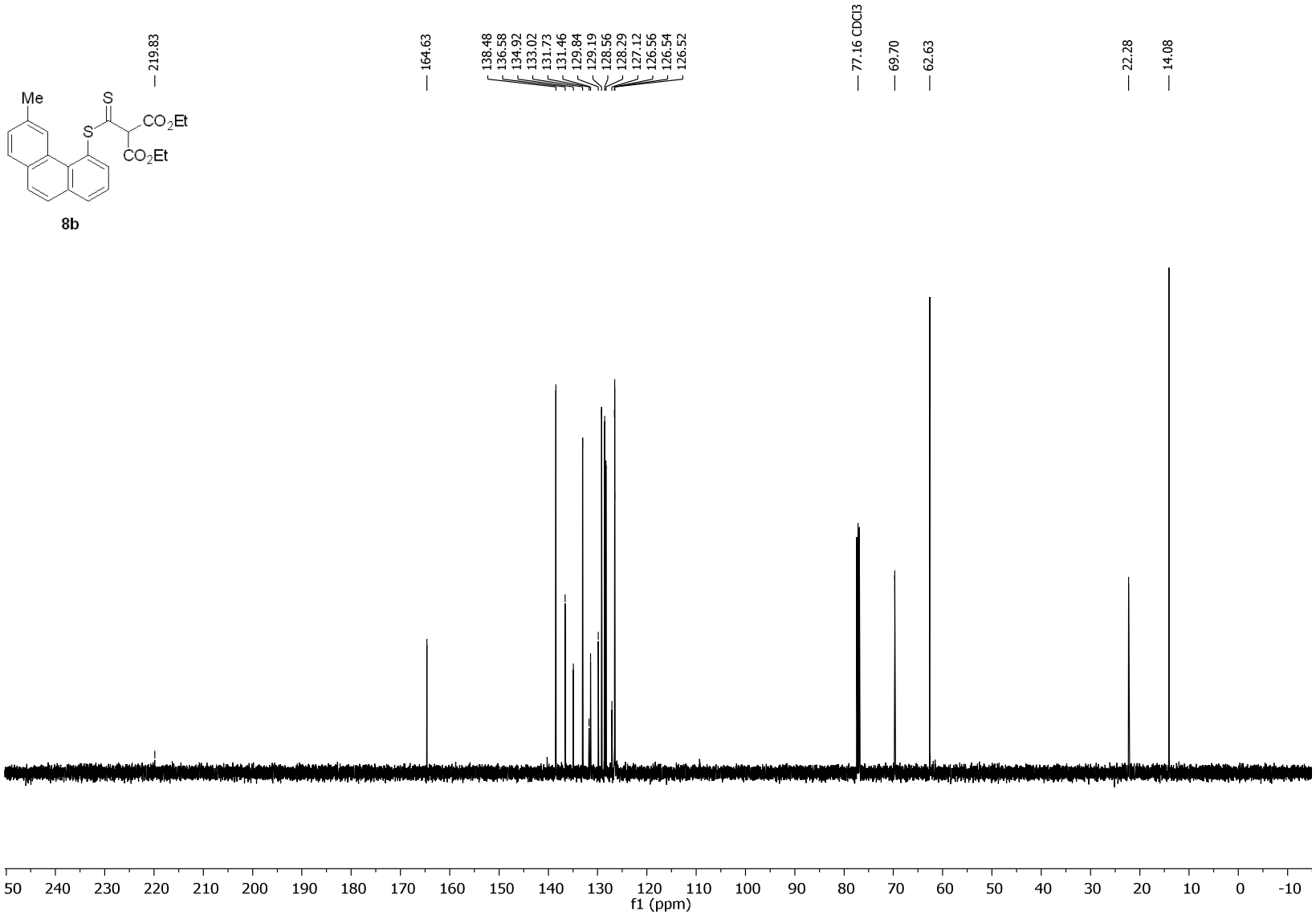

Figure S73. $^{13}C\{^{1}H\}$ NMR spectrum (126 MHz, $CDCl_3$) of **8b**.

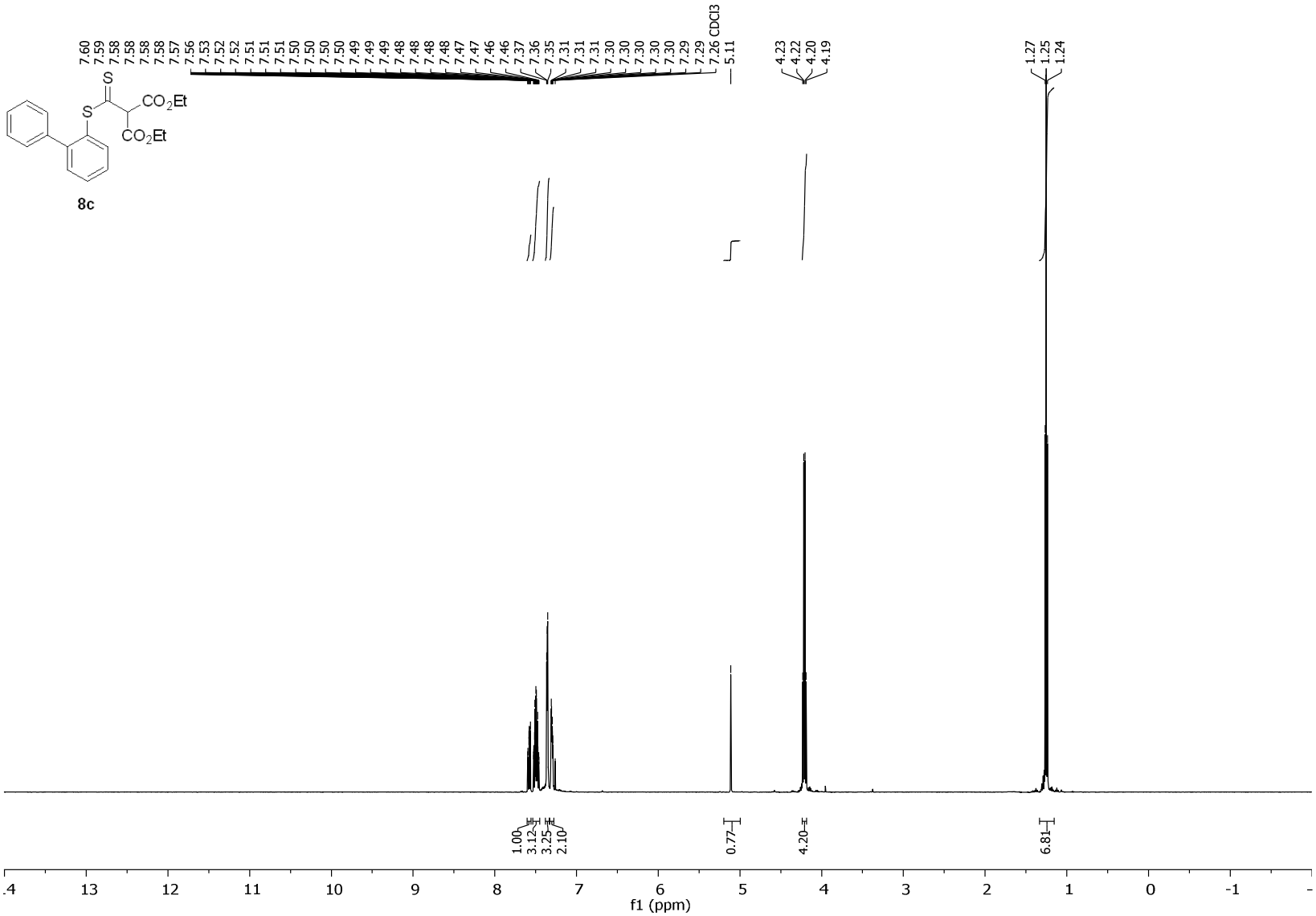

Figure S74. ^{1}H NMR spectrum (500 MHz, $CDCl_3$) of **8c**.

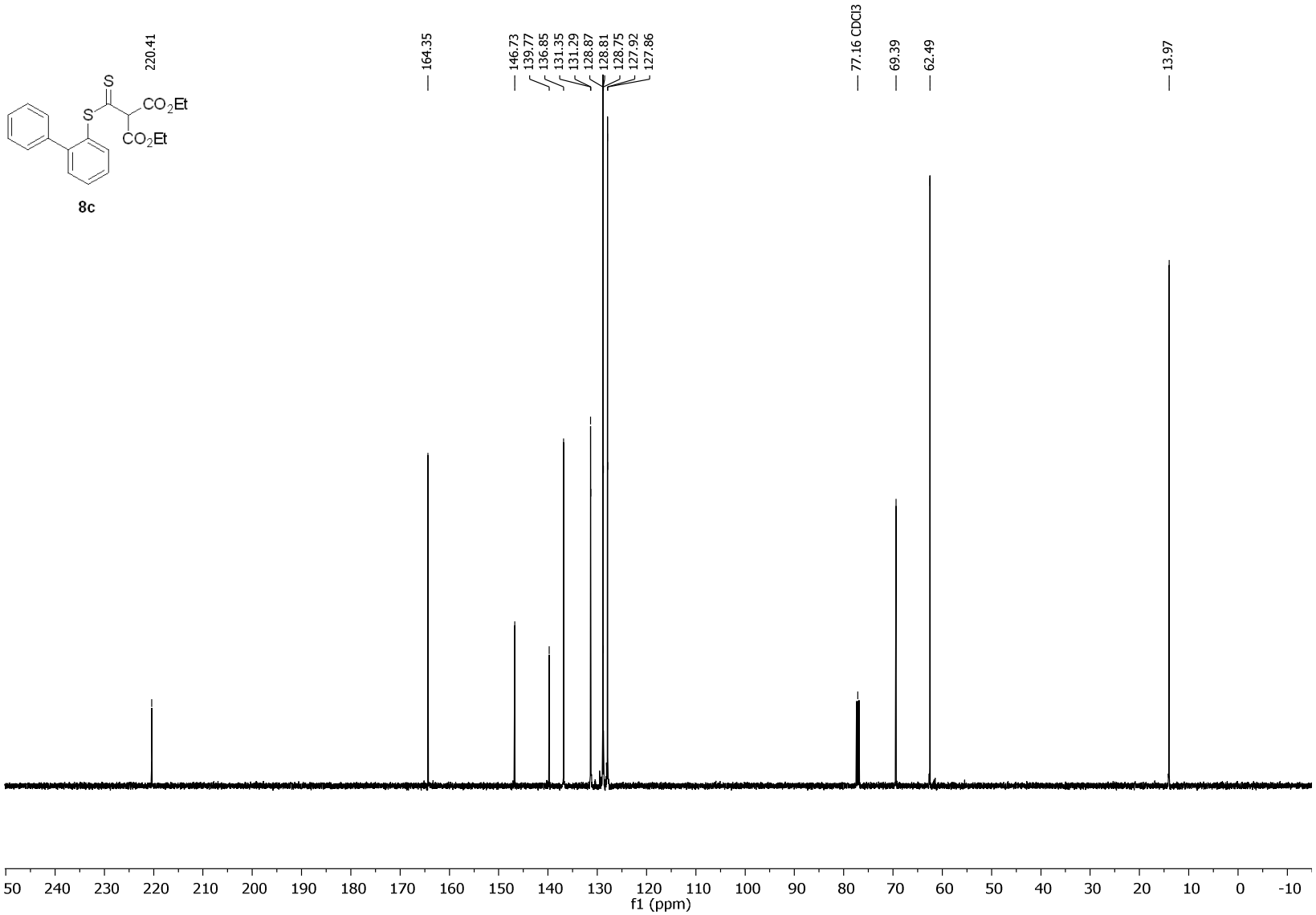

Figure S75. $^{13}C\{^{1}H\}$ NMR spectrum (126 MHz, $CDCl_3$) of **8c**.

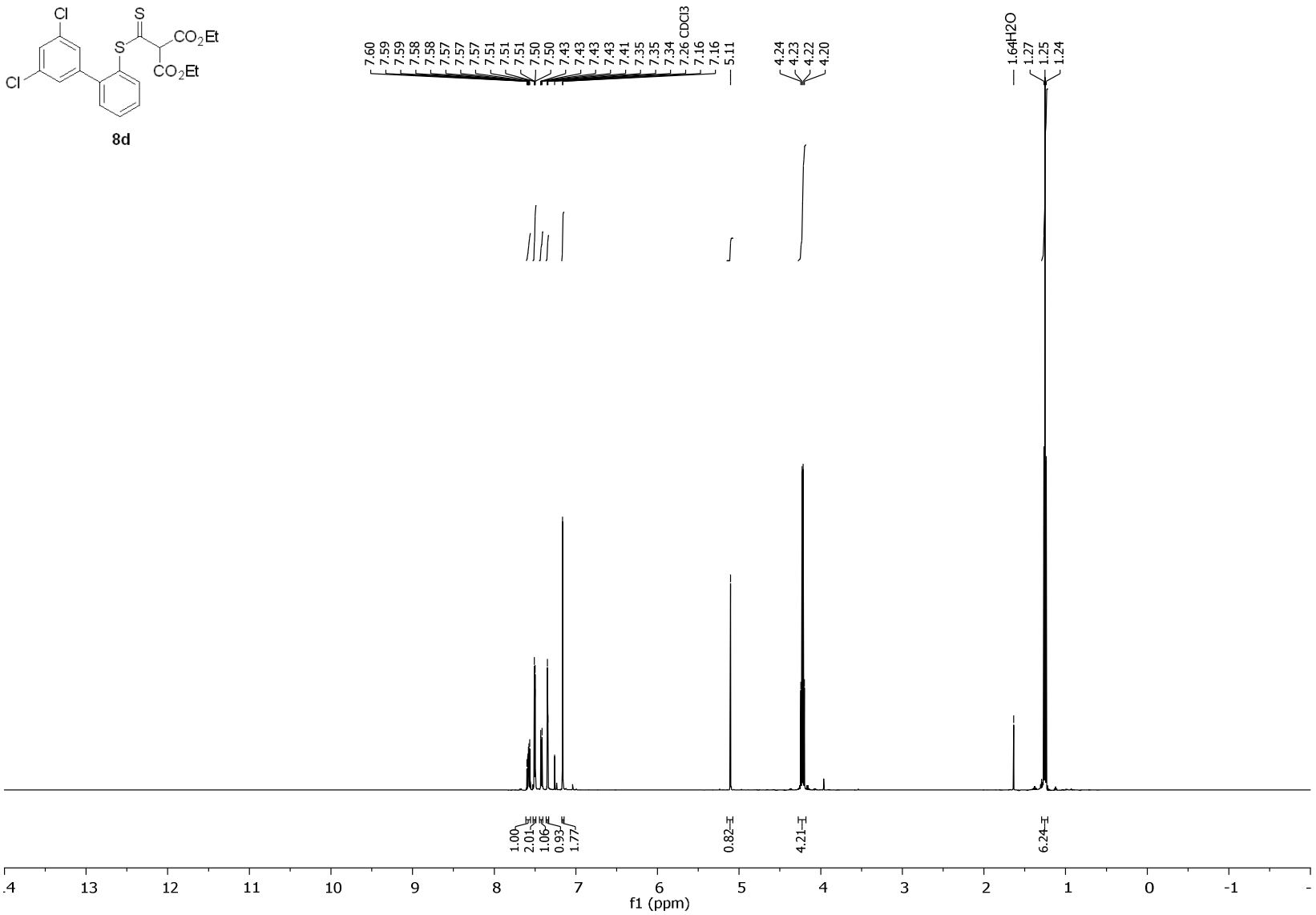

Figure S76. ^{1}H NMR spectrum (500 MHz, $CDCl_3$) of **8d**.

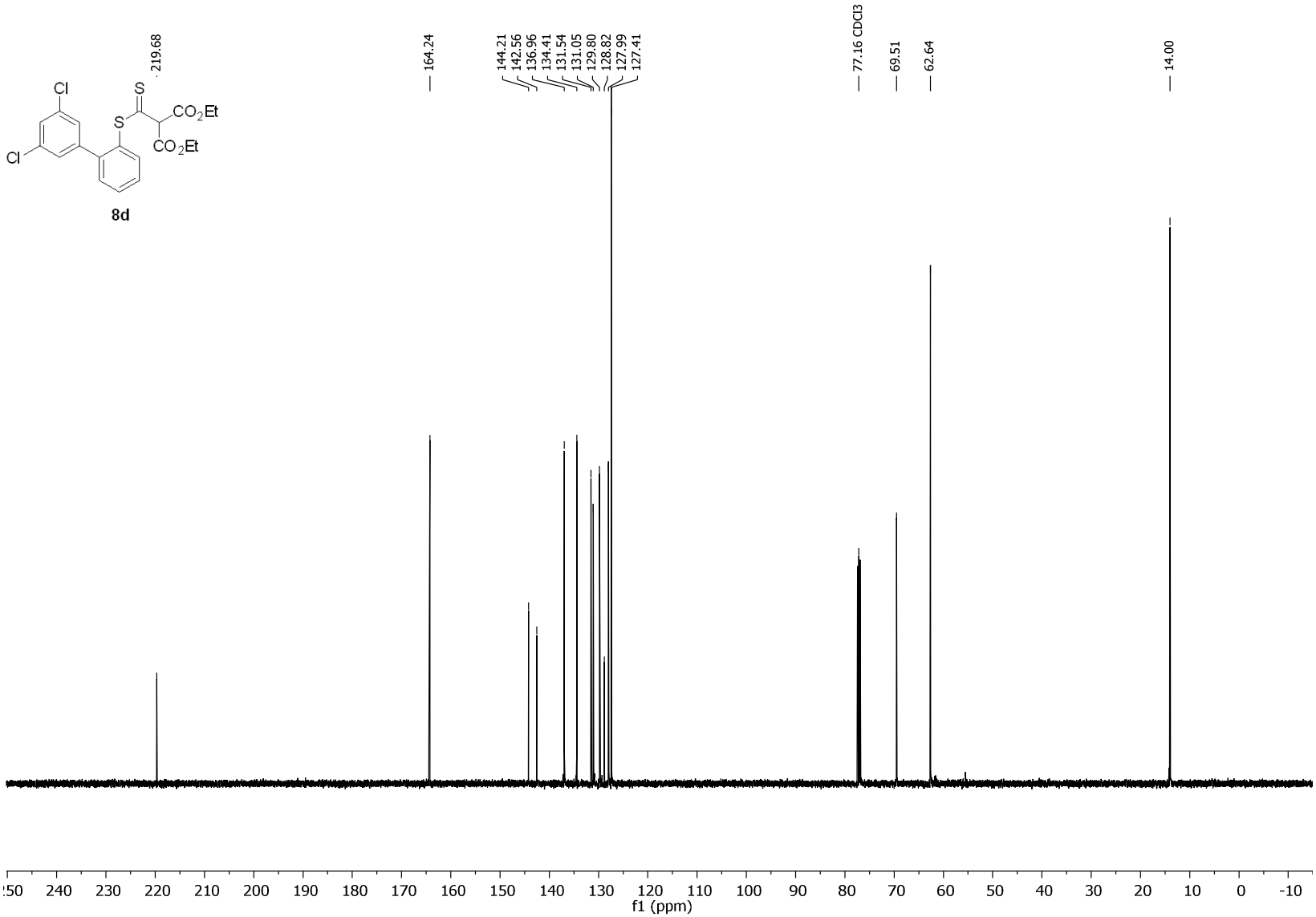

Figure S77. $^{13}C\{^{1}H\}$ NMR spectrum (126 MHz, $CDCl_3$) of **8d**.

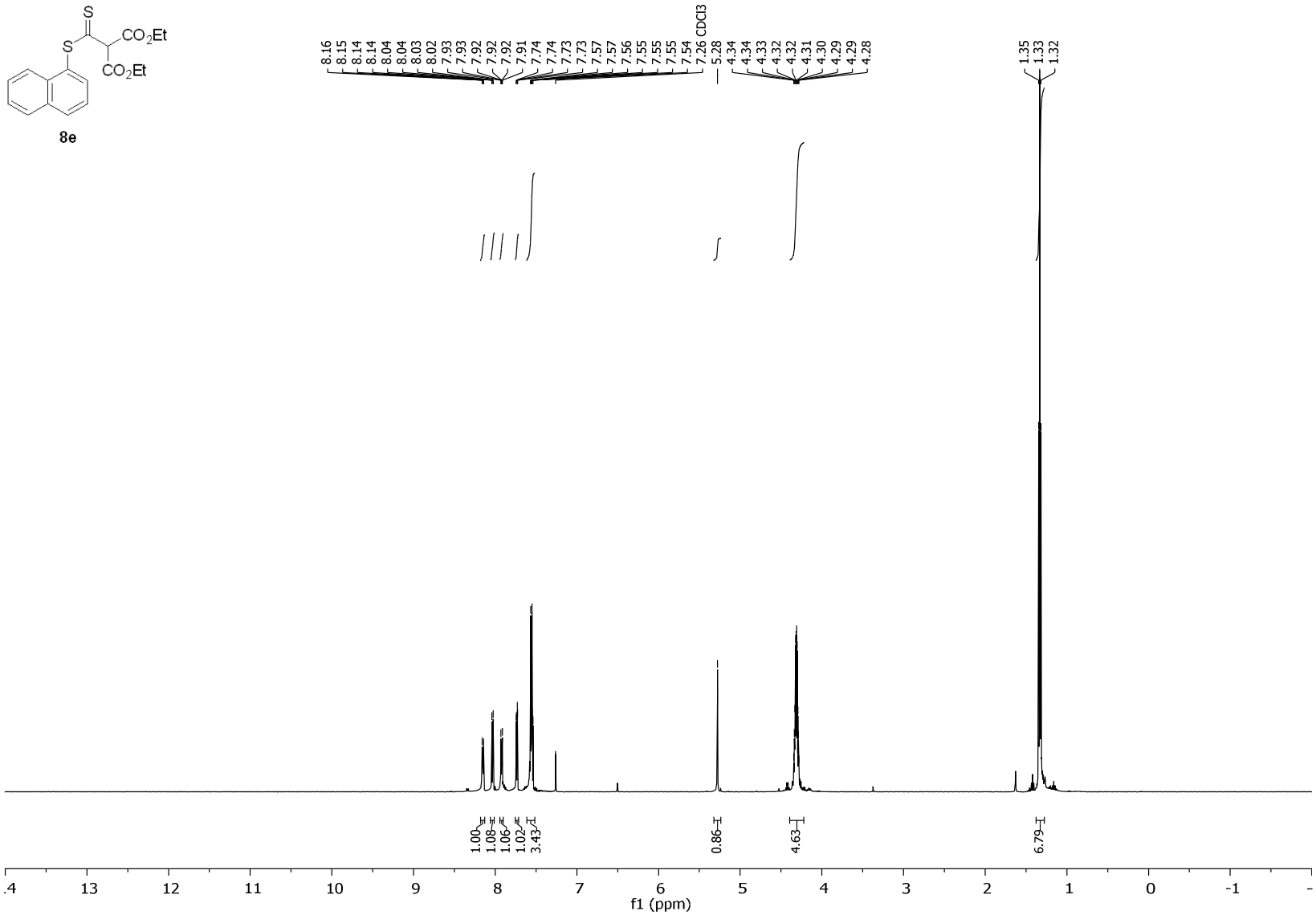

Figure S78. ^{1}H NMR spectrum (500 MHz, $CDCl_3$) of **8e**.

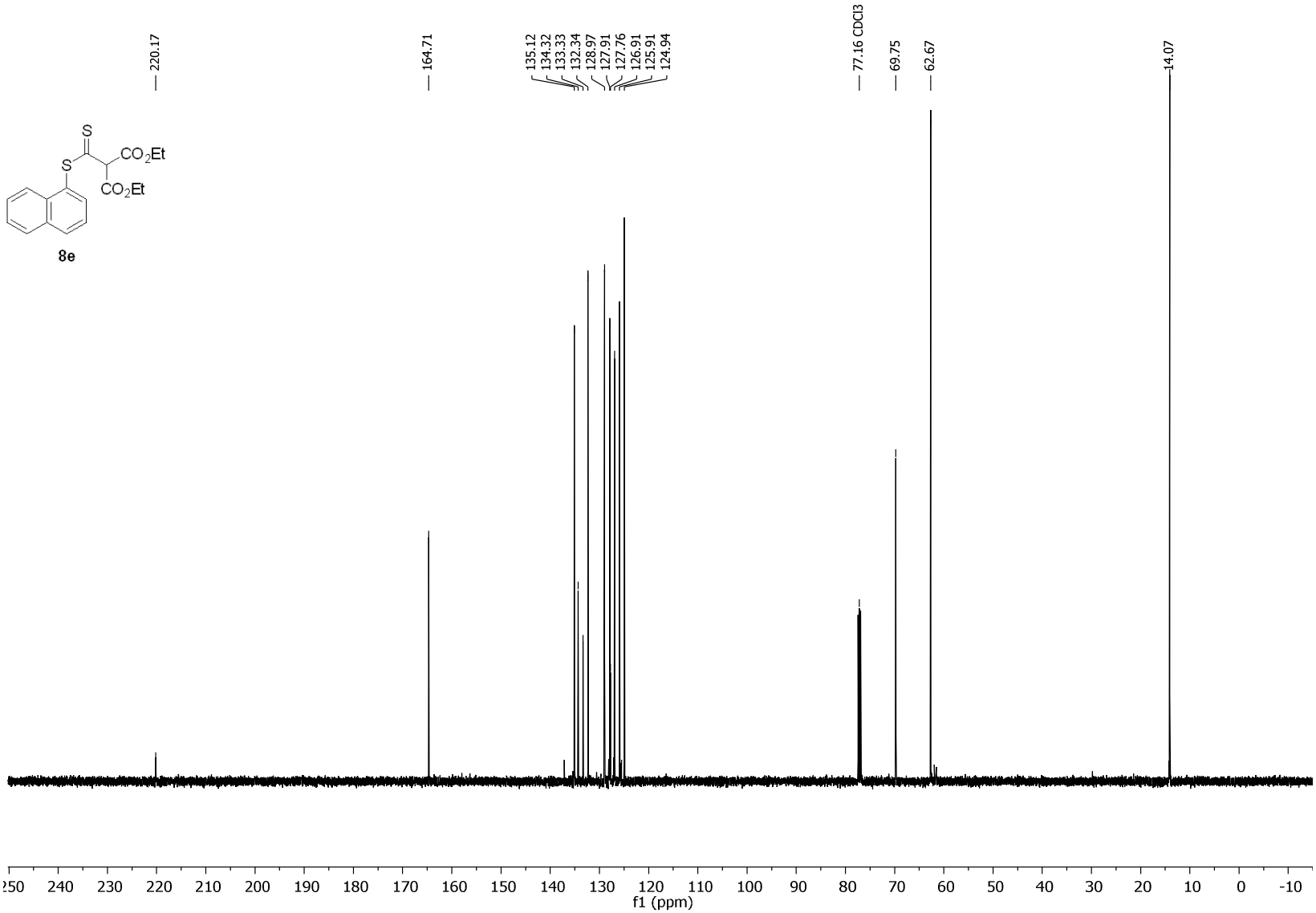

Figure S79. $^{13}C\{^{1}H\}$ NMR spectrum (126 MHz, $CDCl_3$) of **8e**.

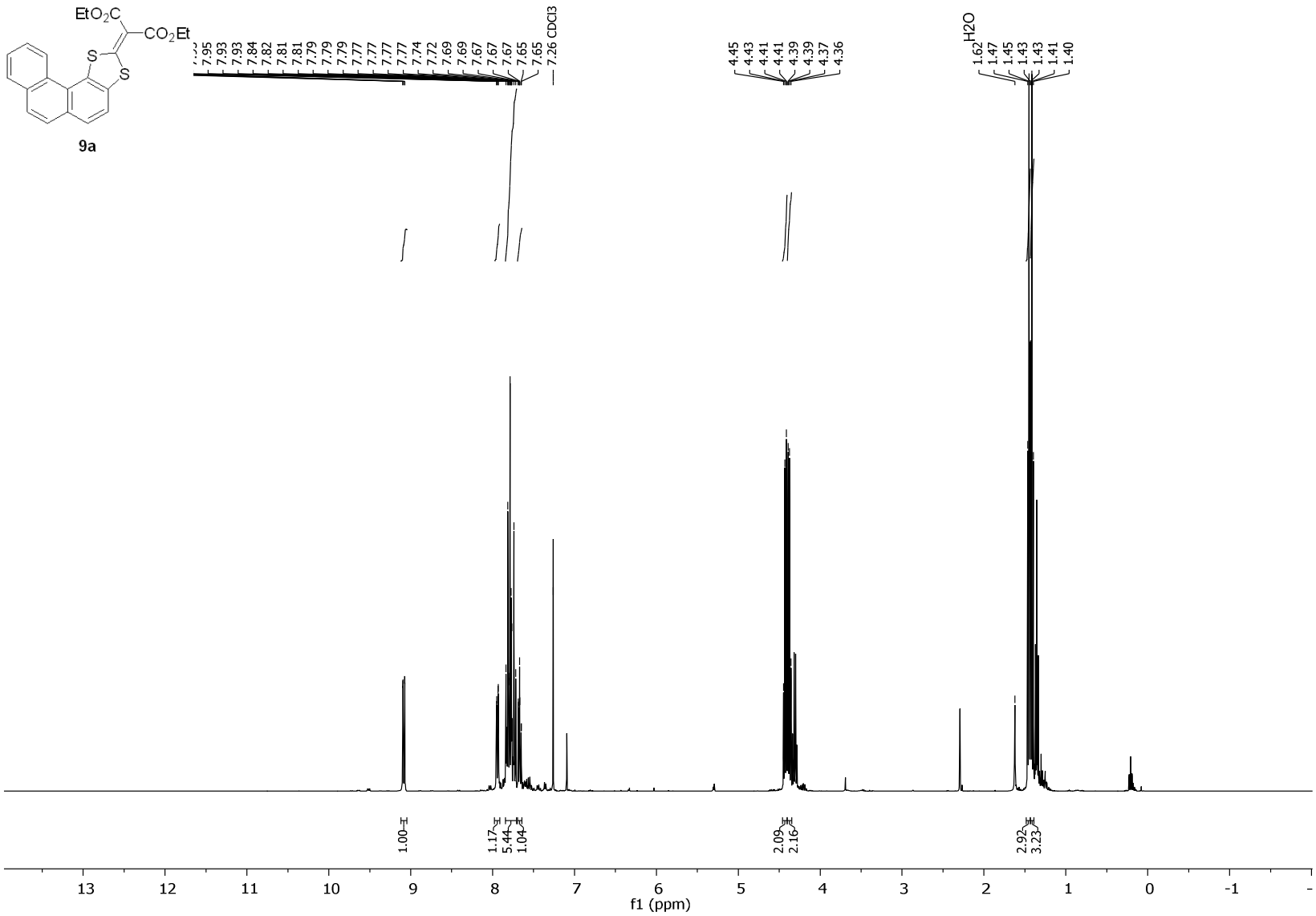

Figure S80. ^{1}H NMR spectrum (400 MHz, $CDCl_3$) of **9a**.

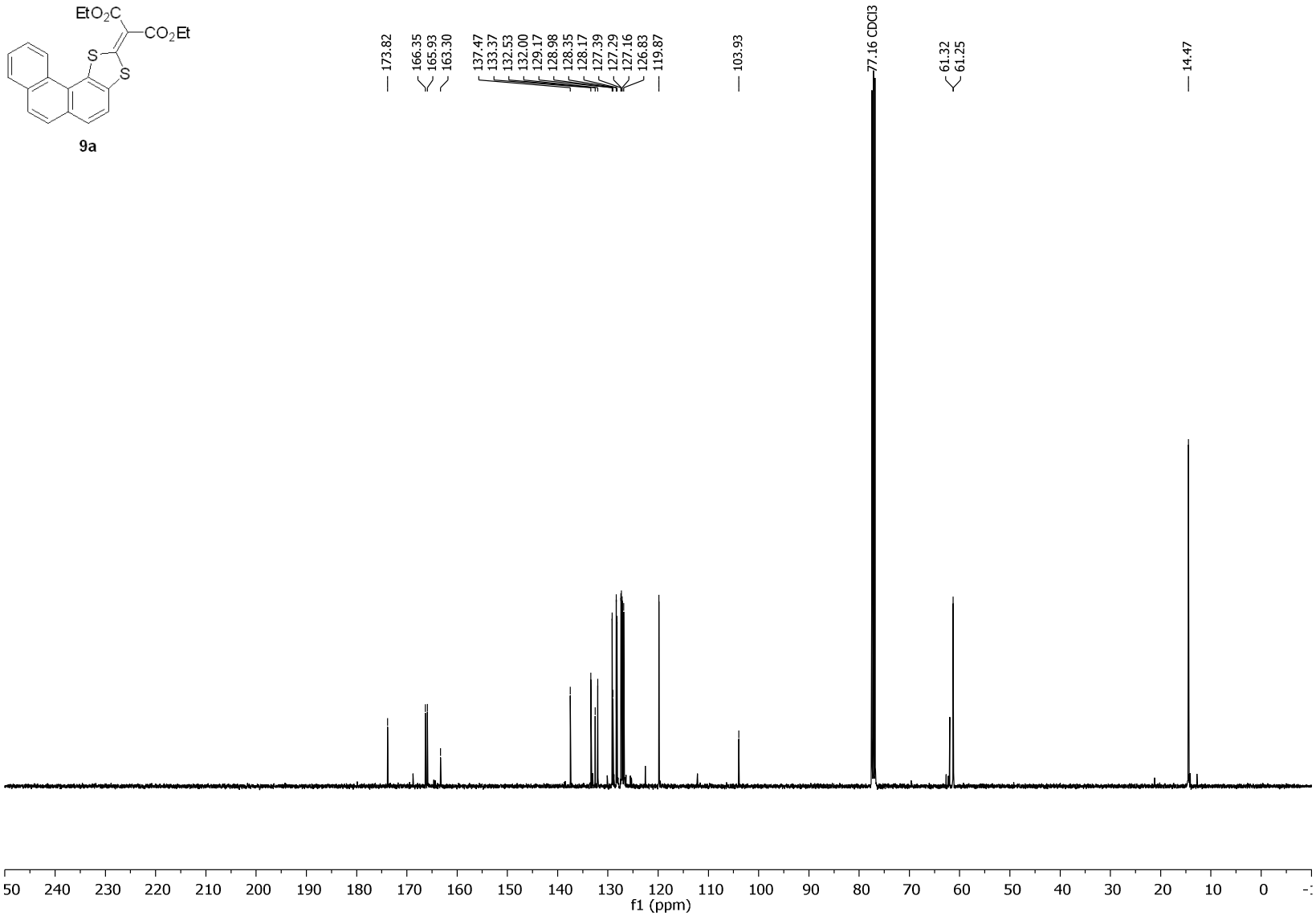

Figure S81. $^{13}C\{^{1}H\}$ NMR spectrum (101 MHz, $CDCl_3$) of **9a**.

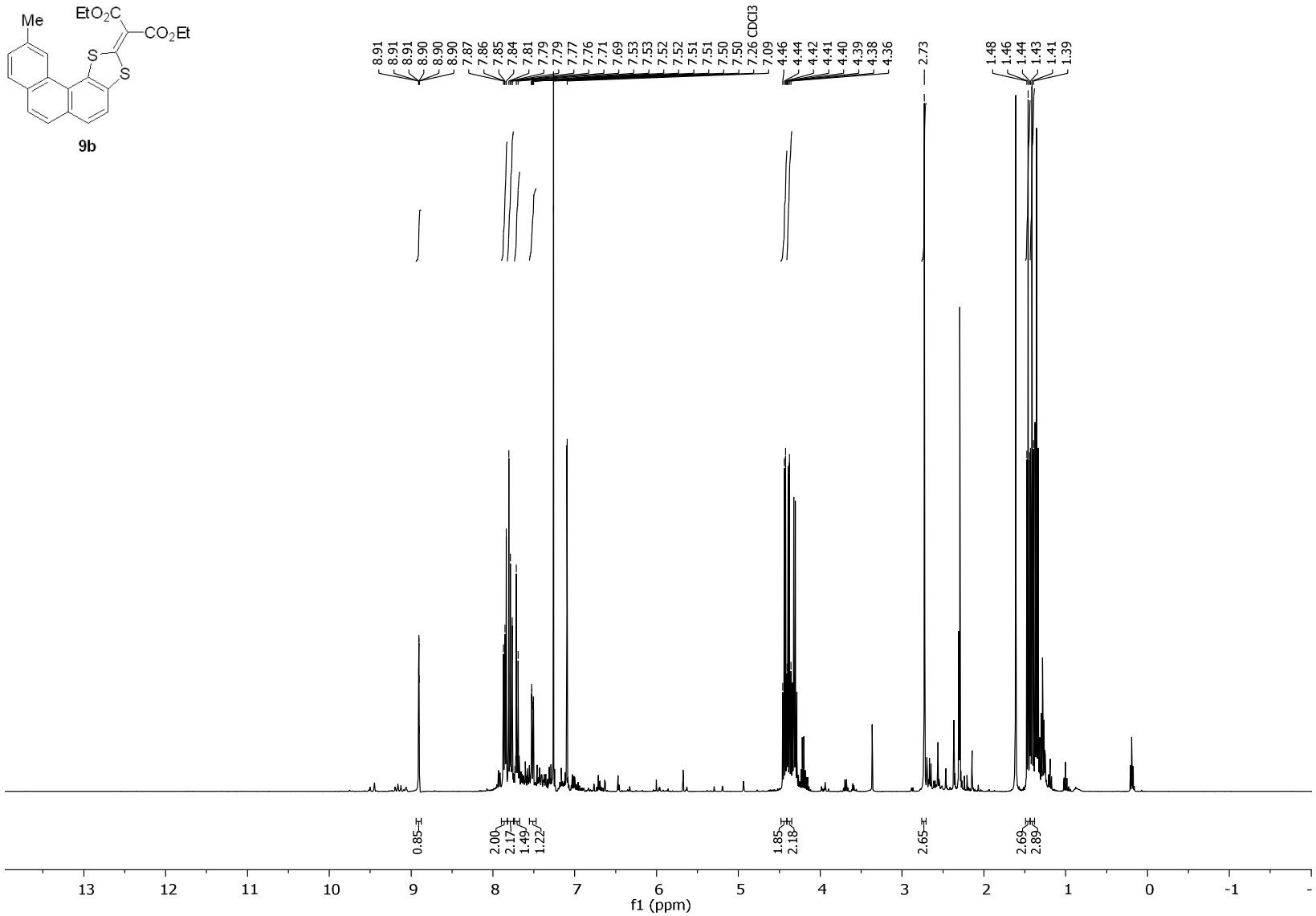

Figure S82. ^{1}H NMR spectrum (400 MHz, $CDCl_3$) of **9b**.

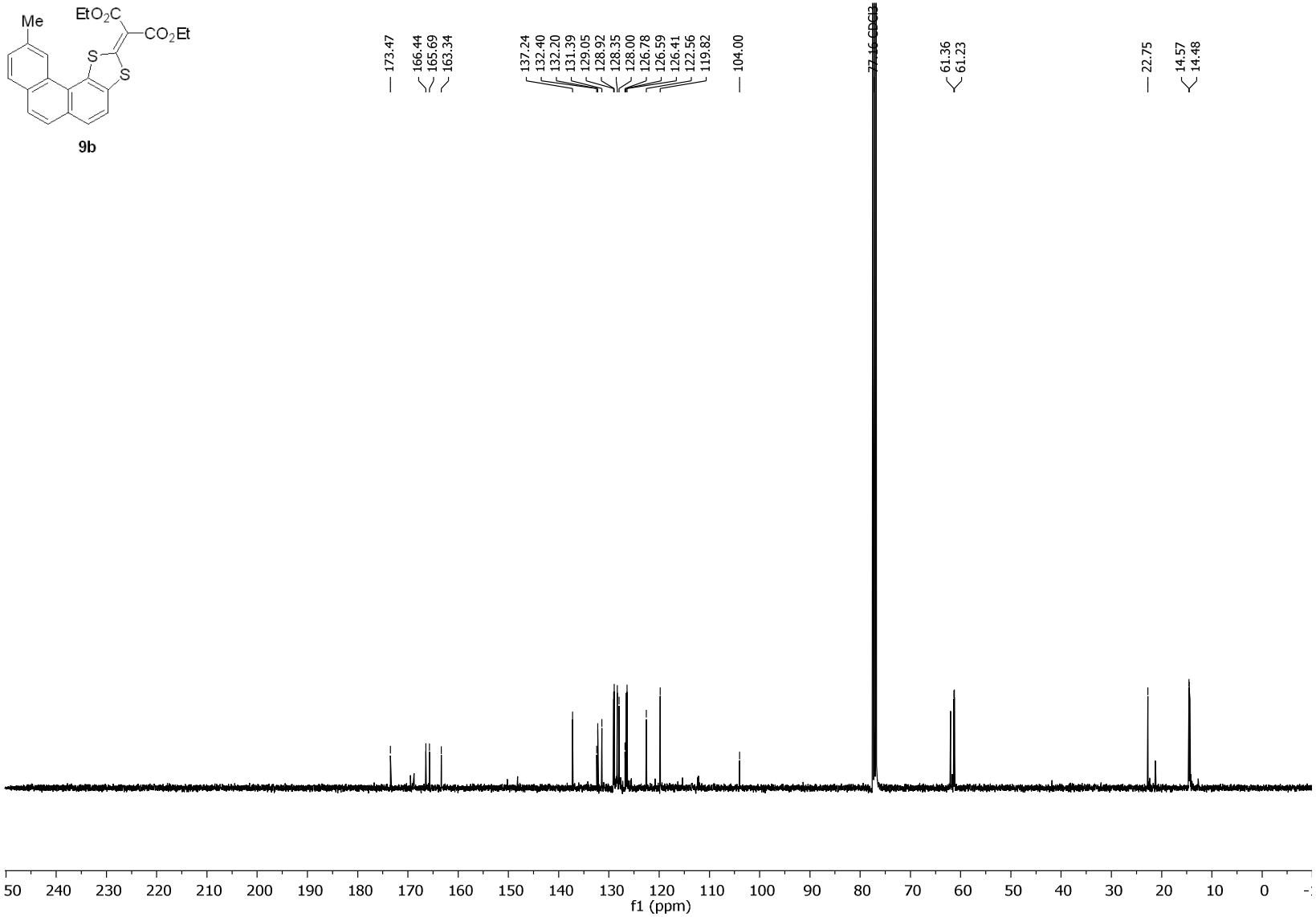

Figure S83. $^{13}C\{^{1}H\}$ NMR spectrum (101 MHz, $CDCl_3$) of **9b**.

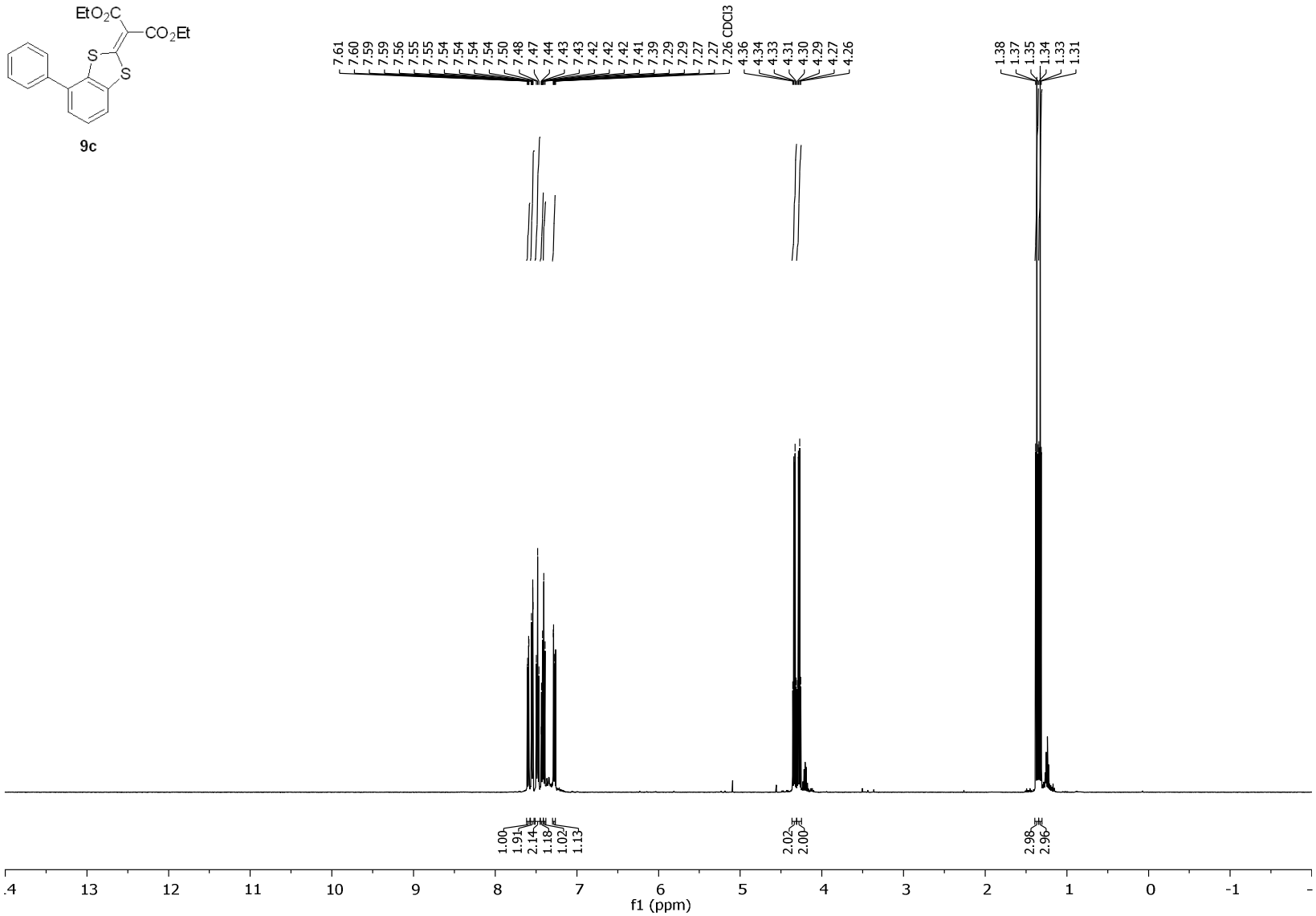

Figure S84. ^{1}H NMR spectrum (500 MHz, $CDCl_3$) of **9c**.

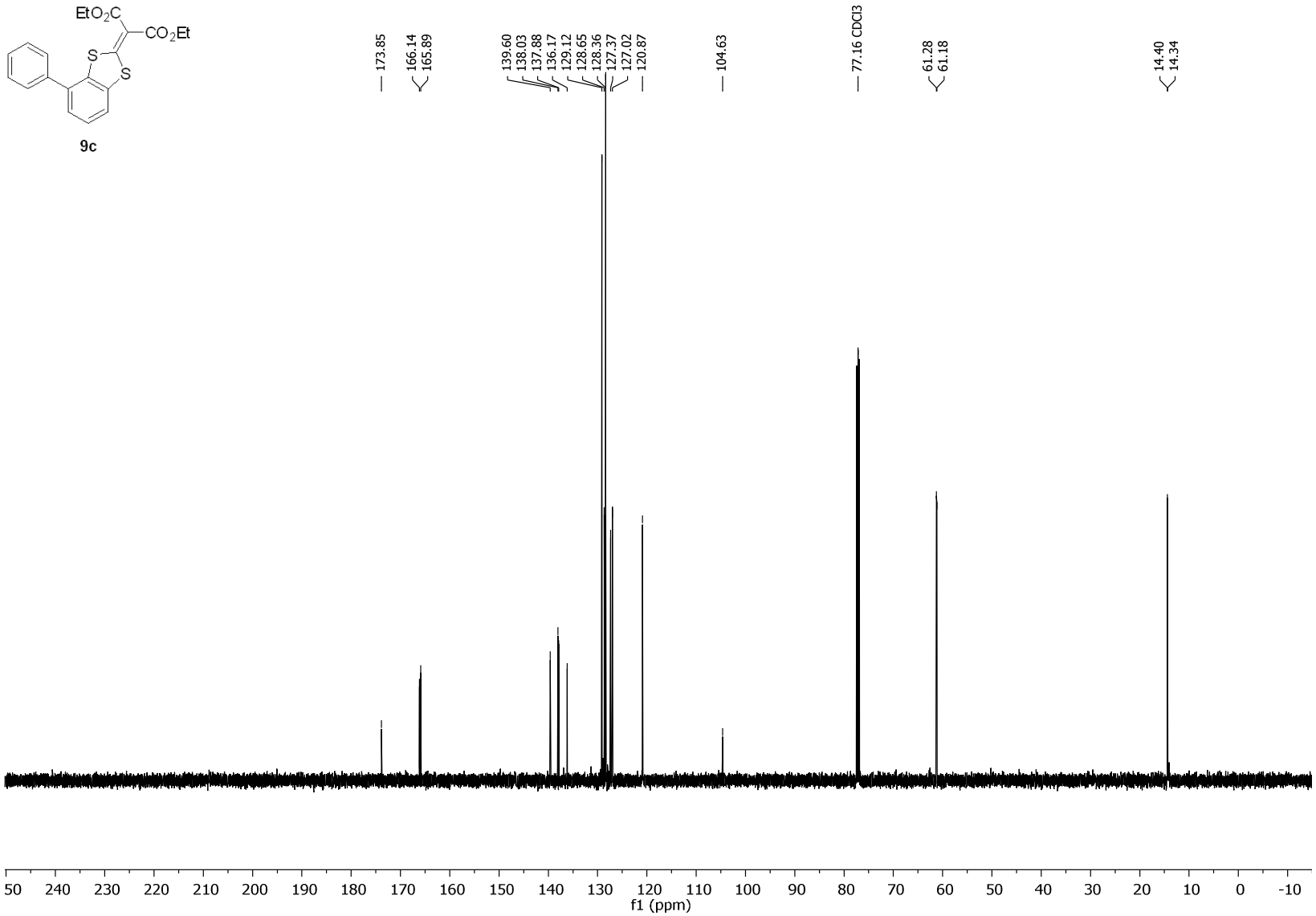

Figure S85. $^{13}C\{^{1}H\}$ NMR spectrum (126 MHz, $CDCl_3$) of **9c**.

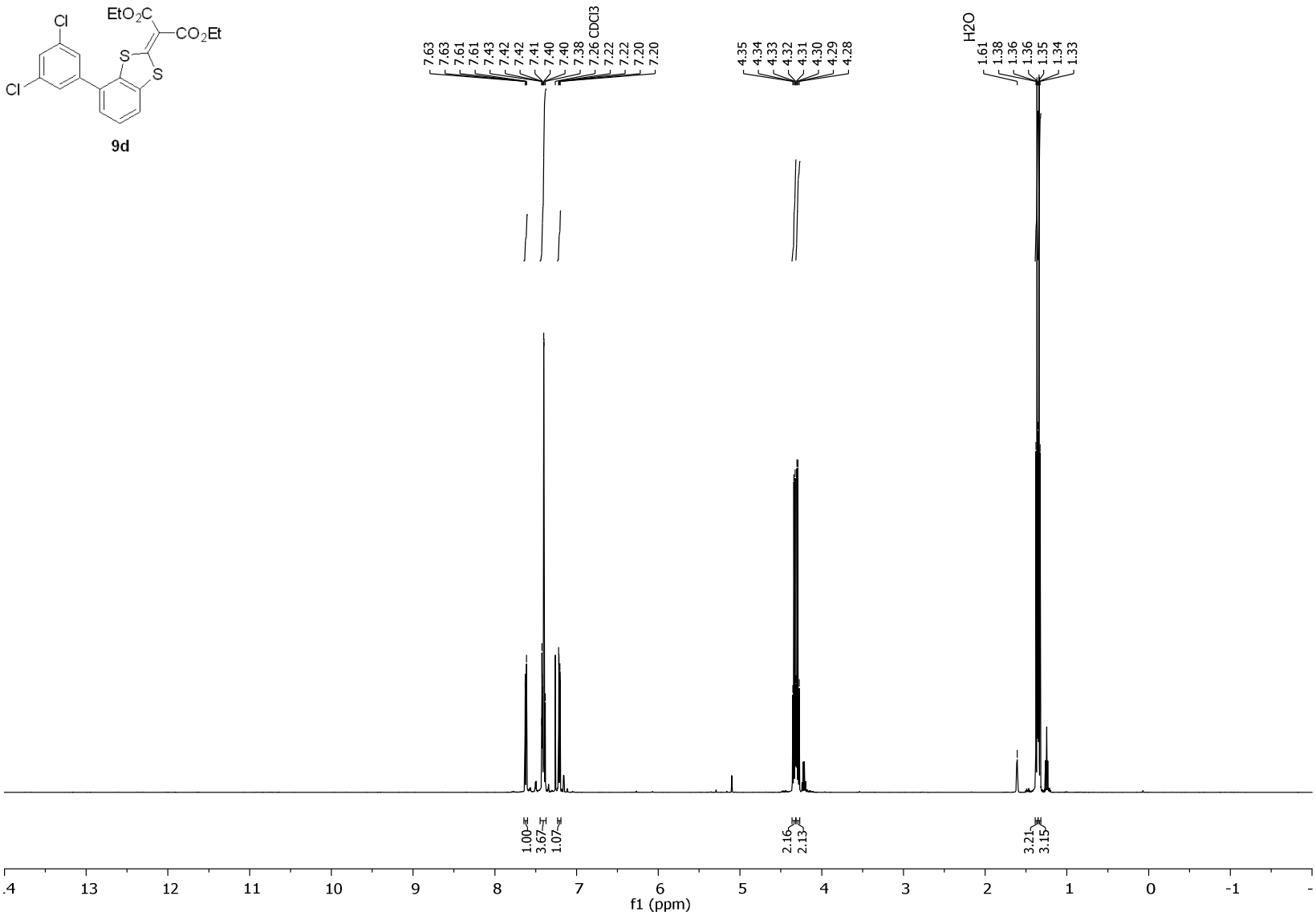

Figure S86. ^{1}H NMR spectrum (500 MHz, $CDCl_3$) of **9d**.

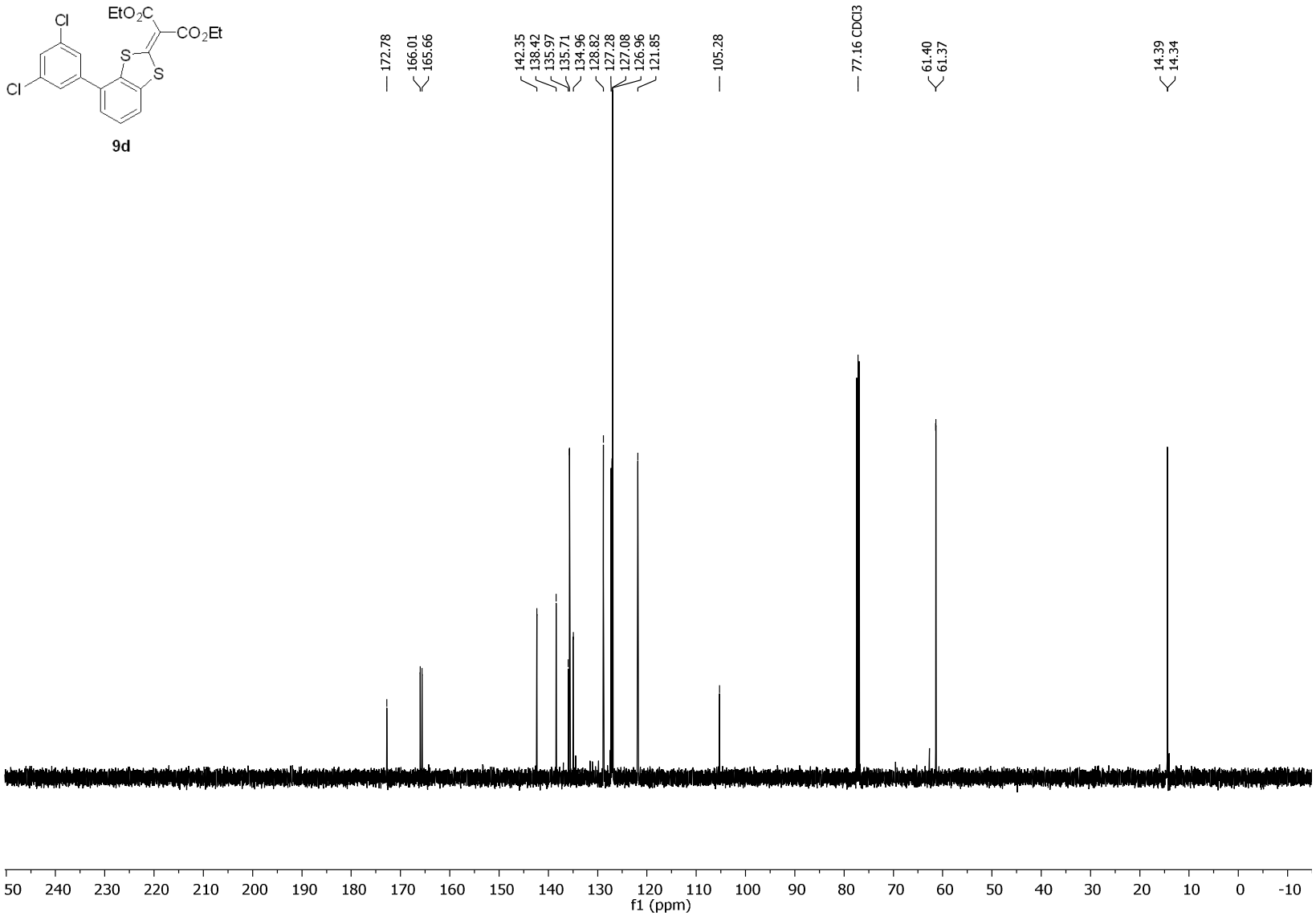

Figure S87. $^{13}C\{^{1}H\}$ NMR spectrum (126 MHz, $CDCl_3$) of **9d**.

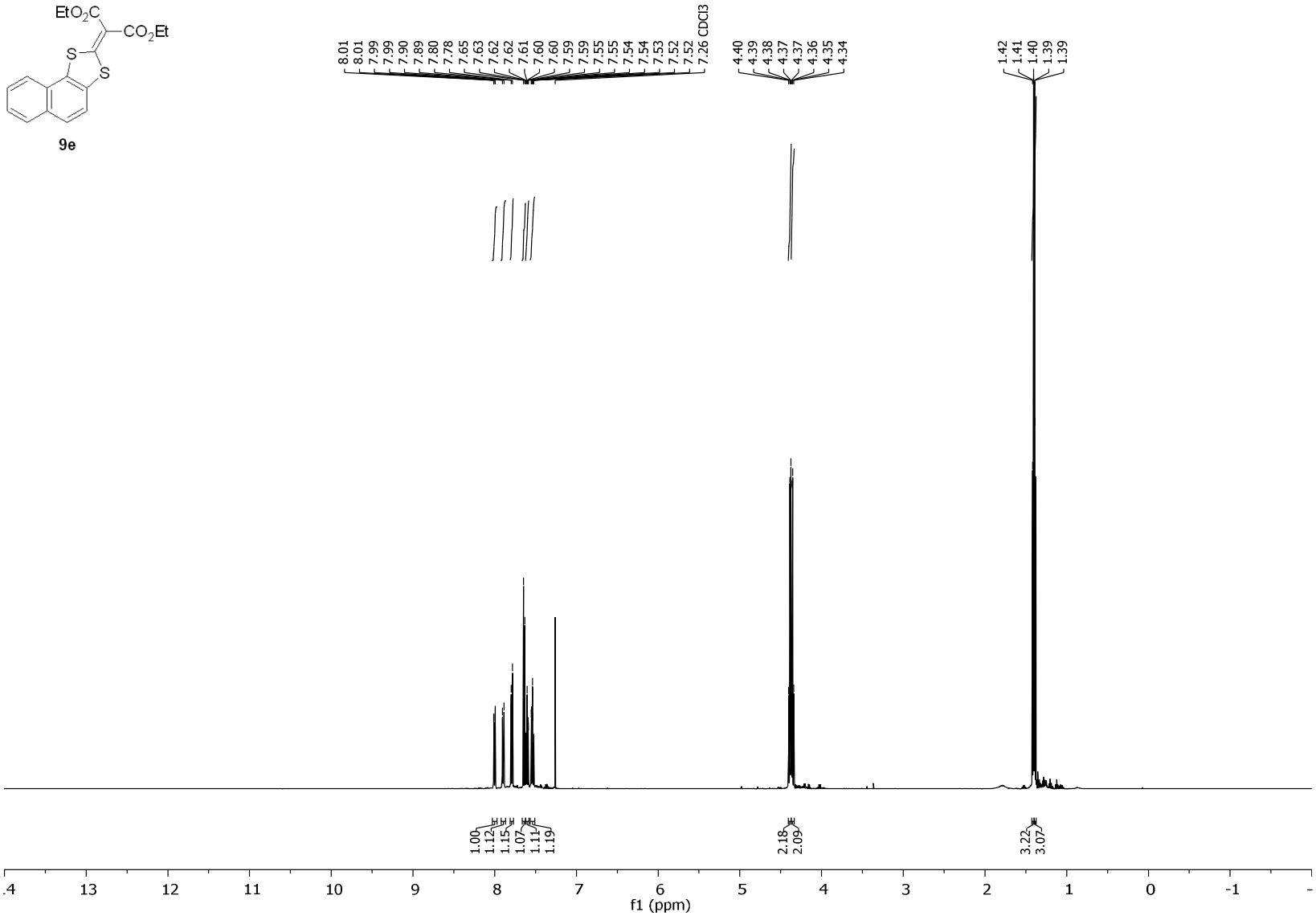

Figure S88. ^{1}H NMR spectrum (500 MHz, $CDCl_3$) of **9e**.

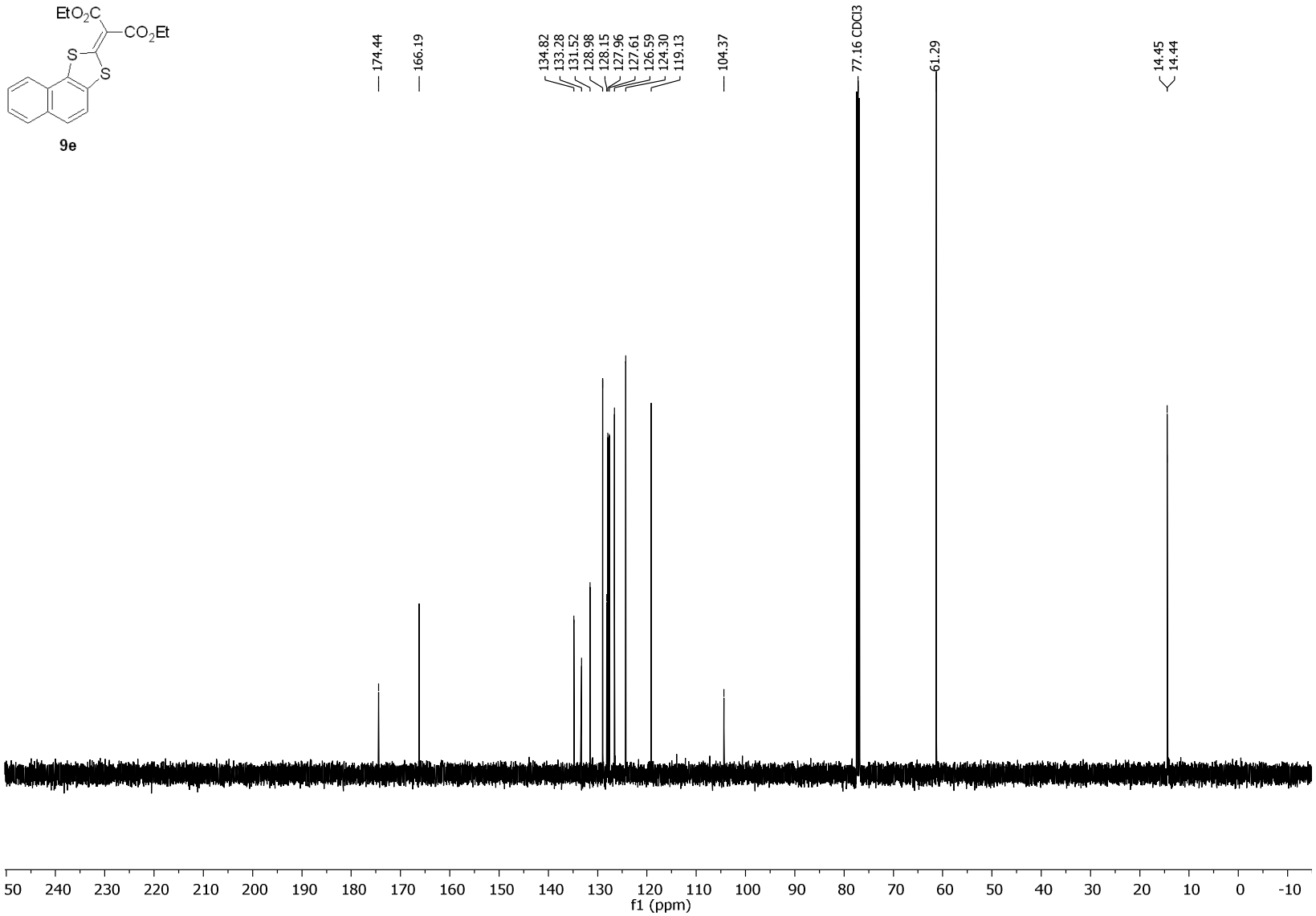

Figure S89. $^{13}C\{^{1}H\}$ NMR spectrum (126 MHz, $CDCl_3$) of **9e**.

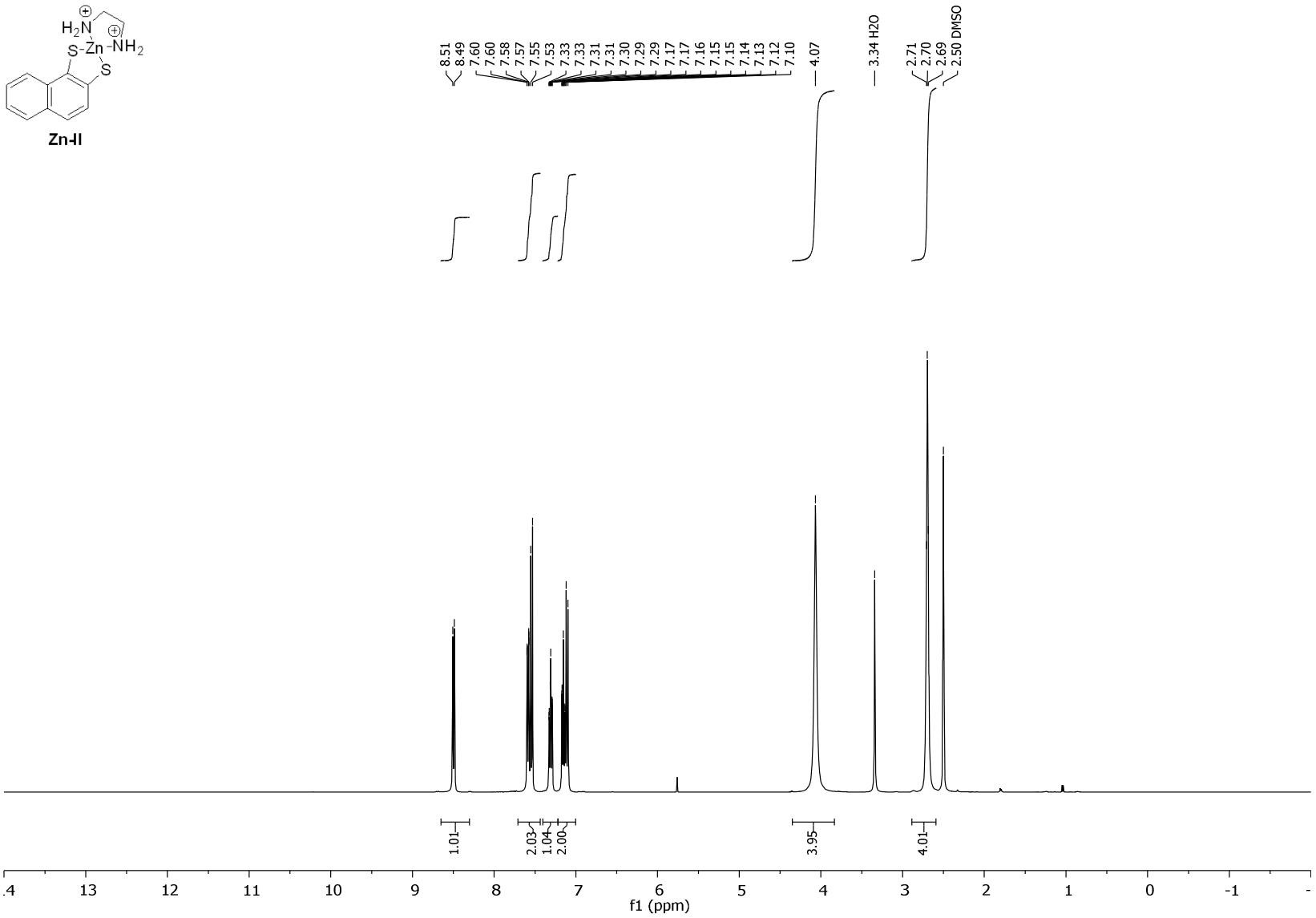

Figure S90. ^{1}H NMR spectrum (400 MHz, DMSO-d_6) of **Zn-II**.

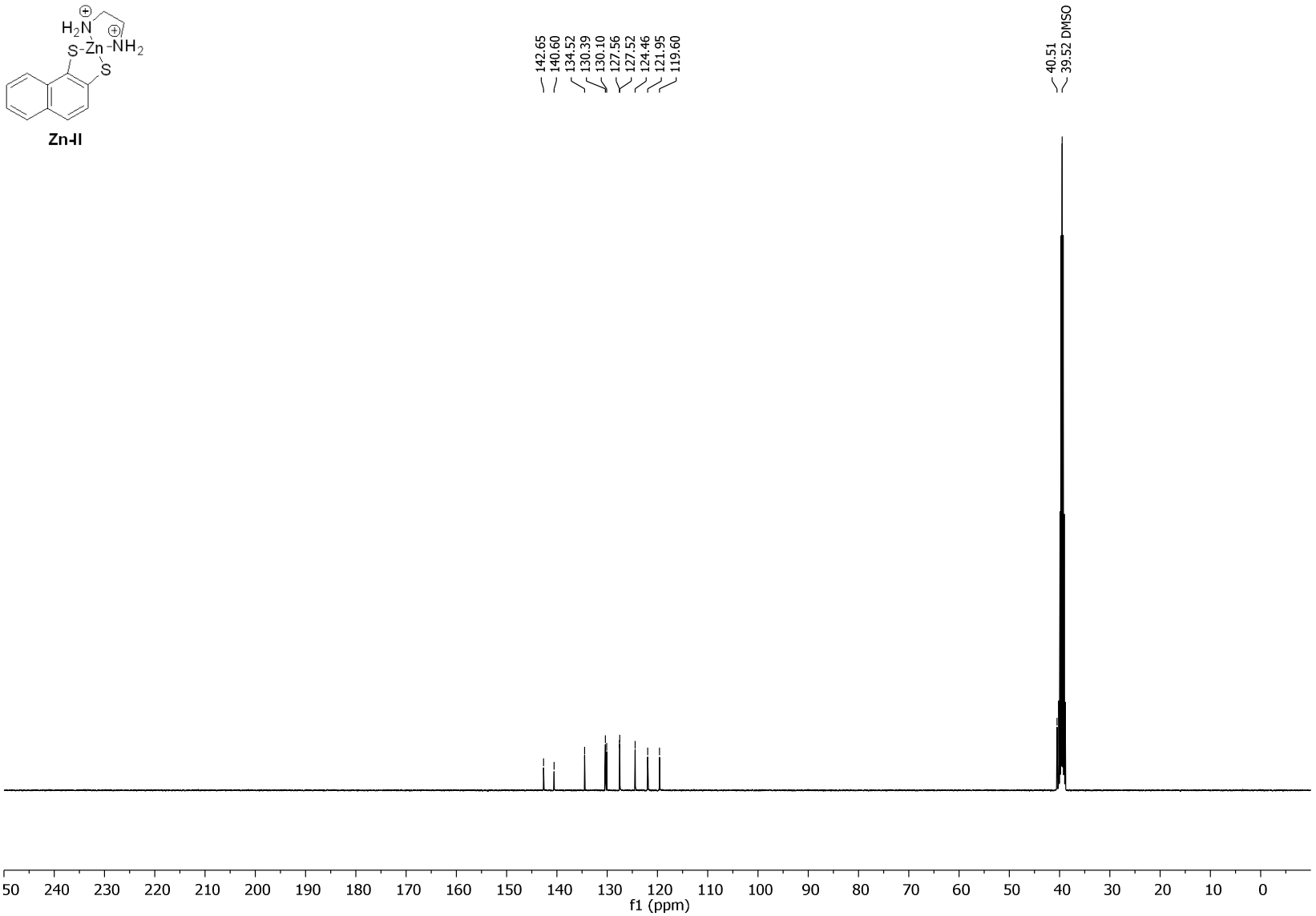

Figure S91. $^{13}C\{^{1}H\}$ NMR spectrum (101 MHz, DMSO-d_6) of **Zn-II**.

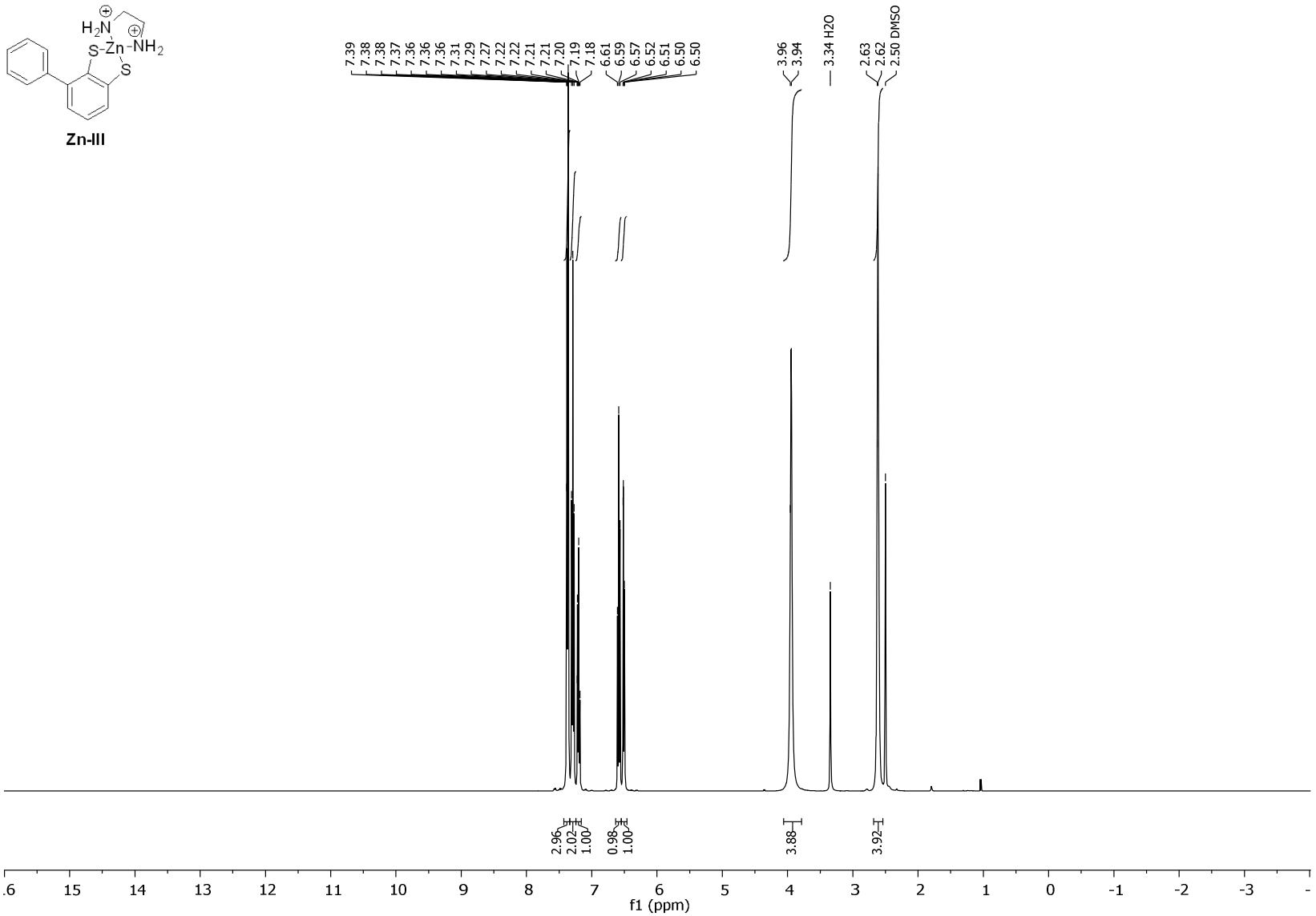

Figure S92. ^{1}H NMR spectrum (400 MHz, DMSO-d_6) of **Zn-III**.

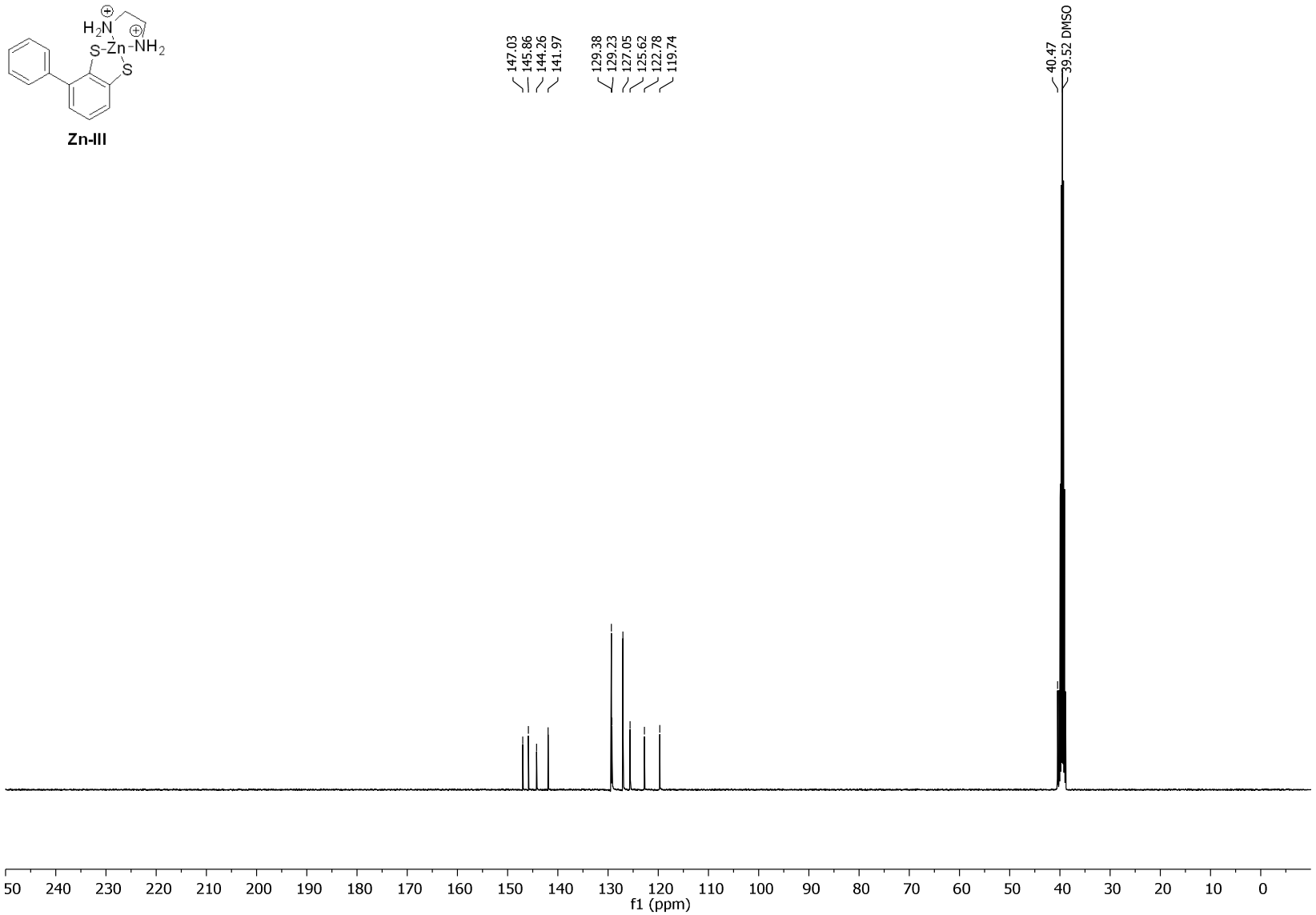

Figure S93. $^{13}C\{^{1}H\}$ NMR spectrum (101 MHz, DMSO-d_6) of **Zn-III**.

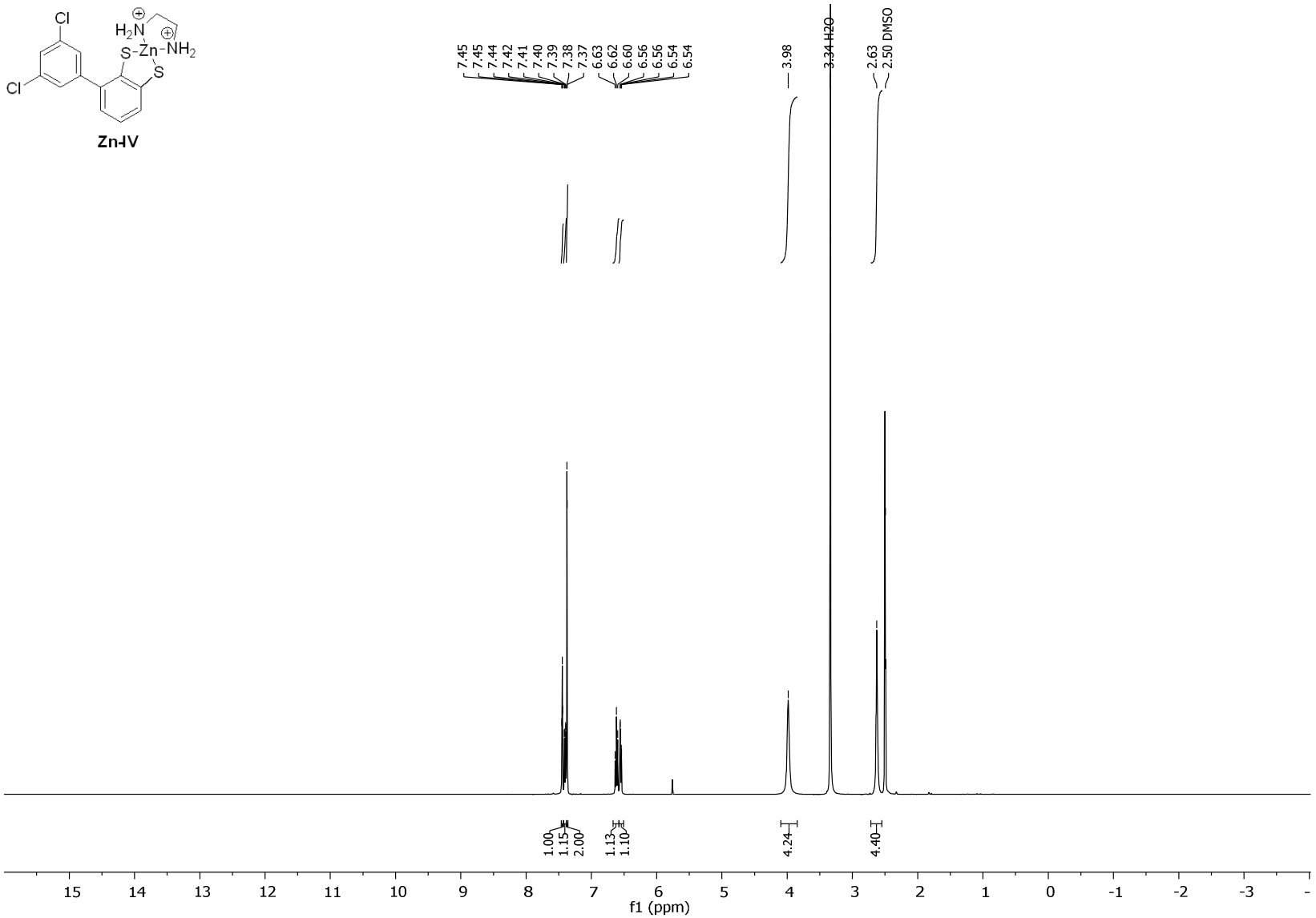

Figure S94. ^{1}H NMR spectrum (400 MHz, DMSO-d_6) of **Zn-IV**.

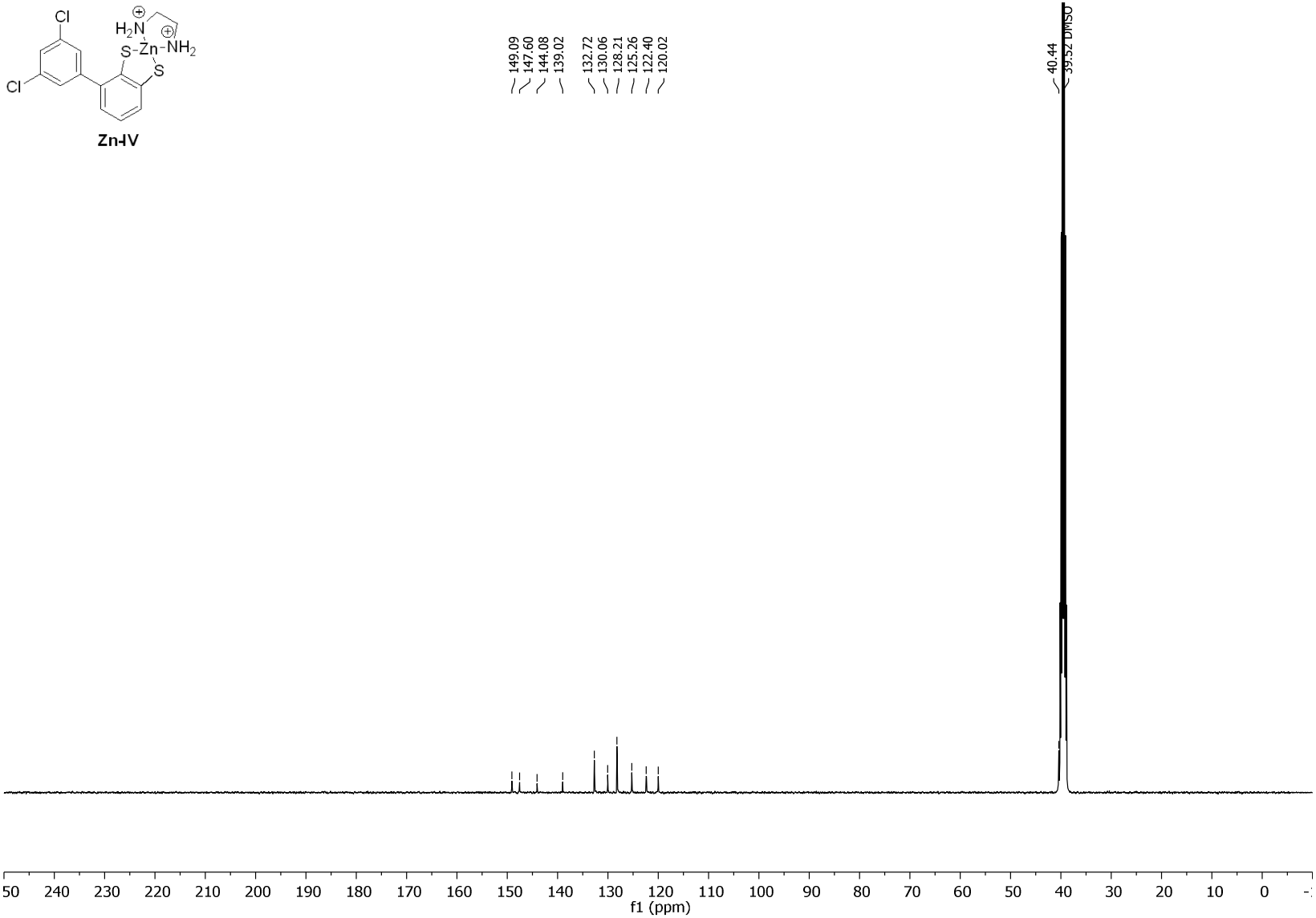

Figure S95. $^{13}C\{^{1}H\}$ NMR spectrum (101 MHz, DMSO-d_6) of **Zn-IV**.

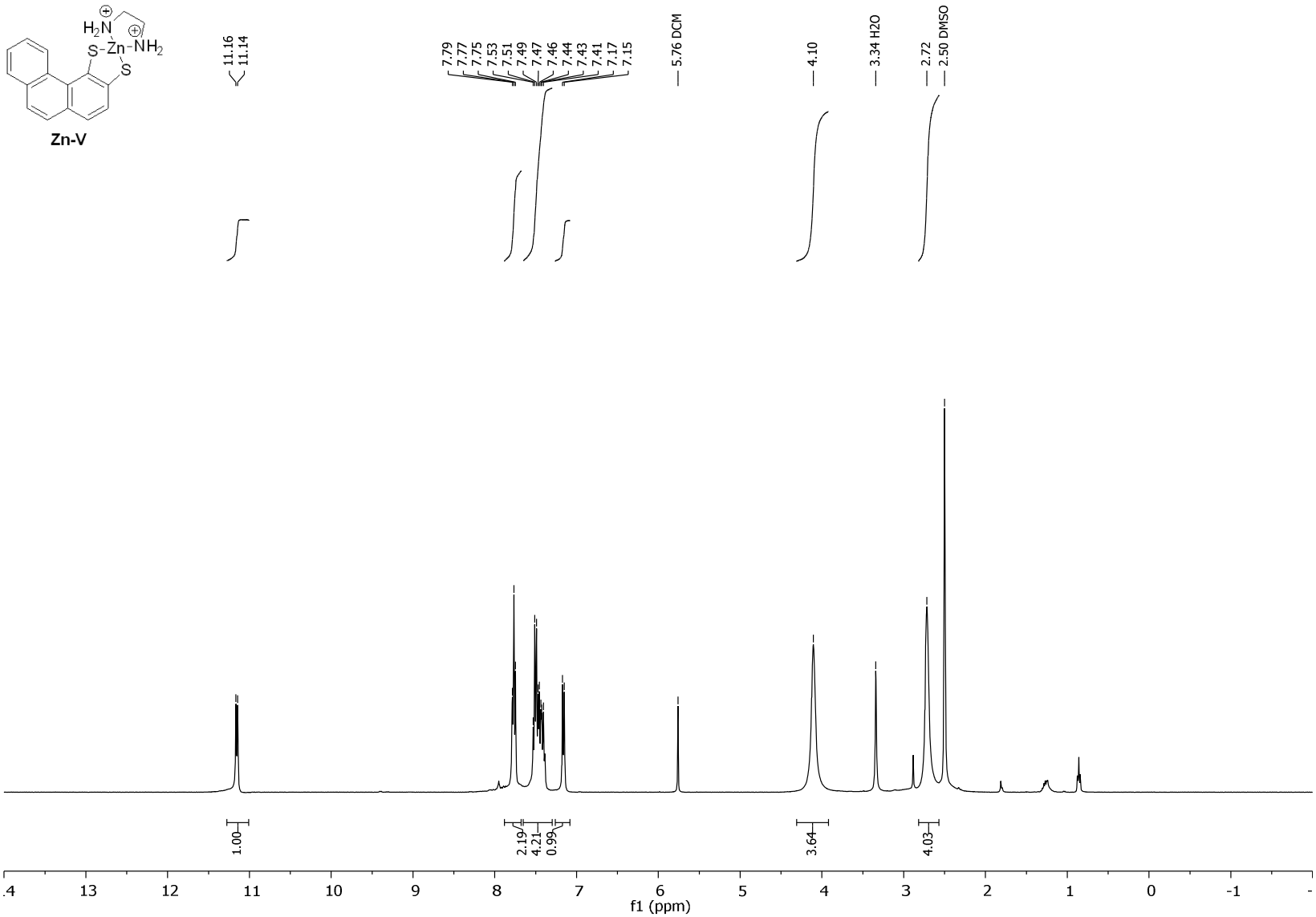

Figure S96. ^{1}H NMR spectrum (400 MHz, DMSO-d_6) of **Zn-V**.

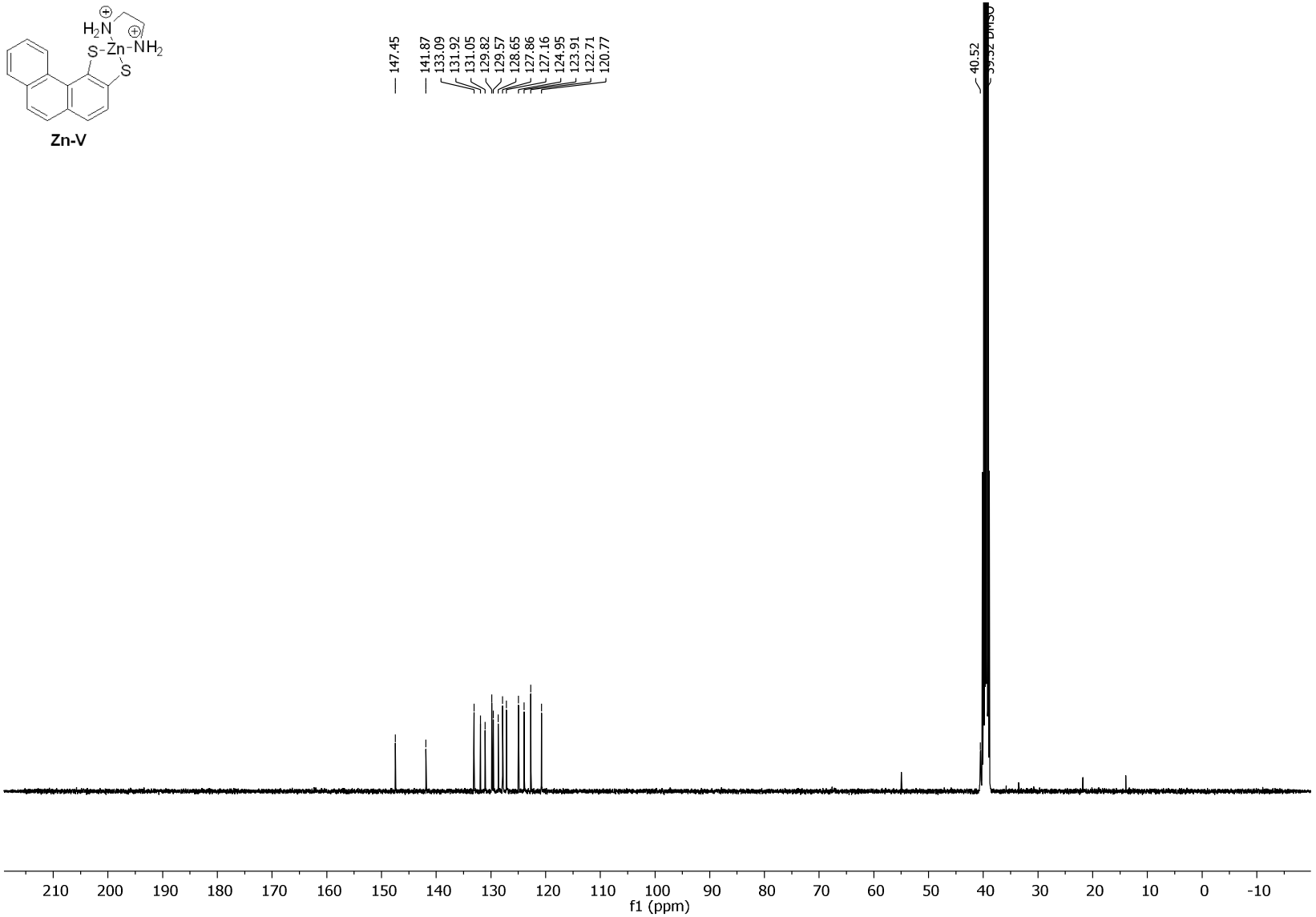

Figure S97. $^{13}C\{^{1}H\}$ NMR spectrum (101 MHz, DMSO-d_6) of **Zn-V**.

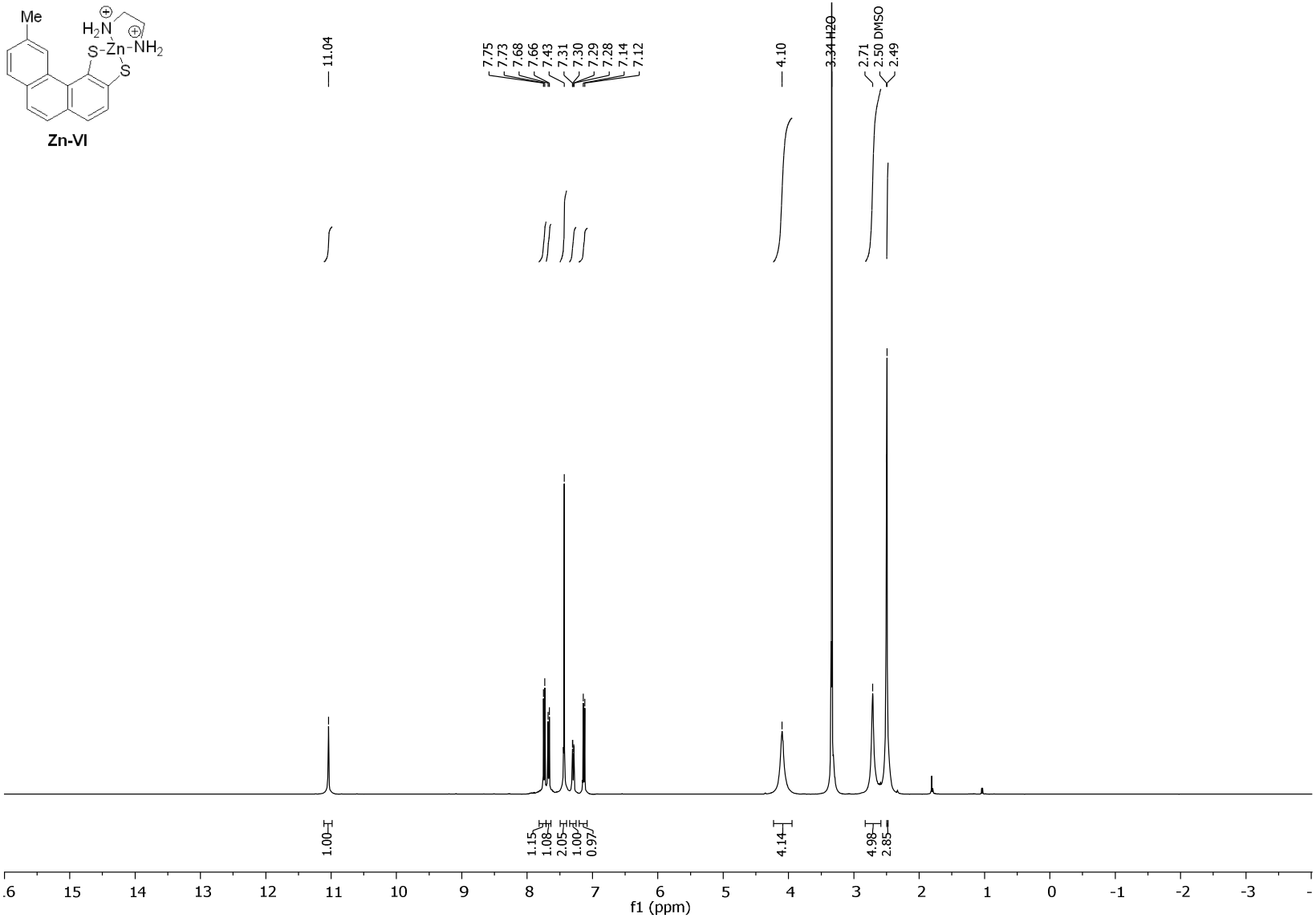

Figure S98. ^{1}H NMR spectrum (400 MHz, DMSO-d_6) of **Zn-VI**.

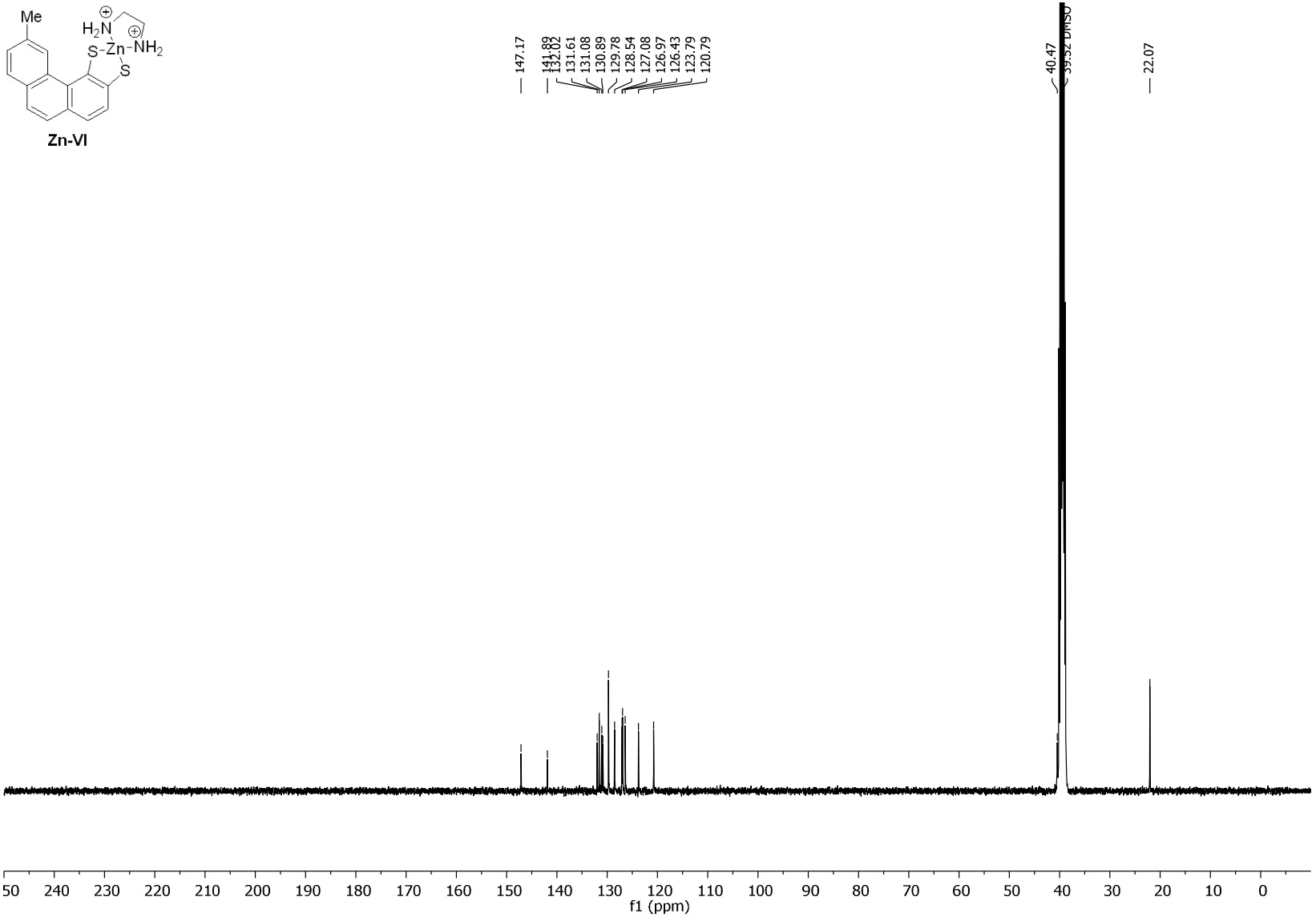

Figure S99. $^{13}C\{^{1}H\}$ NMR spectrum (101 MHz, DMSO-d_6) of **Zn-VI**.

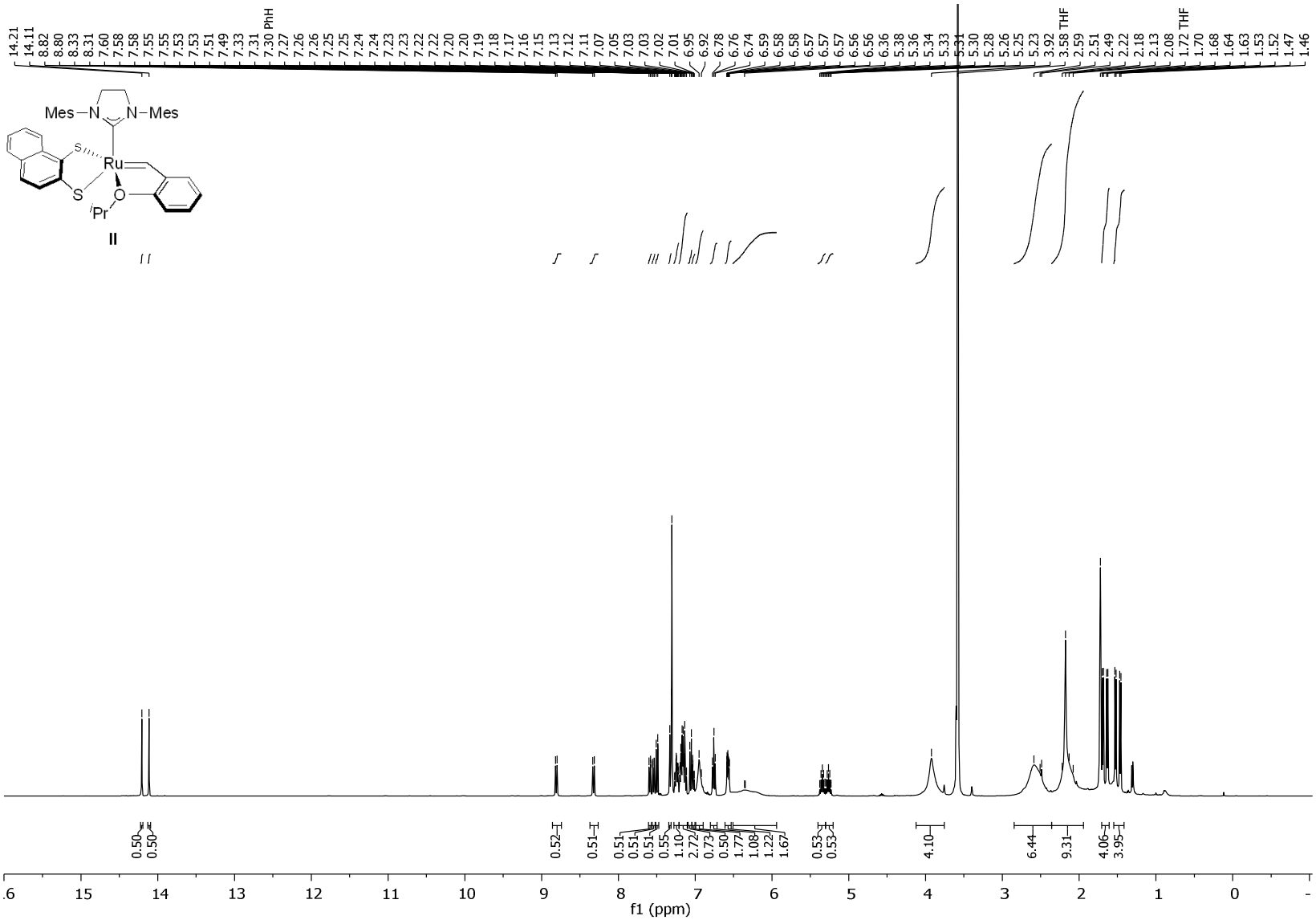

Figure S100. ^{1}H NMR spectrum (400 MHz, THF-d_8) of **II**.

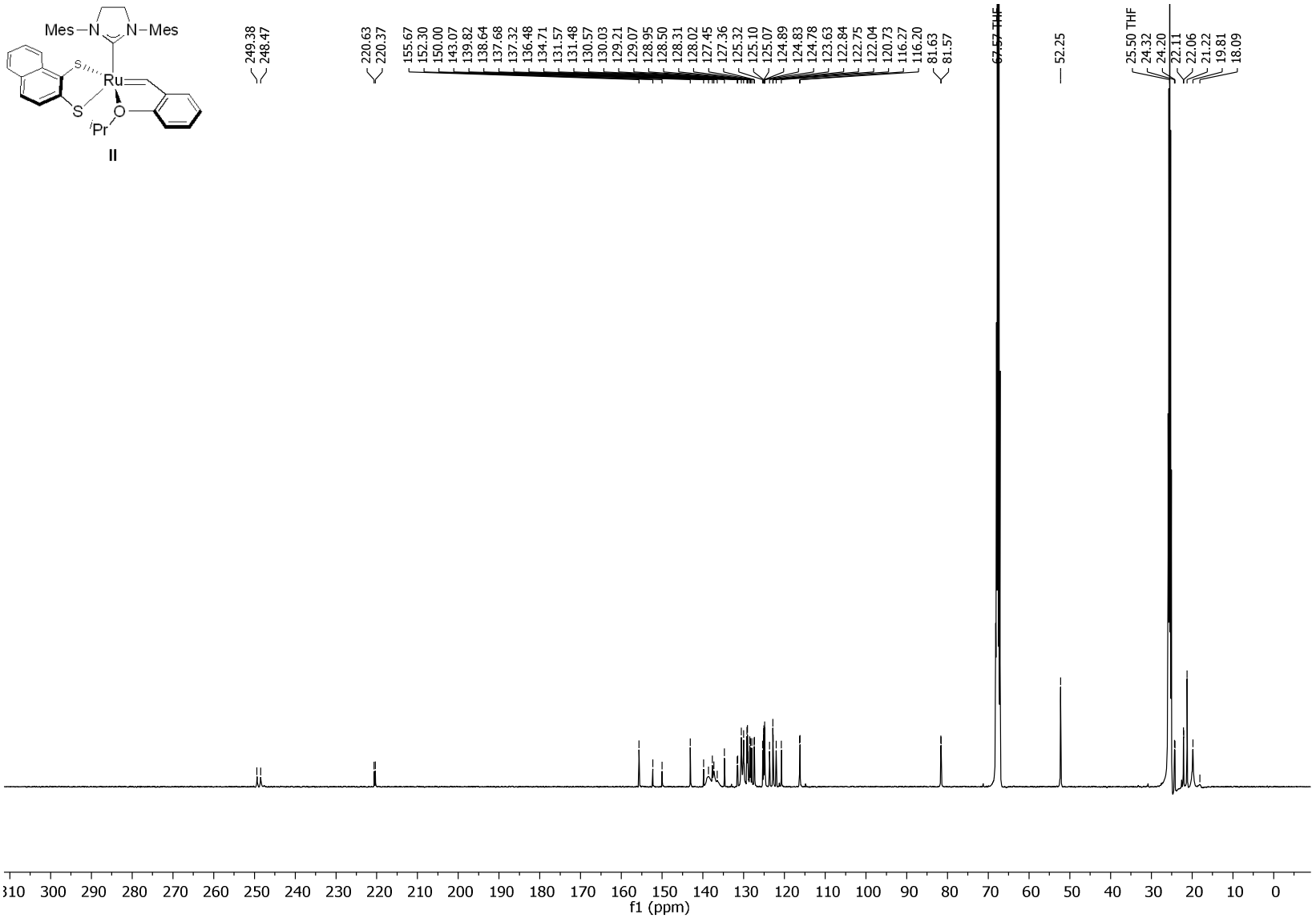

Figure S101. $^{13}C\{^{1}H\}$ NMR spectrum (101 MHz, THF-d_8) of **II**.

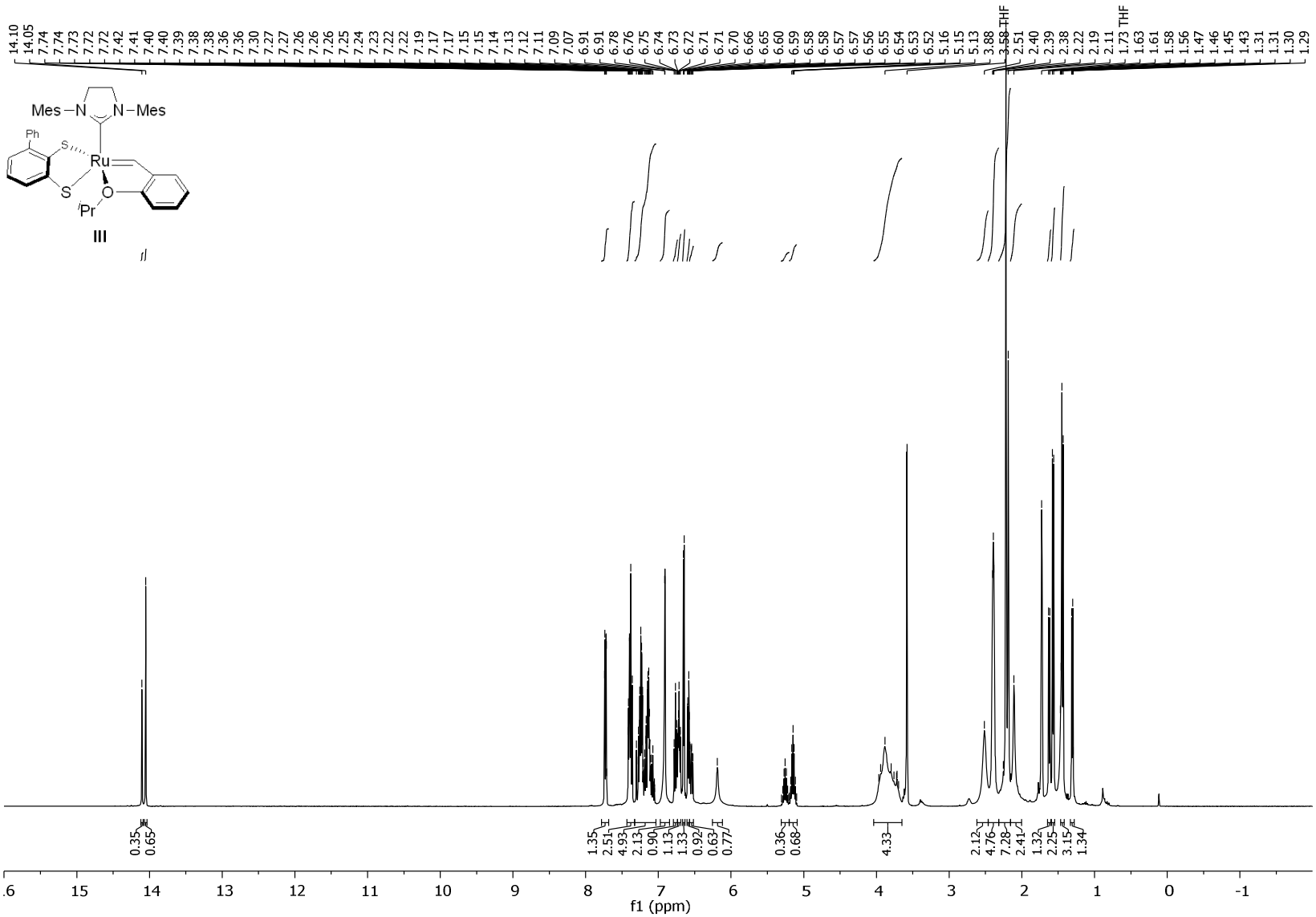

Figure S102. ^{1}H NMR spectrum (400 MHz, THF-d_8) of **III**.

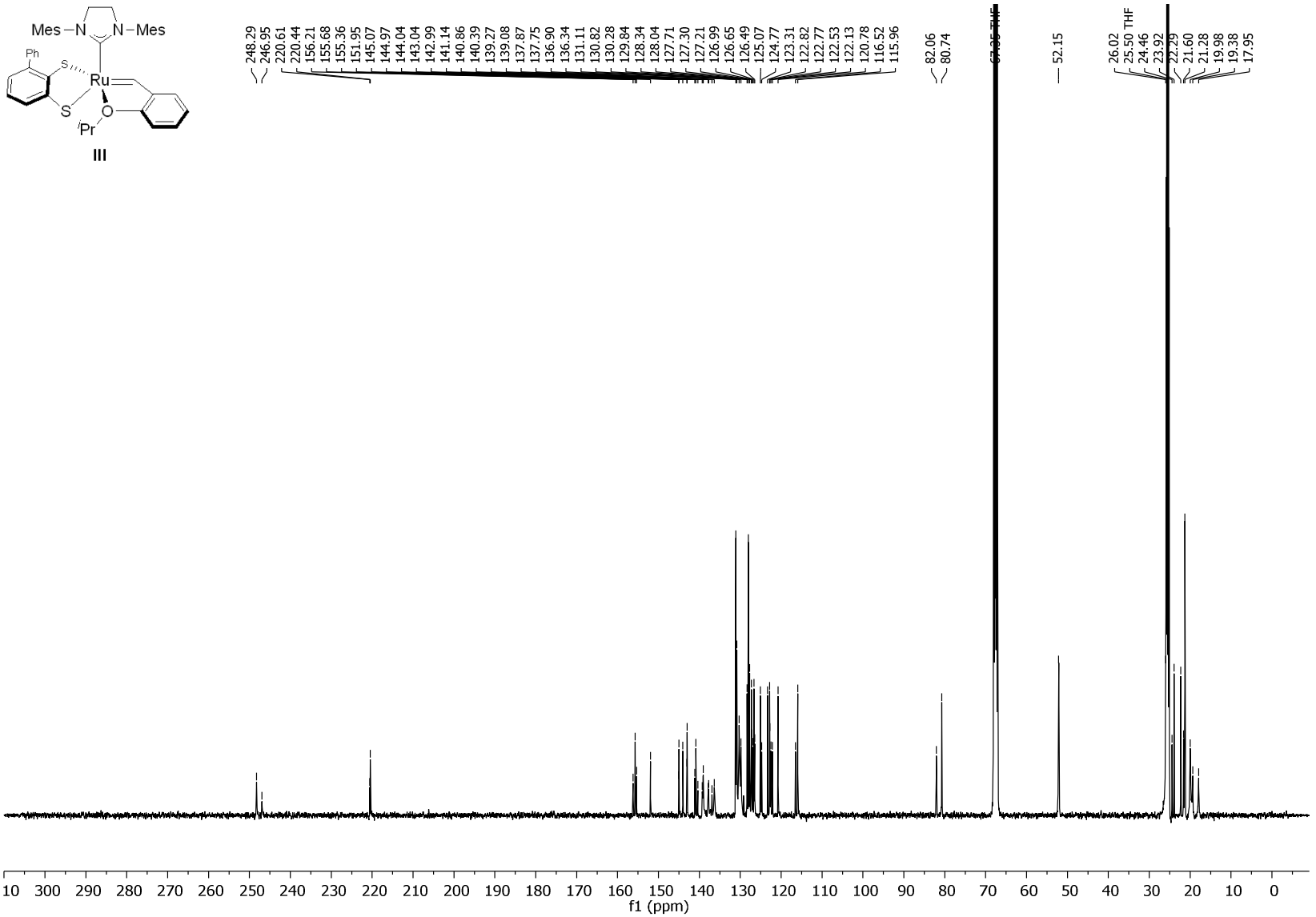

Figure S103. $^{13}C\{^{1}H\}$ NMR spectrum (101 MHz, THF-d_8) of **III**.

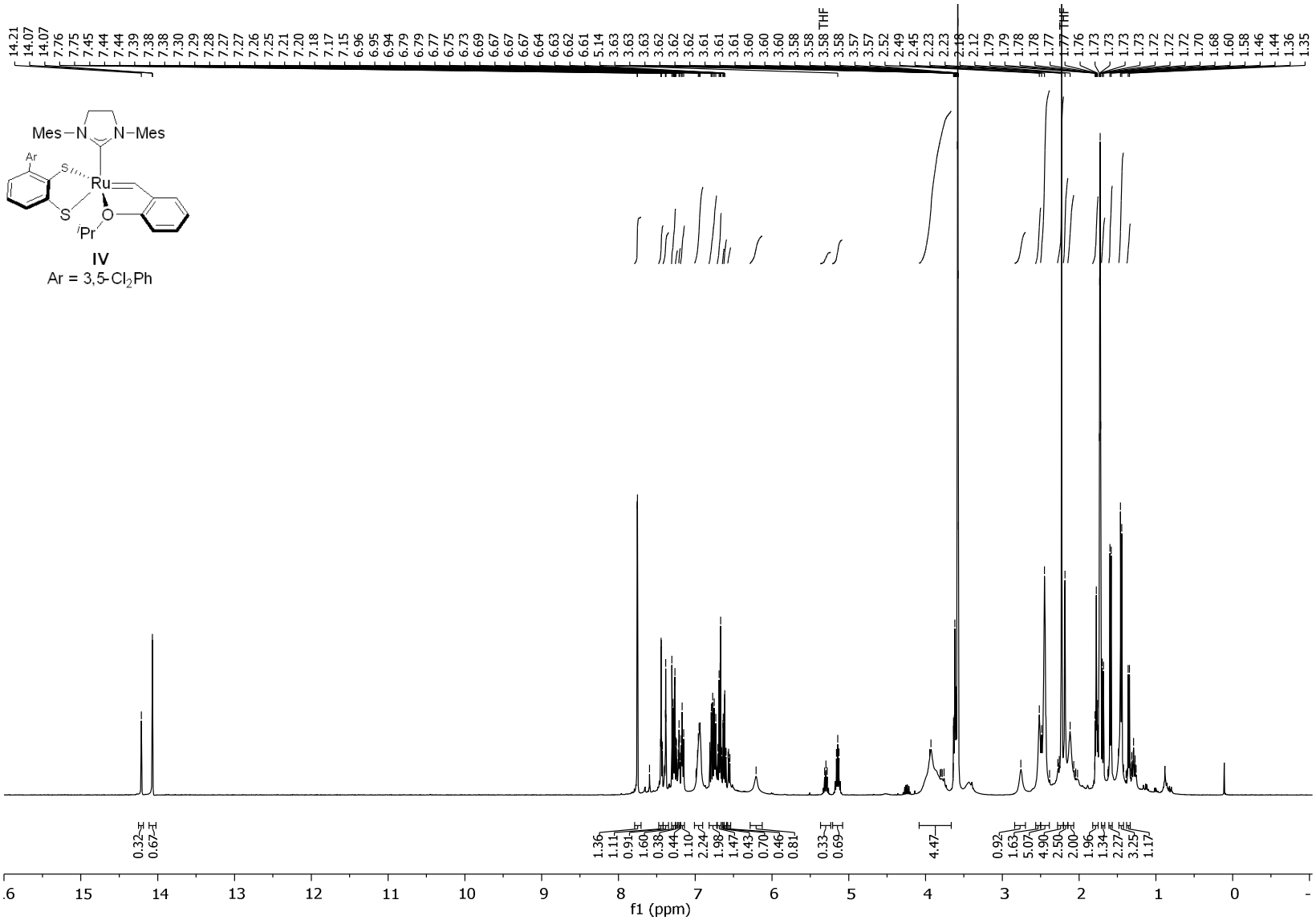

Figure S104. ^{1}H NMR spectrum (400 MHz, THF-d_8) of **IV**.

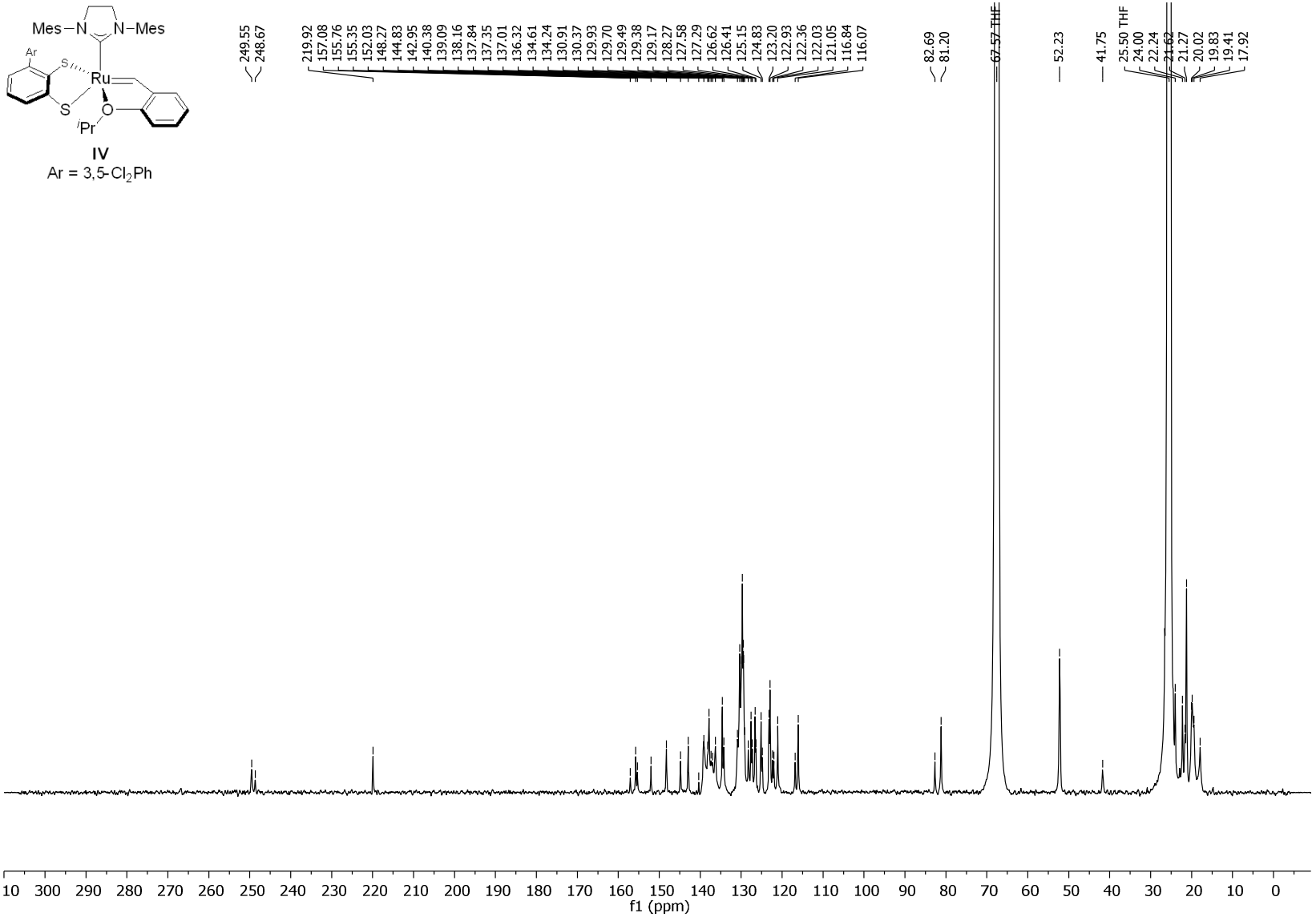

Figure S105. $^{13}C\{^{1}H\}$ NMR spectrum (101 MHz, THF-d_8) of **IV**.

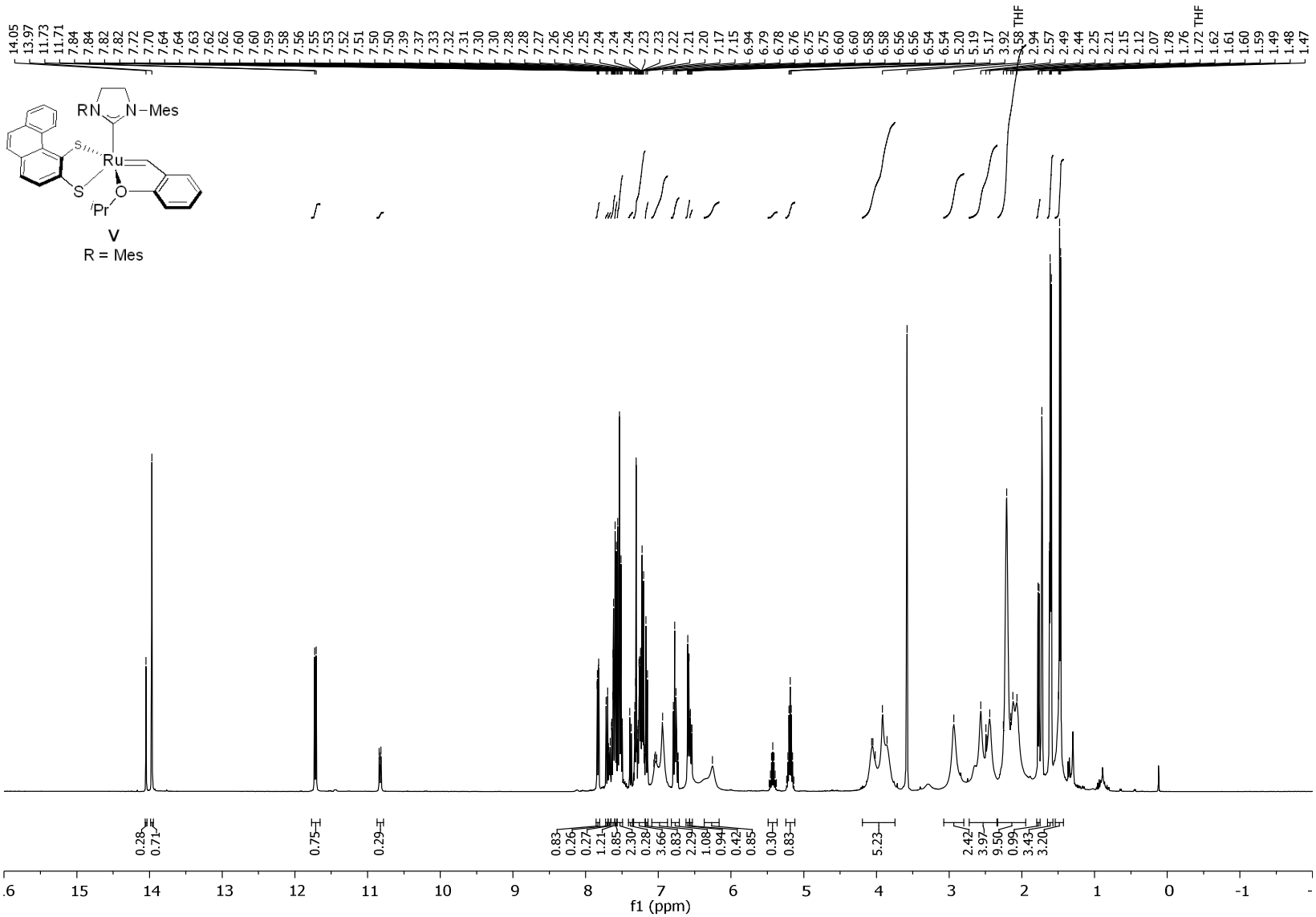

Figure S106. ^{1}H NMR spectrum (400 MHz, THF-d_8) of **V**.

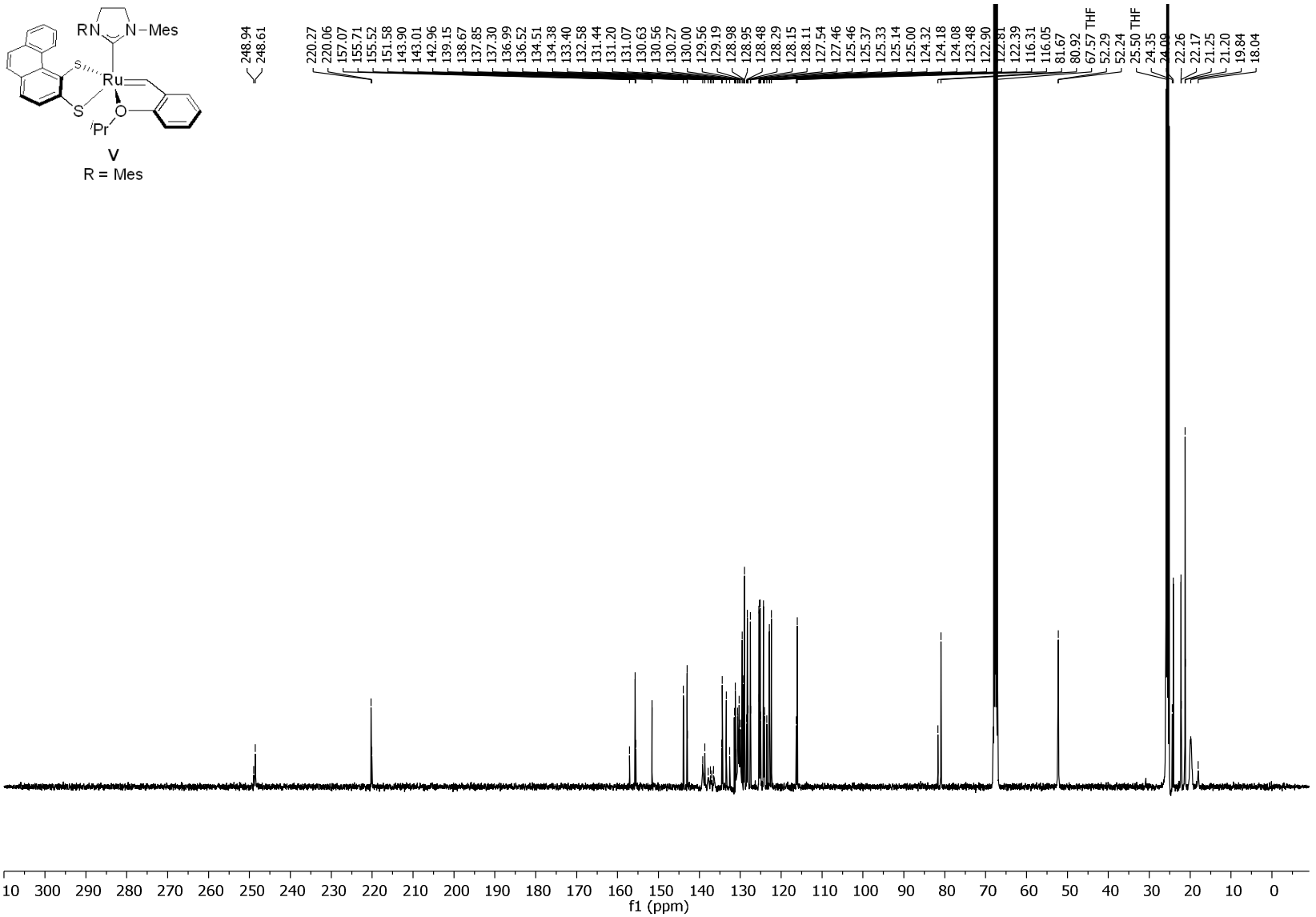

Figure S107. $^{13}C\{^{1}H\}$ NMR spectrum (101 MHz, THF-d_8) of **V**.

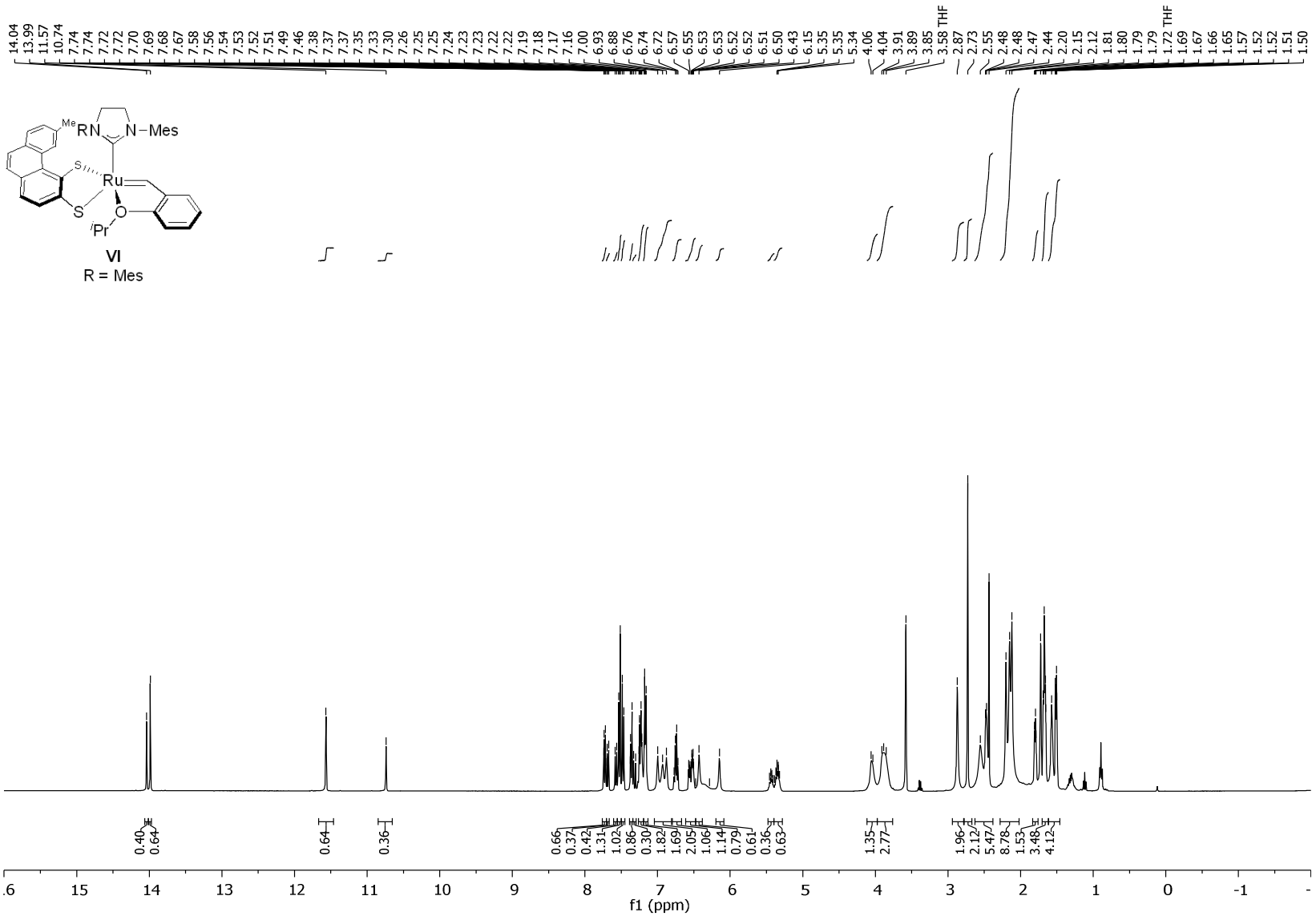

Figure S108. ^{1}H NMR spectrum (400 MHz, THF-d_8) of **VI**.

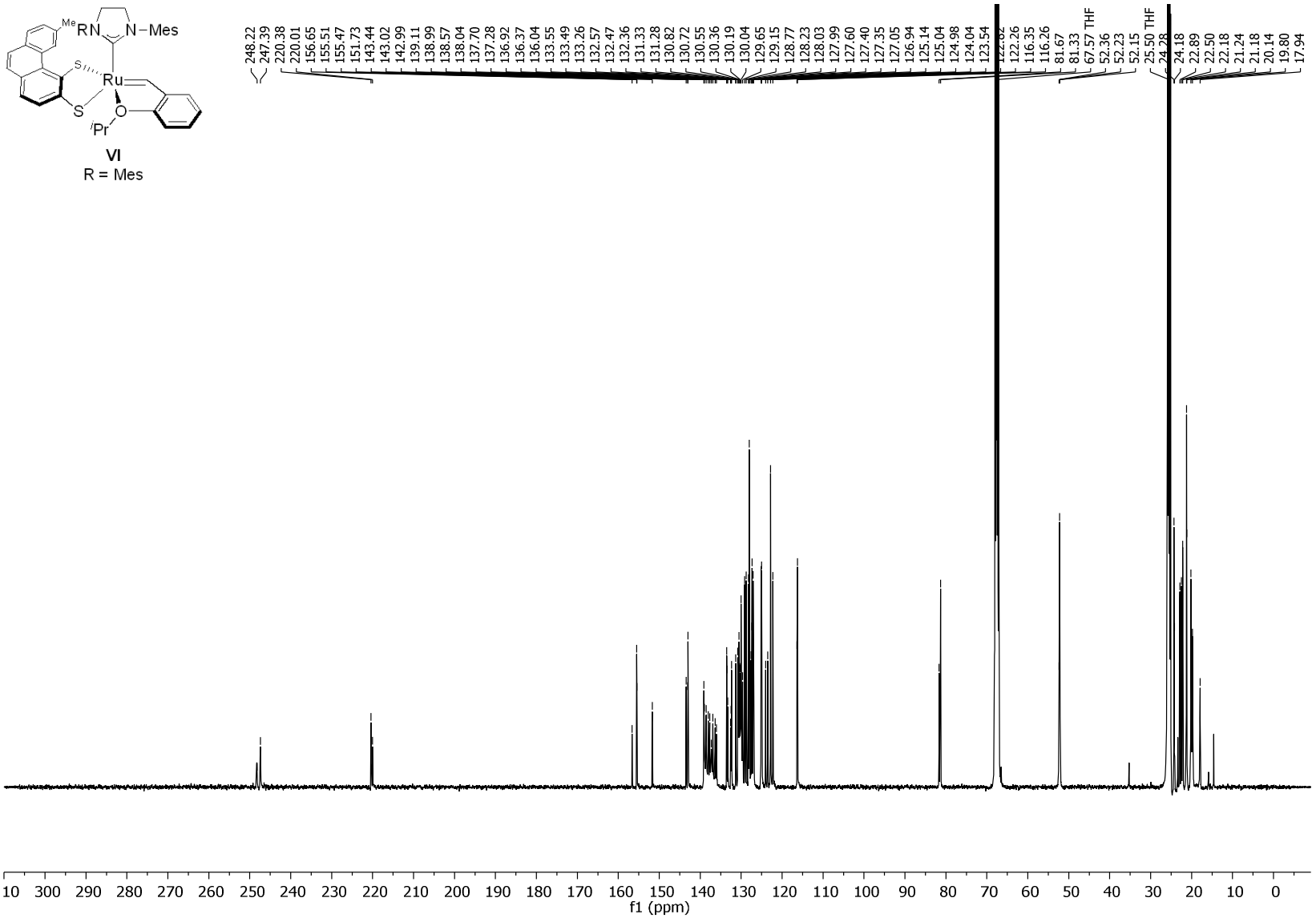

Figure S109. $^{13}C\{^{1}H\}$ NMR spectrum (101 MHz, THF-d_8) of **VI**.

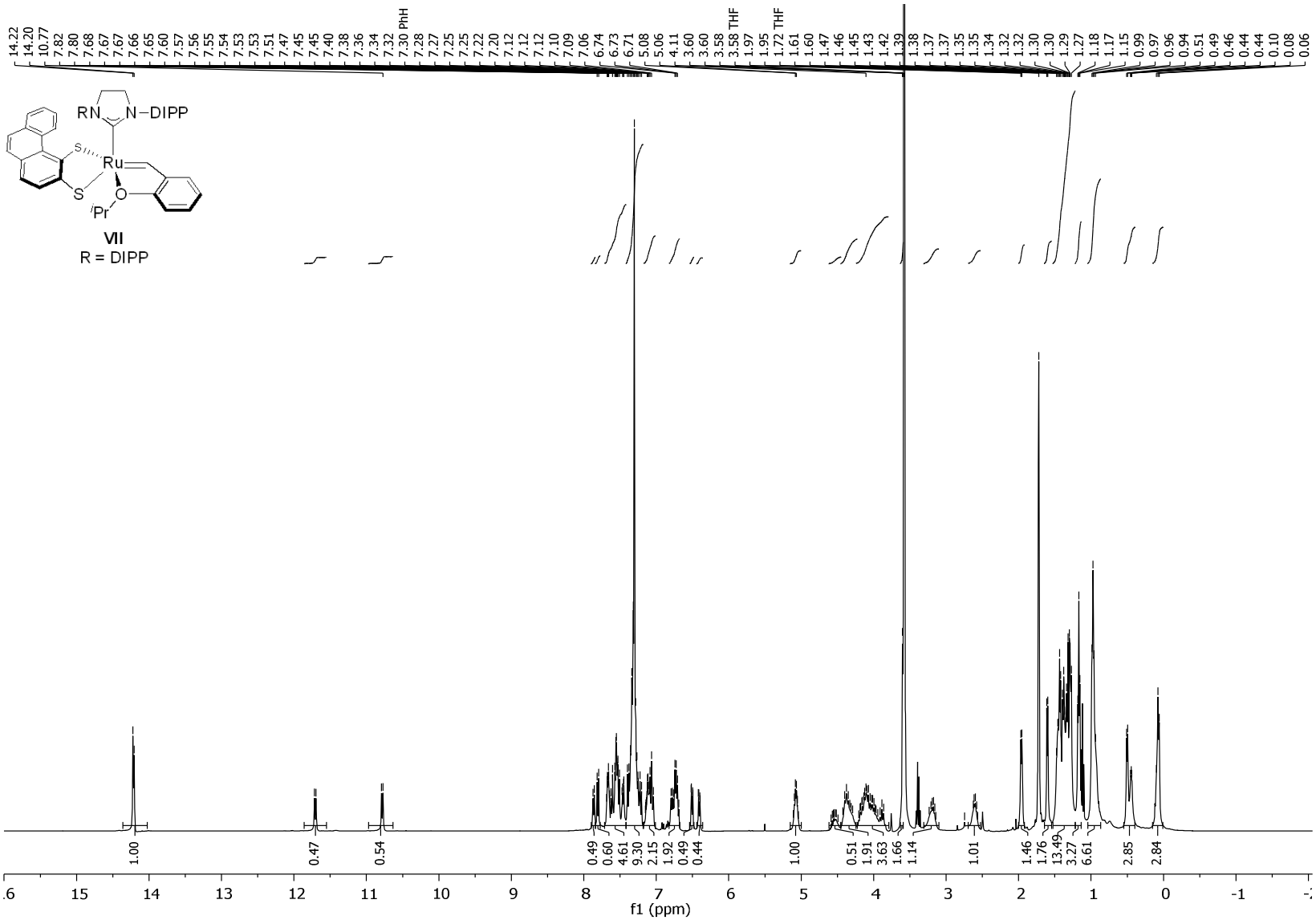

Figure S110. ^{1}H NMR spectrum (400 MHz, THF-d_8) of **VII**.

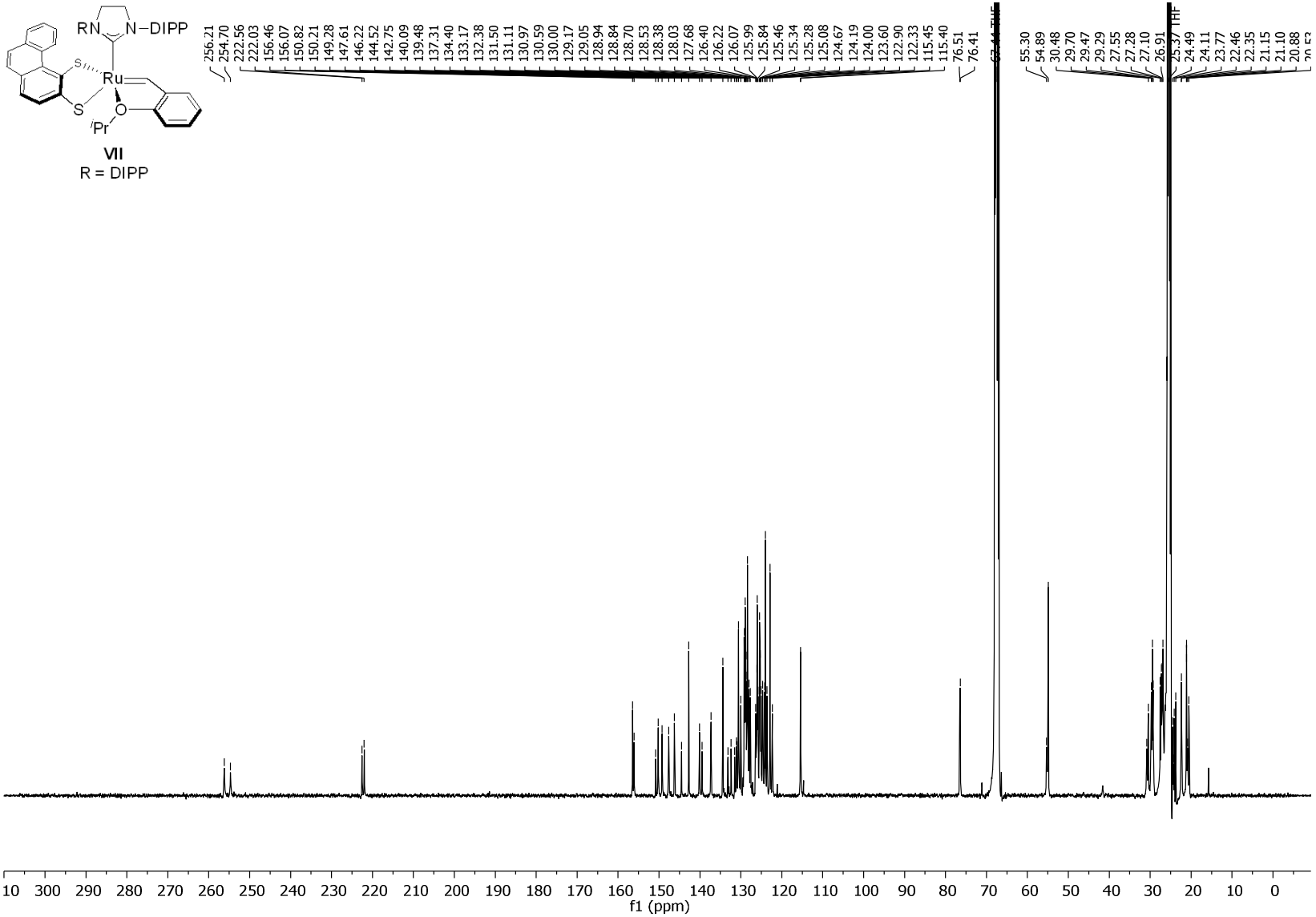

Figure S111. $^{13}C\{^{1}H\}$ NMR spectrum (101 MHz, THF-d_8) of **VII**.